Composite System Thermodynamics of Multiphase Droplet Systems Relevant to Emerging Technologies

by

Fatemeh Eslami

A thesis submitted in partial fulfilment of the requirements for the degree of

Doctor of Philosophy

in

Chemical Engineering

Department of Chemical and Materials Engineering

University of Alberta

Abstract

   Droplets exist widely in our everyday life and various industries. Numerous studies have been done to explore droplet systems and among them Gibbsian surface thermodynamics is a powerful means to investigate these highly curved systems. Due to the development of modern technologies and the introduction of novel materials, new systems have arisen that require this type of investigation. Here we have chosen two multiphase droplet systems of recent interest: the first one is droplet nucleation on a soft substrate as a modern material and the second one is the microdrop concentrating process which is mainly used in microfluidic technologies.

   Gibbsian surface thermodynamics is a rigorous method to predict the behaviour of highly curved surfaces such as droplets, bubbles, capillaries or colloid systems. This approach includes finding the conditions for equilibrium and explores the nature of each equilibrium state, *i.e.*, whether it is stable, unstable or metastable. The stability analysis is done by means of free energy calculation and the amount of an energy barrier determines the required energy for nucleation.

   In the first system of interest, we provide a mathematical explanation for easier droplet nucleation on a soft substrate compared with a rigid surface, an effect which has been observed experimentally by other researchers. In the second system of interest, we study the microdrop concentrating process which has application in microfluidic microdrop platforms. We provide the first thermodynamic description for microdrop concentrating of two types of solutes—those with and without solubility limits—and explore the role of different design parameters on the equilibrium states. Next we perform thermodynamic stability analysis of the process to determine the behaviour of the system at each equilibrium state. Finally, the role of the Ostwald–

Freundlich equation describing the effect of curvature of the precipitated solutes within the microdrops is fully explored.

Preface

Chapter 2 of this thesis, with minor modifications, has been published as: F. Eslami and J. A. W. Elliott, "Thermodynamic Investigation of the Barrier for Heterogeneous Nucleation on a Fluid Surface in Comparison with a Rigid Surface", Journal of Physical Chemistry B 115(36) 10646-10653 (2011).

Chapter 3 of this thesis, with minor modifications, has been published as F. Eslami and J. A. W. Elliott, "Design of Microdrop Concentrating Processes", Journal of Physical Chemistry B 117(7), 2205-2214 (2013).

Chapter 4 of this thesis, with minor modifications, has been published as: F. Eslami and J. A. W. Elliott, "Stability Analysis of Microdrops during Concentrating Processes", Journal of Physical Chemistry B 118(13), 3630−3641 (2014).

Chapter 5 of this thesis is being prepared for submission for publication as: F. Eslami and J. A. W. Elliott, "Role of Precipitating Solute Curvature on Microdrops during Concentrating Processes: The Non-Ideal Ostwald–Freundlich Equation".

"Knowledge gives life to the soul."

Imam Ali (as)

To my lovely parents,

My dear husband,

And my sweetheart son, Hossein

Acknowledgements

I would like to express my sincere gratitude and appreciation to my nice supervisor, Professor Janet A. W. Elliott for her enormous support and patience, helpful discussions and guidance, exceptional motivation and enthusiasm and her great way of teaching. I learnt too much from her not only in my academic career but also for means of living.

I would like to thank my examining committee: Dr. Alan J.H. McGaughey, Dr. Neda Nazemifard, Dr. John Shaw, Dr. Tony Young for their time and great comments.

I gratefully acknowledge our Iranian community in Edmonton, Tasnim, and our kind friends here that provided happy and memorable days in Edmonton for me and my family. I would like to especially thank two of my friends among them: Leila Zargarzadeh for her impressive scientific discussions, sharing the literature and her honest companionship and Sabereh Rezaei for her sincere long term friendship, encouragement and her deep feeling and caring.

I gratefully thank my kind friend Fatemeh Jafari and my lovely mother and father in law that took care of my baby during my thesis preparation.

I am also thankful to Mr. Behzad Vafaeian for his assistance in operating WestGrid and Dr. Alireza Abazari for bringing to our attention the problem addressed in Chapter 3.

I would also like to convey my love and gratitude to my cherished family, my mother Zahra Ansari, my father Mohammad Jafar Eslami, my husband Sadegh Mohit, my sister and brother Narges and Mohammad for their absolute love, support and prayers. I owe my success to my

Table of Contents

List of Figures

Chapter 1: Introduction

1.1. Motivation

From the time of Gibbs to the present, detailed surface thermodynamics has been used to understand the behaviour of systems including curved fluid interfaces. Such systems include nucleation of a drop in a vapor phase, and the equilibrium contact angle or size that will be obtained by a drop on a surface or in another fluid.

Droplets are the topic of interest in many industries and new technologies. Wetting is a major process ubiquitously used in everyday life and pertains to the way that a drop rests on a surface. The intermolecular energies between the drop and the solid surface manage the wettability of the surface and its contact angle. One of the parameters that affects the surface energies and wettability of the surface is the geometry of the surface. From this viewpoint, surfaces can be smooth, rough, rigid or soft. Surface roughness may be produced by a series of grooves which may make the surface hydrophobic.[1-3] Seeking for ultra-hydrophobic materials which have lots of applications[4,5] in self-cleaning surfaces, waterproofing clothes, anti-biofouling paints[5] and microfluidic devices, scientists produce such materials by creating nanometer hierarchical protrusion on the surfaces inspired by the superhydrophobic surfaces in nature, such as Lotus leaves or shark skin.[6-8] Softness is another aspect of the surface that influences the surface energy and hence its wettability. Soft matters are a group of materials, including polymers, gels, elastomers, organic solids and tissues, that nowadays are used extensively everywhere. In addition, when sizes are reduced to nanometers, some rigid materials behave as softer materials.

Although the geometry of the soft surface prior to resting a drop on it is similar to the rigid one, due to elasticity of the surface its geometry will change by placing a drop on it.

A surface can be wetted either by a sessile drop or condensed drops. Condensation is another major process dealing with droplets which takes place in many industrial processes such as air conditioning, thermal processing and power management. Condensation is a phase transition from a vapor phase into a liquid phase and similar to other first-order phase transitions follows a nucleation mechanism which is the formation of the drop in a vapor phase. Nucleation happens in two ways, homogeneous or heterogeneous. The former occurs when the drop forms within the vapor phase and the latter takes place in the case of the presence of a third phase (usually solid) which provides sites for nucleation. In the formation of a nucleus, increasing the volume of the new phase decreases the free energy, while increasing its surface area increases the free energy. At a specific size of the new phase which is the critical size or the Kelvin size, these two phenomena balance each other and the total free energy is an extremum. Filmwise and dropwise are two types of condensation that may occur subject to the wettability of the condensing surface. When the surface is less wettable, condensation happens in the form of drops and much more heat transfers during the phase transition since there is no liquid film as a barrier to heat transfer.

Besides the presence of droplets in the above mentioned industries, by development of technologies, droplets were introduced as a platform in microfluidic technologies to help understand the behaviour of ultra-small volumes of fluid. Actually, from a long time ago, simulating the chemical processes inside cells and sub-cellular organisms was a subject of interest and droplets provide a suitable platform for this simulation. Droplets were considered as micro reactors for analysing very small amounts of materials in a confined space to help manipulating the materials without dilution or diffusion of the material.

Generally speaking, droplets have lots of applications in emerging technologies and due to their high surface-to-volume ratio, detailed surface thermodynamics is needed to find the equilibrium conditions and provide appropriate knowledge for understanding their behaviour in different systems. Although much research in this field has been done on unsophisticated systems such as considering rigid surfaces, single component or ideal solution droplets, by introduction of advanced materials and microfluidic technologies, there are a number of new systems for which surface thermodynamic analysis has not been done yet and is needed. In this work, we have chosen one of the advanced materials—soft substrates—and one of the microfluidic systems—microdrop concentrating processes—on which to perform detailed surface thermodynamics and provide more accurate design parameters. In the following sections, first a brief background on surface thermodynamics is presented and then a literature review about stability analysis of curved fluid interfaces, wetting on soft substrates and microdrop concentrating processes has been submitted. At the end, the scope and objectives of the thesis are presented.

1.2. Surface Thermodynamics Background[9-13]

Thermodynamics is the study of the variation of energy, entropy and the amount and volume of transferring materials at equilibrium conditions. Importantly, thermodynamics maybe used to find the equilibrium state of a system and thermodynamic stability analysis may be used to find the nature of the equilibrium states (stable, unstable, metastable). In systems with highly curved surfaces such as colloids and also in systems with very small scales such as in nanotechnology, surface effects should be considered since by changing the area of surfaces work is done and this work is not negligible.

Based on Gibbs' definitions, systems are simple or composite. A composite system is composed of a number of simple subsystems and a simple system is defined to be macroscopically homogeneous, isotropic and uncharged and has no surface, electrical, magnetic or gravitational effects. When all the simple subsystems of a composite system are at equilibrium, then we can consider the composite system at equilibrium. Entropy and internal energy of the composite system is additive over its constituents.

In order to find the equilibrium state, based on thermodynamic postulates, the entropy of the composite system should be extremized with respect to the system's constraints including energy being constant or the energy should be extremized with respect to constraints including entropy being constant. Equations (1-1) and (1-2) are fundamental equations of thermodynamics and S, U, N_j, V and r are entropy, internal energy, number of molecules (or moles) of each component j, volume and number of components respectively.

$$S = S(U, V, N_1, .., N_r) \qquad (dS)_U = 0 \; at \; equilibrium \qquad (1\text{-}1)$$

$$U = U(S, V, N_1, .., N_r) \qquad (dU)_S = 0 \; at \; equilibrium \qquad (1\text{-}2)$$

For a bulk phase, the differential form of the fundamental equation of thermodynamics is given by equation (1-3) which relates the thermodynamic properties, temperature, pressure and chemical potential, represented by T, P and μ respectively.

$$dU^i = T^i dS^i - P^i dV^i + \sum_{j=1}^{r} \mu_j^i dN_j^i \qquad (1\text{-}3)$$

In equation (1-3) the superscript i represents each bulk subsystem such as liquid or vapor. In addition, the differential forms of the fundamental relation for flat and curved interfaces are given by equations (1-4) and (1-5) respectively:

4

$$dU^{\alpha\beta} = T^{\alpha\beta}dS^{\alpha\beta} + \gamma^{\alpha\beta}dA^{\alpha\beta} + \sum_{j=2}^{r}\mu_j^{\alpha\beta}dN_j^{\alpha\beta} \qquad (1\text{-}4)$$

$$dU^{\alpha\beta} = T^{\alpha\beta}dS^{\alpha\beta} + \gamma^{\alpha\beta}dA^{\alpha\beta} + \sum_{j=1}^{r}\mu_j^{\alpha\beta}dN_j^{\alpha\beta} \qquad (1\text{-}5)$$

In the above relations γ and A stand for surface tension and surface area and the superscript $\alpha\beta$ identifies the interface subsystems. Equations (1-4) and (1-5) are based on "Gibbs' dividing surface approximation" and "Gibbs' surface of tension approximation" respectively. To explain the Gibbs' dividing surface concept, consider a system which contains two phases of α and β with the interface $\alpha\beta$ being flat. In reality the surface phase has a small thickness and each chemical component and density has a constant value in one phase and changes in a continuous way to reach another constant value in the other phase. But based on Gibbs' convention, there is a way of describing the real system with an infinitesimal thin surface which separates two phases and has no volume but has area of $A^{\alpha\beta}$. He places the dividing surface at the level for which the number of moles of one of the components has no magnitude in the surface phase. Hence the summation in equation (1-4) begins at $j=2$ if the first component is supposed to be zero at the interface. By fixing this ideal dividing surface, the remaining extensive properties can be determined at the interface and they are referred as "surface excess quantities". In the case of curved interfaces the Gibbs' surface of tension approximation is used for placing the dividing surface. In order to avoid explicit dependency of the surface tension on the curvature, for curved interfaces all species have excess quantities at interface. Hence the summation in equation (1-5) begins at $j=1$.

There are also two important equations in capillary science which describe the equilibrium state of curved interfaces. One of them is the Laplace–Young equation which relates the curvature of the interface to the pressure difference of the bulk phases:

$$P^\alpha - P^\beta = \gamma^{\alpha\beta}\left(\frac{1}{R_1} + \frac{1}{R_2}\right) \tag{1-6}$$

In equation (1-6), R_1 and R_2 are two principal radii of curvature of the interface. In case of a drop or bubble this interface will be a sphere, so $R_1=R_2=R_{sphere}$. The Young equation is the other basic equation which determines the contact angle θ between a liquid–vapor interface and a solid:

$$\gamma^{LV}\cos\theta = (\gamma^{SV} - \gamma^{SL}) \tag{1-7}$$

In view of the fact that intensive properties like temperature and pressure are easily measurable quantities, by means of Legendre transforms of the fundamental relation, different free energies including Helmholtz, Gibbs and Grand potential functions can be derived. In chemical engineering thermodynamics, most of the time the potential energy which should be extremized is the Gibbs free energy. This is due to the fact that, without considering surface effects, the temperature and pressure should be constant in the equilibrium state, but as the Laplace–Young equation illustrates, there is a pressure difference across curved interfaces which affects the free energy. Based on this concept, the thermodynamic potential of each system should be determined carefully. In fact, the nature of interactions between system and reservoir dictates which function acts as the potential function.

The system and reservoir can exchange energy, mass or volume with each other. They can be considered together as an isolated system. In this case, by writing the Euler equation for the reservoir and considering the new equilibrium state for the system plus reservoir and keeping in mind that the intensive properties of the reservoir do not change, the free energy which acts as a potential function and should be extremized will be found.

As an illustration of a curved surface existing in a system consider a drop. Formation of a drop in a vapor phase is an example of homogeneous nucleation. Nucleation is accompanied by forming an interface around the border of the new phase. When nucleation happens spontaneously inside a phase without interference of another phase it is called homogeneous nucleation. In the case of the presence of another phase (usually solid) which provides sites for nucleation, heterogeneous nucleation will take place. When there is a nucleus in a system, by means of surface thermodynamics the equilibrium radius (R_c) of the bubble or drop can be found and also whether R_c corresponds to a stable equilibrium state or an unstable one. R_c can be determined from the equilibrium conditions and associated relations. In order to determine the stability of equilibrium states, the second derivative of free energy with respect to size of the drop or bubble should be explored at the equilibrium radii. If the second derivative is negative, R_c represents an unstable equilibrium. If the second derivative is positive, R_c represents a stable equilibrium. Metastable equilibria are located at local minima in the potential function. At an instant, if a drop forms in a vapor phase and it is larger than the unstable size, it will grow bigger and bigger, or if the drop radius is smaller than the unstable size, the drop will evaporate. But if the drop radius is in stable equilibrium, whether fluctuations cause its size to become bigger or smaller it will return to the stable size and remains unaffected by small perturbations.

Usually the critical radius of the nucleus can be found from physical properties of the system combined with assumed equations of state for the phases giving extra relations for chemical potentials. For example, the vapor phase can be treated as an ideal gas. In the case of moderate pressure the liquid phase can be considered as an incompressible fluid. However, if a constraint on the system is no volume change then the assumption of constant isothermal compressibility is more realistic for the liquid phase.

In addition, one of the important quantities in potential functions is the volume of the phases (*i.e.*, the bubble or drop) and the area of phase interfaces such as the liquid–vapor and solid–vapor interfaces. Therefore the geometry of the surface plays an important role in the stability analysis.

1.3. Literature Review

1.3.1. Stability Analysis of Curved Interfaces and the Kelvin Equation

Research has been done in the field of stability analysis of curved fluid surfaces using the approach of surface thermodynamics. Ward and his research group have done several works in this field. They studied the stability of a pure sessile drop on a rigid surface[14] and explored the role of adsorption on solid–fluid interfaces.[15,16] They also found the equilibrium contact angle of a sessile drop[17,18] by means of Gibbs adsorption equation and a given isothermal adsorption equation. In addition, they have investigated the homogeneous[19] and heterogeneous[12] nucleation of bubbles in weak gas–liquid solutions at constant pressure[20] and volume and explored the stability analysis[21] of these systems. They verified that in homogeneous nucleation dissolved components increase the pressure and decrease the superheat for the onset of nucleation.[19] In order to examine a weak gas–liquid solution in heterogeneous nucleation they used the conical shaped pit for preparing sites for nucleation. In this system, in the case of a closed and constant volume system[12] they got the Helmholtz free energy to be the potential function and in the case of a closed and constant pressure system[20] they got a new potential function named "*B*". In addition, it was found that when a bubble nucleates in a liquid–gas solution a minimum amount of dissolved gas is required so that both stable and unstable equilibriums states exist for the bubbles.[21] Studying the surface thermodynamics and equilibrium conditions in capillary systems is another subject of investigation which has several applications in porous media.[22-25]

Zargarzadeh and Elliott explored the stability of the pure fluid confined in a solid cone and between a sphere and a flat plate and between two flat plates and investigated the role of different geometrical properties on the presence of liquid forming out of vapor (and vapor forming out of liquid) in these systems.[24,25]

The Kelvin equation is an important relation in surface thermodynamics which can provide the correct answer for vapor pressure and melting point of curved interfaces, solubility of small particles, nucleation, capillary rise, *etc*.[26] However, Kelvin had predicted that his equation would not be valid for the microscopic scale while his derivation was based on macroscopic thermodynamics. Therefore, many experiments have been performed to recognize the range of validity of the Kelvin equation.[27] It is concluded that the most deviations from the Kelvin equation arise from the presence of contaminants on the interface and that there is good support for the validity of the Kelvin equation for drops and capillaries up to mean curvature of 3-4 nm.[27]

Apart from ideal rigid, smooth substrates, several thermodynamic analyses[7,28-31] have been done for a sessile drop resting on rough or superhydrophobic surfaces. It was found that in the case of rough surfaces the Young equation is not valid anymore and instead the Wenzel[32] or Cassie[33] equations govern the contact angles. In the former case the liquid penetrates into the grooves while in the latter case air entraps in the grooves and the liquid remains on the top of surface. The transition between these two states and which is the more stable one has been determined by means of free energy analysis.[7]

Generally speaking, Gibbsian surface thermodynamics is a useful method to understand the behaviour of highly curved surfaces and by means of stability analysis valuable information

about different equilibrium states will be obtained. Here we are going to implement this method to some modern systems containing droplets.

1.3.2. Wetting on Soft Substrates

Wetting of a soft substrate by a sessile drop has been investigated both experimentally[34-38] and theoretically.[39-46] Considering an elastic solid as a soft substrate, a drop deforms the surface: Laplace pressure inside the drop pushes the substrate downward and the surface tensions pulls the contact line upward and creates a ridge around it. Deformation of the surface affects the validity of the Young equation, a law regarding contact angle in capillary science. In fact the relation proposed by Young describes the force balance in the horizontal direction for a rigid, plane solid. But he didn't say anything about the vertical component of surface tension. For wetting on a rigid surface this issue is not very important but in case of deformable substrates it will play an important role.[47] The Young equation is valid for wetting on an infinitely rigid substrate and Neumann's triangle law of forces is used for wetting on a liquid surface which is an infinitely soft surface. Since a soft surface acts between these two limits, wetting on soft substrates would be governed by a relation between them.[48] Finding the correct contact angle and equilibrium shape of the deformed soft solid is challenging due to the stress singularity and infinite deformation at the contact line resulting from classic elastic theory.[41] Different methods have been used to deal with this problem: Lester[39] and Rusanov[40] considered a thickness (t) for the liquid–vapor interface of molecular dimensions and Shanahan[49] considered other types of behaviour such as plastic or non-linear elastic for a very small zone (ε) in the vicinity of the triple line. White attributed the presence of these vague length scales such as t and ε to unclear transmission of surface tension to the substrate which relates to the intersurface forces at the microscopic scale.[44] He found that the microscopic contact angle is zero and in the case of the

macroscopic contact angle a modified Young equation which has a "line-tension-like"

modification is valid. Olives[50] used Gibbsian surface thermodynamics and incorporated a new

idea of "ideal transmission" into the "Gibbs dividing surface" and found the conditions for

equilibrium for drops placed on deformable solids. He recently[51] performed careful mathematics

and found finite displacement at the triple line by considering the validity of "Green's formula"

at the triple line. Shanahan used minimization of free energy which contains the interfacial free

energy term and the elastic energy of deformation with constant volume as a constraint and

submitted a modification for the Young equation which pertains to the Laplace pressure at the

mesoscopic scale.

Kern and Muller[46] performed the minimization of free energy for a thin elastic solid and found

a pseudo-parabolic shape for the deformable substrate. They attributed the presence of a ridge in

previous works to superposing the forces. Yu and Zhao[45] investigated the role of surface

thickness on the deformation profile and found a "saturation thickness" for each substrate. They

figured out that only substrates which have a thickness bigger than this magnitude obey the result

of Lester[39] and Rusanov[40] since they performed their analysis for "semi-infinite surfaces".

Pericet-Camara *et al.*[35] performed a set of experiments and by means of laser scanning confocal

microscopy and white light confocal profilometer observed the deformation profile of the

substrate with different thickness. They observed the ridge at the triple line but confirmed that

substrate deformation below a certain thickness decays by exponential oscillation rather than in a

monotonic way.

After the publication of Chapter two of this thesis, Style and Dufresne[48] reported an analytical

calculation and verified that in the case of very small droplets or for any size of droplet at

microscopic scales, the soft surface acts like a fluid surface and the Neumann triangle relation

governs the contact angle of the system. Therefore, the deformation shape near the contact line is a general feature only governed by interfacial tensions and surface stresses. Using this feature, Style *et al.*[52] proposed a new method for evaluating the surface stresses of the solids without requiring the solid body's information. In addition, they discovered a novel technique for transferring a droplet on a homogeneous flat surface only by changing the thickness of the soft material throughout the substrate. The reason for this migration is lower free energy of the system on softer surfaces. This characteristic is very useful in microfluidic devices and enhances control of the drops on the surfaces.[53,54]

Apart from investigating the wettability of sessile drops on soft surfaces, Sokuler *et al.*[55] performed a set of experiments and studied the nucleation of drops on soft surfaces. They used PDMS as a substrate and by changing the monomer and cross-linker ratios of the surface changed the softness of the substrate. They observed that on softer surfaces the density of nucleation is higher and the drop coalescence is slower and suggested that this observation may relate to a smaller free energy of nucleation on softer surfaces. Here, we provide a mathematical justification for this observation for the first time. Due to the importance of condensation in industries, using the soft substrates enhances the heat transfer and subsequently the overall energy efficiency of the processes.

1.3.3. Microdrop Concentrating Processes

Another form of the presence of droplets in industries is in emulsion format which means the presence of the drop in an immiscible continuous fluid rather than on a solid. Microfluidic technologies provide a new tool for better exploitation of emulsions. By means of this novel technology high rate generation and various manipulations of emulsion droplets are now

possible.[56] One of the motivations for development of microfluidics was miniaturization and seeking for understanding and resproducing the behaviour of chemistry of tiny materials in ultra-small volumes such as cells.[57,58] Microdroplets such as those in water-in-oil emulsions facilitate this investigation since they act as compartmentalized micro-reactors for the minute encapsulated analytes in high throughput experiments. In addition, microdroplets offer an impenetrable confined container for the inner solute which prevents dilution of the solute.[59] If the continuous phase is an organic phase with slight solubility of water such as soybean oil and the aqueous microdrop contains a solute that has a small partition coefficient in the organic phase then concentration of the solute is possible. Increasing the temperature enhances the solubility of water in the organic phase which results in more mass transfer from the droplet into the organic phase and hence concentrating the solute.[60] The high surface-to-volume ratio of microdroplets enhances the mass transfer since it was found that the rate of change in concentration is proportional to the fifth power of the surface-to-volume ratio. Since preparing droplets with a certain composition is very hard experimentally, this process takes advantage of adjusting the concentration by means of temperature change which is easy to control.[61]

Concentrating the encapsulated solutes within microdrops has many applications in biology. It helps detection and control of tiny amounts of materials such as biomarkers, DNA, proteins and sub-cellular organelles.[62] Cryobiology is another field that can exploit microdrop concentrating processes. In some protocols for the cryopreservation of cells a high concentration of cryoprotective agents is needed while at the same time too long an exposure of cells to that high concentration is fatal. Using the microdrop concentrating process allows increasing the cryoprotective agent concentration in very short time.[63] After the publication of Chapter three of this thesis, Kojima and Takayama applied the microdrop concentrating technique to find the

binodal curves of aqueous two phase systems (ATPS) which is a method for molecular separations at the macroscale.[64] Traditionally, ATPS binodal curves are found by diluting a concentrated two phase system up to disappearance of the phase boundary while utilizing the microdrop concentrating process acts in the opposite direction and is useful when only a small sample of material is available. Microdrop concentrating is also applicable in protein crystallization since protein crystallization is a sensitive process that needs precise control over concentration. Shim *et al.*[61] exploit the microdrop concentrating mechanism by modifying it and designing a Phase Chip as a microfluidic device. The chip contains two layers which are connected via a Polydimethylsiloxane (PDMS) membrane. One layer contains microdrop emulsions in oil which are stored in wells and the other layer is the reservoir and the water diffuses from the microdrop into the reservoir or vice versa via the membrane. They have used this device for protein crystallization. Actually nucleation processes in protein crystallization need high supersaturation while high supersaturation leads to the growth of many defects in the crystal. In order to obtain large and defect-free crystals first the seed should be produced at high concentration via nucleation and then by lowering the concentration the seed can grow large without defects.[61] Wang *et al.* apply concentrating process to polymer solution microdroplets and obtain toroidal particles at the end of the process.[65] Microdrop concentrating processes are accompanied by droplet shrinkage and volume change. It was found that preparing droplets in very small sizes such as femtoliters is very challenging and energy consuming. The "shrunk to femtoliter" method exploits this microdrop dehydration to produce a certain small size of the droplets more easily.[66] Bajpayee *et al.* use this process for the desalination of water. They extract pure water out of saline water-in-oil emulsion in a more energy-efficient technique.[67]

The above mentioned applications elucidate the significance of microdrop concentrating processes. Many dynamic studies have been done on microdrop concentrating processes to figure out the kinetics of the process.[60,62,63,68-70] For example, Jeffries *et al*. proposed a model for heat and mass transfer of microdrops and verified their model by performing an experiment on pure aqueous microdrops in decanol and acetophenone.[69] Shen *et al*. studied the dynamics of the dehydration process in a system of encapsulated particles in aqueous microdrops in oil phase and investigated the role of the number of particles and surfactant concentration on water removal.[70]

In general, although the microdrop concentrating process is an important and applied method in microfluidics we found no thermodynamic investigation of this process: thermodynamics can provide important information for better design of such systems.

1.4. Scope of the Thesis

In this thesis, Gibbsian thermodynamics of composite systems is used to develop understanding of two different multiphase droplet systems of scientific and industrial importance: *i*) nucleation of a liquid drop on a liquid or solid surface, and *ii*) microfluidic droplet concentrating processes. The thesis objectives are:

1. To provide an explanation for the experimentally observed ease of nucleation on soft surfaces by investigating the thermodynamic stability of a sessile drop on either a rigid surface or a fluid surface at constant vapor phase pressure and comparing their energy barriers (Chapter 2).[*]

---

[*] In Chapters 1 and 2, γ stands for surface tension while in Chapters 3, 4 and 5 surface tensions are denoted by σ and the activity coefficient is denoted by γ.

2. To develop the first equilibrium thermodynamic description of microdrop concentrating processes, necessary for design of such processes, by considering limited and unlimited solubility substances as solutes (Chapter 3).[†]

3. To analyze the microdrop concentrating system from the thermodynamic stability point of view and to find the nature of different equilibrium states of the system which determines to which equilibrium state the system will physically converge (Chapter 4).

4. To investigate the effect of curvature of the solid precipitate and the solid–drop interfacial tension on microdrop concentrating processes thermodynamically, including stability analysis when the limited solubility solute precipitates in the drop phase (Chapter 5).

1.5. References

1. Marmur, A. Wetting on Hydrophobic Rough Surfaces: To Be Heterogeneous or Not to Be? *Langmuir* **2003***, 19*, 8343-8348.

2. Milne, A. J. B.; Elliott, J. A. W.; Zabeti, P.; Zhou, J.; Amirfazli, A. Model and Experimental Studies for Contact Angles of Surfactant Solutions on Rough and Smooth Hydrophobic Surfaces. *Phys. Chem. Chem. Phys.* **2011***, 13*, 16208-16219.

3. Sheng, Y.; Jiang, S.; Tsao, H. Effects of Geometrical Characteristics of Surface Roughness on Droplet Wetting. *J. Chem. Phys.* **2007***, 127*, 234704.

4. Bittoun, E.; Marmur, A. The Role of Multiscale Roughness in the Lotus Effect: Is It Essential for Super-Hydrophobicity? *Langmuir* **2012***, 28*, 13933-13942.

5. Marmur, A. Underwater Superhydrophobicity: Theoretical Feasibility. *Langmuir* **2006***, 22*, 1400-1402.

6. Marmur, A. The Lotus Effect: Superhydrophobicity and Metastability. *Langmuir* **2004***, 20*, 3517-3519.

7. Li, W.; Amirfazli, A. Microtextured Superhydrophobic Surfaces: A Thermodynamic Analysis. *Adv. Colloid Interface Sci.* **2007***, 132*, 51-68.

[†] The numerical methods and flowcharts regarding to Chapters 3, 4 and 5 are provided in the Appendix.

8. Kwon, Y.; Patankar, N.; Choi, J.; Lee, J. Design of Surface Hierarchy for Extreme Hydrophobicity. *Langmuir* **2009**, *25*, 6129-6136.

9. Gibbs, J. W. On the Equilibrium of Heterogeneous Substances. *Trans. Conn. Acad. Arts Sci.3* **1876**, 108–248; **1878**, 343–524, in "The Scientific Papers of J. Willard Gibbs," Ox Bow, Woodridge, CT (1993), Vol. I, pp. 55–353.

10. Callen, H. B. *Thermodynamics and an Introduction to Thermostatistics;* Wiley: New York, 1985; pp 36.

11. Hunter, R. J. *Introduction to Modern Colloid Science;* Oxford University Press Inc.: New York, 1993; Vol. 1, pp 344.

12. Ward, C. A.; Johnson, W. R.; Venter, R. D.; Ho, S.; Forest, T. W.; Fraser, W. D. Heterogeneous Bubble Nucleation and Conditions for Growth in a Liquid Gas System of Constant Mass and Volume. *J. Appl. Phys.* **1983**, *54*, 1833-1843.

13. Elliott, J. A. W. On the Complete Kelvin Equation. *Chem. Eng. Educ.* **2001**, *35*, 274-278.

14. McGaughey, A. J. H.; Ward, C. A. Droplet Stability in a Finite System: Consideration of the Solid-Vapor Interface. *J. Appl. Phys.* **2003**, *93*, 3619-3626.

15. Ghasemi, H.; Ward, C. A. Surface Tension of Solids in the Absence of Adsorption. *J. Phys. Chem. B.* **2009**, *113*, 12632-12634.

16. Ward, C. A.; Wu, J. Effect of Adsorption on the Surface Tensions of Solid-Fluid Interfaces. *J. Phys. Chem. B.* **2007**, *111*, 3685-3694.

17. Ghasemi, H.; Ward, C. A. Sessile-Water-Droplet Contact Angle Dependence on Adsorption at the Solid-Liquid Interface. *J. Phys. Chem. C* **2010**, *114*, 5088-5100.

18. Wu, J.; Farouk, T.; Ward, C. A. Pressure Dependence of the Contact Angle. *J. Phys. Chem. B.* **2007**, *111*, 6189-6197.

19. Forest, T. W.; Ward, C. A. Homogeneous Nucleation of Bubbles in Solutions at Pressures Above Vapor-Pressure of Pure Liquid. *J. Chem. Phys.* **1978**, *69*, 2221-2230.

20. Ward, C. A.; Levart, E. Conditions for Stability of Bubble Nuclei in Solid-Surfaces Contacting a Liquid-Gas Solution. *J. Appl. Phys.* **1984**, *56*, 491-500.

21. Ward, C. A.; Tikuisis, P.; Venter, R. D. Stability of Bubbles in a Closed Volume of Liquid-Gas Solution. *J. Appl. Phys.* **1982**, *53*, 6076-6084.

22. Attard, P. Thermodynamic Analysis of Bridging Bubbles and a Quantitative Comparison with the Measured Hydrophobic Attraction. *Langmuir* **2000**, *16*, 4455-4466.

23. Elliott, J. A. W.; Voitcu, O. On the Thermodynamic Stability of Liquid Capillary Bridges. *Can. J. Chem. Eng.* **2007**, *85*, 692-700.

24. Zargarzadeh, L.; Elliott, J. A. W. Comparative Surface Thermodynamic Analysis of New Fluid Phase Formation between a Sphere and a Flat Plate. *Langmuir* **2013***, 29*, 3610-3627.

25. Zargarzadeh, L.; Elliott, J. A. W. Surface Thermodynamic Analysis of Fluid Confined in a Cone and Comparison with the Sphere-Plate and Plate-Plate Geometries. *Langmuir* **2013***, 29*, 12950-12958.

26. Reiss, H.; Koper, G. The Kelvin Relation - Stability, Fluctuation, and Factors Involved in Measurement. *J. Phys. Chem.* **1995***, 99*, 7837-7844.

27. Fisher, L. R.; Israelachvili, J. N. Experimental Studies on the Applicability of the Kelvin Equation to Highly Curved Concave Menisci. *J. Colloid Interface Sci.* **1981***, 80*, 528-541.

28. Sajadinia, S. H.; Sharif, F. Thermodynamic Analysis of the Wetting Behavior of Dual Scale Patterned Hydrophobic Surfaces. *J. Colloid Interface Sci.* **2010***, 344*, 575-583.

29. Li, W.; Amirfazli, A. A Thermodynamic Approach for Determining the Contact Angle Hysteresis for Superhydrophobic Surfaces. *J. Colloid Interface Sci.* **2005***, 292*, 195-201.

30. Zhang, H.; Li, W.; Cui, D.; Hu, Z.; Xu, L. Design of Lotus-Simulating Surfaces: Thermodynamic Analysis Based on a New Methodology. *Colloid Surface A.* **2012***, 413*, 314-327.

31. Long, J.; Hyder, M. N.; Huang, R. Y. M.; Chen, P. Thermodynamic Modeling of Contact Angles on Rough, Heterogeneous Surfaces. *Adv. Colloid Interface Sci.* **2005***, 118*, 173-190.

32. Wenzel, R. Resistance of Solid Surfaces to Wetting by Water. *Ind. Eng. Chem.* **1936***, 28*, 988-994.

33. Cassie, A.; Baxter, S. Wettability of Porous Surfaces. *T. Faraday Soc.* **1944***, 40*, 0546-0550.

34. Extrand, C. W.; Kumagai, Y. Contact Angles and Hysteresis on Soft Surfaces. *J. Colloid Interface Sci.* **1996***, 184*, 191-200.

35. Pericet-Camara, R.; Auernhammer, G. K.; Koynov, K.; Lorenzoni, S.; Raiteri, R.; Bonaccurso, E. Solid-Supported Thin Elastomer Films Deformed by Microdrops. *Soft Matter* **2009***, 5*, 3611-3617.

36. Pericet-Camara, R.; Best, A.; Butt, H.; Bonaccurso, E. Effect of Capillary Pressure and Surface Tension on the Deformation of Elastic Surfaces by Sessile Liquid Microdrops: An Experimental Investigation. *Langmuir* **2008***, 24*, 10565-10568.

37. Carre, A.; Gastel, J. C.; Shanahan, M. E. R. Viscoelastic Effects in The Spreading of Liquids. *Nature* **1996***, 379*, 432-434.

38. Jerison, E. R.; Xu, Y.; Wilen, L. A.; Dufresne, E. R. Deformation of an Elastic Substrate by a Three-Phase Contact Line. *Phys. Rev. Lett.* **2011***, 106*, 186103.

39. Lester, G. R. Contact Angles of Liquids at Deformable Solid Surfaces. *J. Colloid Sci.* **1961***, 16*, 315-&.

40. Rusanov, A. I. Theory of Wetting of Elastically Deformed Bodies .1. Deformation with a Finite Contact-Angle. *Colloid J. Ussr+* **1975***, 37*, 614-622.

41. Shanahan, M. E. R.; de Genns, P. G. In *Adhesion 11;* Allen, K. W., Ed.; Elsevier Applied Science Publ: London, 1987; Vol. 11, pp 71-81.

42. Shanahan, M. E. R. The Spreading Dynamics of a Liquid-Drop on a Viscoelastic Solid. *J. Phys. D. Appl. Phys.* **1988***, 21*, 981-985.

43. Shanahan, M. E. R.; Carre, A. Spreading and Dynamics of Liquid Drops Involving Nanometric Deformations on Soft Substrates. *Colloid Surf. A.* **2002***, 206*, 115-123.

44. White, L. R. The Contact Angle on an Elastic Substrate. 1. The Role of Disjoining Pressure in the Surface Mechanics. *J. Colloid Interface Sci.* **2003***, 258*, 82-96.

45. Yu, Y.; Zhao, Y. Elastic Deformation of Soft Membrane with Finite Thickness Induced by a Sessile Liquid Droplet. *J. Colloid Interface Sci.* **2009***, 339*, 489-494.

46. Kern, R.; Muller, P. Deformation of an Elastic Thin Solid Induced by a Liquid Droplet. *Surf Sci.* **1992***, 264*, 467-494.

47. Yu, Y.; Yang, Z.; Zhao, Y. Role of Vertical Component of Surface Tension of the Droplet on the Elastic Deformation of PDMS Membrane. *J. Adhes. Sci. Technol.* **2008***, 22*, 687-698.

48. Style, R. W.; Dufresne, E. R. Static Wetting on Deformable Substrates, from Liquids to Soft Solids. *Soft Matter* **2012***, 8*, 7177-7184.

49. Shanahan, M. E. R. The Influence of Solid Micro-Deformation on Contact-Angle Equilibrium. *J. Phys. D. Appl. Phys.* **1987***, 20*, 945-950.

50. Olives, J. Surface Thermodynamics, Surface Stress, Equations at Surfaces and Triple Lines for Deformable Bodies. *J. Phys. Condens. Mat.* **2010***, 22*, 085005.

51. Olives, J. Green's Formula and Singularity at a Triple Contact Line. Example of Finite-Displacement Solution. *Int. J. Solids Struc.* **2014***, 51*, 314-324.

52. Style, R. W.; Boltyanskiy, R.; Che, Y.; Wettlaufer, J. S.; Wilen, L. A.; Dufresne, E. R. Universal Deformation of Soft Substrates Near a Contact Line and the Direct Measurement of Solid Surface Stresses. *Phys. Rev. Lett.* **2013***, 110*, 066103.

53. Squires, T. M. Drops on Soft Surfaces Learn the Hard Way. *P. Natl. Acad. Sci. USA.* **2013***, 110*, 12505-12506.

54. Style, R. W.; Che, Y.; Park, S. J.; Weon, B. M.; Je, J. H.; Hyland, C.; German, G. K.; Power, M. P.; Wilen, L. A.; Wettlaufer, J. S.; Dufresne, E. R. Patterning Droplets with Durotaxis. *P. Natl. Acad. Sci. USA.* **2013**, *110*, 12541-12544.

55. Sokuler, M.; Auernhammer, G. K.; Roth, M.; Liu, C.; Bonaccurso, E.; Butt, H. The Softer the Better: Fast Condensation on Soft Surfaces. *Langmuir* **2010**, *26*, 1544-1547.

56. Bremond, N.; Bibette, J. Exploring Emulsion Science with Microfluidics. *Soft Matter* **2012**, *8*, 10549-10559.

57. Chiu, D. T.; Lorenz, R. M.; Jeffries, G. D. M. Droplets for Ultrasmall-Volume Analysis. *Anal. Chem.* **2009**, *81*, 5111-5118.

58. Huebner, A.; Sharma, S.; Srisa-Art, M.; Hollfelder, F.; Edel, J. B.; deMello, A. J. Microdroplets: A Sea of Applications? *Lab Chip* **2008**, *8*, 1244-1254.

59. Kuo, J. S.; Chiu, D. T. Controlling mass Transport in Microfluidic Devices. *Annu. Rev. Anal. Chem.* **2011**, *4*, 275-296.

60. He, M.; Sun, C.; Chiu, D. T. Concentrating Solutes and Nanoparticles within Individual Aqueous Microdroplets. *Anal. Chem.* **2004**, *76*, 1222-1227.

61. Shim, J.; Cristobal, G.; Link, D. R.; Thorsen, T.; Jia, Y.; Piattelli, K.; Fraden, S. Control and Measurement of the Phase Behavior of Aqueous Solutions using Microfluidics. *J. Am. Chem. Soc.* **2007**, *129*, 8825-8835.

62. Ji, J.; Nie, L.; Li, Y.; Yang, P.; Liu, B. Simultaneous Online Enrichment and Identification of Trace Species Based on Microfluidic Droplets. *Anal. Chem.* **2013**, *85*, 9617-9622.

63. Bajpayee, A.; Edd, J. F.; Chang, A.; Toner, M. Concentration of Glycerol in Aqueous Microdroplets by Selective Removal of Water. *Anal. Chem.* **2010**, *82*, 1288-1291.

64. Kojima, T.; Takayama, S. Microscale Determination of Aqueous Two Phase System Binodals by Droplet Dehydration in Oil. *Anal. Chem.* **2013**, *85*, 5213-5218.

65. Wang, B.; Shum, H. C.; Weitz, D. A. Fabrication of Monodisperse Toroidal Particles by Polymer Solidification in Microfluidics. *Chemphyschem* **2009**, *10*, 641-645.

66. Wu, T.; Hirata, K.; Suzuki, H.; Xiang, R.; Tang, Z.; Yomo, T. Shrunk to Femtolitre: Tuning High-Throughput Monodisperse Water-In-Oil Droplet Arrays for Ultra-Small Micro-Reactors. *Appl. Phys. Lett.* **2012**, *101*, 074108.

67. Bajpayee, A.; Luo, T.; Muto, A.; Chen, G. Very Low Temperature Membrane-Free Desalination by Directional Solvent Extraction. *Energy Environ. Sci.* **2011**, *4*, 1672-1675.

68. Jeffries, G. D. M.; Kuo, J. S.; Chiu, D. T. Dynamic Modulation of Chemical Concentration in an Aqueous Droplet. *Angew. Chem. Int. Ed.* **2007**, *46*, 1326-1328.

69. Jeffries, G. D. M.; Kuo, J. S.; Chiu, D. T. Controlled Shrinkage and Re-Expansion of a Single Aqueous Droplet inside an Optical Vortex Trap. *J. Phys. Chem. B.* **2007***, 111*, 2806-2812.

70. Shen, A. Q.; Wang, D.; Spicer, P. T. Kinetics of Colloidal Templating Using Emulsion Drop Consolidation. *Langmuir* **2007***, 23*, 12821-12826.

Chapter 2: Thermodynamic Investigation of the Barrier for Heterogeneous Nucleation on a Fluid Surface in Comparison with a Rigid Surface

2.1. Nomenclature

S	Entropy	*Subscripts*	
U	Internal energy	U	Upper
T	Temperature	L	Lower
P	Pressure	c	Critical
V	Volume	∞	Saturation
μ_i	Chemical potential of component i	0	Reference state
γ	Surface tension	*Superscripts*	
N_i	Number of moles of component i	L	Liquid
A	Area	V	Vapor
R	Radius	S	Solid
φ	Dummy variable of integration	SL	Solid–liquid
θ	Contact angle on a rigid surface	SV	Solid–vapor

β	Contact angle on a fluid surface	LV	Liquid–vapor
α	Deformation angle	R	Reservoir
$\bar{R}$	Universal gas constant	L'	Fluid substrate
G	Gibbs free energy	LL'	Liquid–fluid substrate
F	Helmholtz free energy	$L'V$	Fluid substrate–vapor
B	Free energy given by equation 2-20	eq	Equilibrium
		w	Water
		d	Dodecane

2.2. Introduction

Nucleation is one of the processes accompanying first-order phase transitions.[1] Formation of a bubble in a liquid phase, or a drop in a vapor phase, is an example of homogeneous nucleation. Heterogeneous nucleation, the topic of interest in this chapter, takes place in the case of the presence of a third phase (usually solid), which provides sites for nucleation. Heterogeneous nucleation can be important[2] in heat transfer[3] and vapor deposition.[4] Nucleation on soft surfaces is important since many natural and technological substances such as tissues and polymers are soft materials. In addition, at very small scales such as nanometers, many of the substances that seem to be rigid act like soft matter, as interfacial forces overcome the strength of the small amount of material.
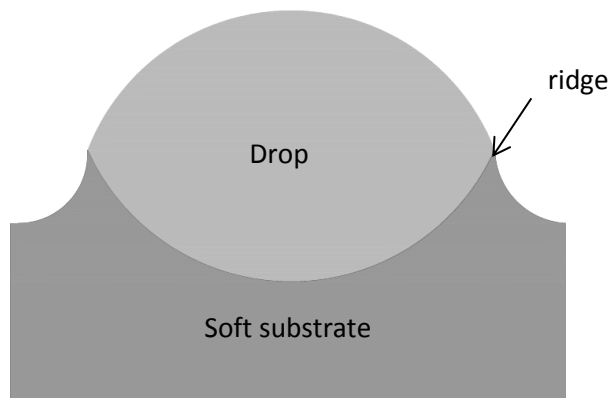
Figure 2-1 Schematic of a sessile drop on a soft substrate and ridge formation around the contact line. Adopted from reference [2]

Due to the importance of nucleation of a sessile drop on soft surfaces, several works have been done in this area. However, most researchers treat the soft surface as an elastic solid. The sessile drop deforms a soft surface, the deformation being the result of the vertical component of surface tension around the contact line, which pulls the solid upward, and also the Laplace pressure inside the drop, which pushes the solid downward.[5] Several mathematical functions describing the surface deformation have been proposed.[6-9] There are two approaches to find the equilibrium shape of a soft surface on which a liquid droplet rests. One approach is a mechanical approach via force balances and the other one is a thermodynamic approach through minimization of free energy. Shanahan[10] is one of the researchers that applied the minimization of free energy to explore the nucleation of a drop on a soft surface. He considered interfacial free energy and the elastic energy of deformation in the free energy and, by imposing constant volume as a constraint and applying the calculus of variations, minimized the free energy. He found a modification for the Young equation for the mesoscopic scale and attributed the contact angle change with drop size to the role of Laplace pressure at the mesoscopic scale rather than line tension.

Lester[6] and Rusanov[7] considered a semi-infinite surface for nucleation of a drop and by means of stress analysis found the deformation profile for the surface. However, in order to avoid infinite stress at the triple line, they had to consider a thickness (t) for the liquid–vapor interface. Lester concluded that the Young equation is not applicable unless deformation of the surface does not happen.

On the other hand, Shanahan and de Gennes[11] performed stress analysis and found a logarithmic deformation profile. They pointed out that in the vicinity of the triple line, linear elasticity is invalid since the radial stress will go to infinity. Therefore, they considered a small distance (ε) around the triple line in which linear elasticity is not applicable, and instead plastic or other nonlinear elasticity governs that area. Alternatively, White[12] believes that the reason for which these unclear length scales such as t and ε are brought into the calculations is the absence of intersurface forces at the microscopic scale. He considered the transmission force of the surface tension to the substrate by introducing the effect of disjoining pressure to his calculations and proposed profiles for the drop and substrate in integral forms.

In addition to semi-infinite soft surfaces, some researchers investigated the deformation of thin elastic surfaces[13] such as thin plates[14] and membranes[8] under the presence of a sessile drop. It was found that the deformation profile for the sessile drop on the thin plates has a pseudoparabolic[9] shape, but for membranes the ridge will still appear around the triple line. Yu and Zhao[8] studied the effect of the thickness of the membrane on its deformation shape. They figured out that each membrane has a "saturated thickness". If its thickness is thicker than that, it can be considered as a semi-infinite body; otherwise thickness has an important effect on the deformation of the solid induced by a water droplet. Besides these various deformation profiles

for substrates, there exist controversial discussions about the contact angle of sessile drops on soft surfaces.

In addition to these theoretical works on the nucleation of a drop on a soft surface, several experimental investigations have been done. For example the presence of the ridge around the triple line was observed by means of scanning white light interferometric microscopy by Carre *et al.*[15] They found a good conformity between their observations and their estimation for its height. Based on their estimation, ridge height is proportional to the vertical component of surface tension and inversely proportional to the shear modulus of the substrate (G).

Sokuler *et al.*[2] performed experiments and recognized that nucleation happens more easily on soft surfaces compared to rigid ones. They manufactured a soft surface and observed that on the softer surfaces the nucleation density is higher. They suggested that this phenomenon can be attributed to a lower barrier for nucleation, which originates from the lower free energy in the case of soft surfaces. They mention that, although for soft surfaces the system has an extra energy of elasticity and the interfacial energy of the liquid–solid interface is larger due to its higher area, the smaller liquid–vapor interfacial area due to the presence of the ridge overcompensates these energies, and the system faces a lower free energy and hence the lower barrier. They also concluded that, for softer surface, coalescence of nucleates is delayed. Since the ridge height is inversely proportional to G, the higher the ridge, the later the nucleates merge, hence liquid covers a larger area on softer solids.

On the whole, Sokuler *et al.*[2] performed experiments and submitted a physical argument without any kind of mathematical derivation that nucleation happens easier on soft surfaces. Therefore, one of the goals of this chapter is to prove this phenomenon theoretically by means of

detailed surface thermodynamics. As we have discussed, the elasticity of the solid introduces

several complexities in calculations. For example some of the consequences of the elastic solid

are: *i*) no explicit solid deformation profile, *ii*) care should be taken in how contact angle is

defined and *iii*) the presence of unclear length scales such as capillary layer thickness in the

calculations. Here we plan to answer the question of whether nucleation is easier on a rigid

surface or a soft surface. However, due to the difficulties of considering soft-elastic surfaces, we

demonstrate that by considering only the fluidity of a surface (*i.e.*, by considering a fluid surface

as an infinitely soft material and comparing a fluid surface with a rigid surface), thermodynamics

will predict that nucleation is easier on soft surfaces.

Hence, we investigate the thermodynamic stability of a sessile drop on either a rigid surface or

a fluid surface at constant vapor phase pressure and compare their energy barriers. We note that

several works have been done before on homogeneous and heterogeneous nucleation. Of

particular relevance, Nepomnyashchy *et al.*[16] compared the free energy barrier of homogeneous

nucleation and heterogeneous nucleation at a liquid–gas interface and showed that

heterogeneous nucleation of a drop at a liquid–gas interface is more favorable than homogeneous

nucleation of a drop in the vapor phase; Forest[17] and Ward investigated the nucleation of a

bubble in liquid–gas solutions both homogeneously and at the liquid–liquid interface, showing

that the surface and interfacial tensions must meet a specific criterion for the bubble to form

heterogeneously; and Jarvis *et al.*[18] showed that a liquid lens can exist at the interface if specific

criteria are met for the magnitudes of surface and interfacial tensions (see Chapter 2 Appendix

for details). However, to the best of our knowledge, the comparison of heterogeneous nucleation

on a rigid surface with that on a fluid surface has not been done previously. In this regard, we

have chosen the surface tensions and interfacial tension such that the criteria for heterogeneous

nucleation are met (see the Chapter 2 Appendix for detailed discussion on the conditions imposed on surface and interfacial tensions), and we assume that either the liquid lens or the sessile drop forms at the interface rather than homogeneously so that we can compare the heterogeneous nucleation on the rigid surface with that on the fluid surface.

There has been other research performed in the field of surface thermodynamic stability analysis of systems with curved surfaces. However, most of these works pertain to systems with finite size[19-23] or capillary bridges systems.[24,25] Depending on the constraints and the conditions of the system, different free energies and stabilities are found for these systems.

2.3. Governing Equations

In order to determine the stability of equilibrium states, the second derivative of free energy with respect to size of the drop or bubble should be explored at the equilibrium radii, R_c. If the second derivative is negative, R_c represents an unstable equilibrium. If the second derivative is positive, R_c represents a stable equilibrium. Metastable equilibria are located at local minima in the free energy function. As a result, if a drop forms spontaneously in a vapor phase with a radius larger than the unstable size, it will grow larger. On the other hand, if a drop forms spontaneously with a radius smaller than the unstable size, the drop will evaporate. But if the drop radius is in stable equilibrium, the drop is unaffected by small perturbations (larger or smaller), after which it will return to the stable size. Generally, to perform the stability analysis the following procedure is followed:

i) derivation of conditions for equilibrium, *ii*) combining conditions for equilibrium with equations of state to find the equation for the equilibrium radius, *iii*) determining what function

acts as the thermodynamic potential (or free energy), and *iv*) use of free energy to determine the number and stability of equilibrium states.

Herein, we perform these procedures first for the nucleation of a sessile drop on a rigid surface and then repeat it for nucleation on a fluid surface. Throughout, we neglect the effects of gravity due to the small size of the drops.

2.3.1. Nucleation of a Sessile Drop on a Rigid Surface:

Figure 2-1*a* shows a sessile drop with radius R and contact angle θ on a rigid solid. The liquid phase and the vapor phase consist of component 1 and the solid phase consists of component 2. The surroundings, or "reservoir", including the container, are considered to be another phase with constant pressure and temperature (P^R and T^R as shown in Figure 2-1). The reservoir can exchange energy and volume with the system through the walls of the system and movable piston. The system is closed and cannot exchange mass with the reservoir. The nature of interactions between system and reservoir dictate the constraints for the composite system.

We know that at equilibrium, the entropy (S) of the system plus the reservoir together will be an extremum, so we require

$$dS^L + dS^V + dS^S + dS^{LV} + dS^{SL} + dS^{SV} + dS^R = 0 \tag{2-1}$$

In equation (2-1), superscripts R, L, V, S, SL, LV, and SV represent the reservoir, liquid, vapor, solid, solid–liquid, liquid–vapor and solid–vapor phases respectively.

For a bulk phase, a flat interface, or a curved interface, the differential form of the fundamental equation of thermodynamics is given by equations (2-2), (2-3), or (2-4), respectively, which

relate changes in the volume, V, the area, A, and the thermodynamic properties temperature, T, pressure, P, and chemical potential, μ, to changes in the internal energy, U.

$$dU^i = T^i dS^i - P^i dV^i + \sum_{j=1}^{r} \mu_j^i dN_j^i \tag{2-2}$$

$$dU^{ab} = T^{ab} dS^{ab} + \gamma^{ab} dA^{ab} + \sum_{j=2}^{r} \mu_j^{ab} dN_j^{ab} \tag{2-3}$$

$$dU^{ab} = T^{ab} dS^{ab} + \gamma^{ab} dA^{ab} + \sum_{j=1}^{r} \mu_j^{ab} dN_j^{ab} \tag{2-4}$$

where superscript i denotes each bulk phase, i.e., liquid, vapor or solid, N_j is the number of moles of component j in phase i, γ is surface tension and the superscript "ab" identifies the interface subsystems, i.e., SL, LV, or SV. The constraints that are imposed on the system are described below:

i) The system and reservoir together are isolated:

$$dU^V = -dU^L - dU^S - dU^{LV} - dU^{SL} - dU^{SV} - dU^R \tag{2-5}$$

ii) The system is closed, so that there is no mass exchange between the system and reservoir:

$$dN_1^V = -dN_1^L - dN_1^{LV} - dN_1^{SL} - dN_1^{SV} \tag{2-6}$$

$$dN_1^R = 0 \qquad dN_2^R = 0 \tag{2-7}$$

iii) A moveable piston separates the system from the reservoir:

$$dV^V = -dV^L - dV^S - dV^R \tag{2-8}$$

iv) The solid is non-volatile and incompressible:

$$dN_2^S = 0 \qquad dV^S = 0 \tag{2-9}$$
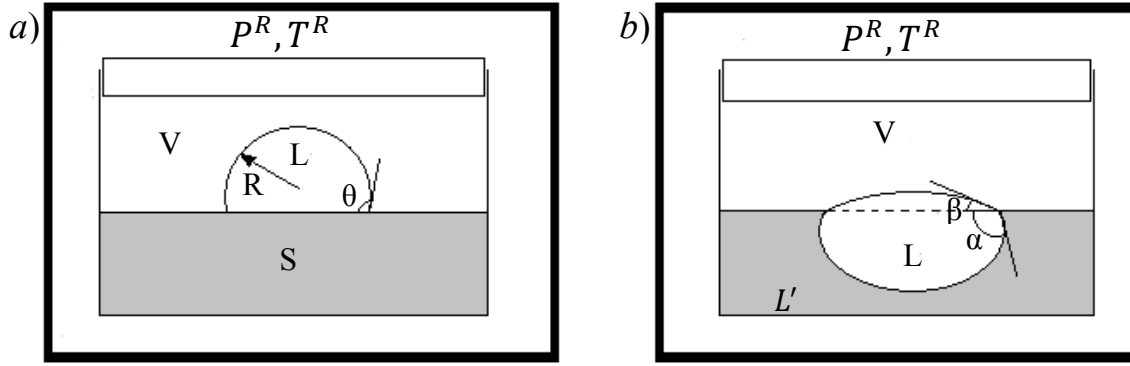
Figure 2-2 Geometry for (*a*) nucleation on a rigid surface, and (*b*) nucleation on a fluid surface

In addition, based on the "Gibbs' dividing surface" approach, the excess surface quantity for N_2 is taken to be zero for the flat interfaces SV and SL; therefore $N_2^{SL} = 0$ and $N_2^{SV} = 0$.

As a consequence of the existence of derivatives of bulk volumes and interfacial areas in relations (2-2) to (2-4), the geometry of the system must be specified. The drop volume and areas for the LV and SL interfaces are given by the following relations:[22]

$$V^L = \int_0^\theta \pi R^3 sin^3\varphi \, d\varphi = \frac{\pi R^3}{3}[2 - \cos\theta(2 + sin^2\theta)] \tag{2-10}$$

$$A^{LV} = \int_0^\theta 2\pi R^2 \sin\varphi \, d\varphi = 2\pi R^2(1 - \cos\theta) \tag{2-11}$$

$$A^{SL} = \pi R^2 sin^2\theta \tag{2-12}$$

In order to find the derivatives, the volume and areas should be differentiated with respect to both θ and R. Substituting equations of the form (2-2) for the bulk phases (liquid, vapor, solid, and reservoir), equations of the form (2-3) for the flat interfaces SV and SL, an equation of the form (2-4) for the curved LV interface, the constraints (2-5) to (2-9) and derivatives of the geometry relations (2-10) to (2-12) into equation (2-1) and collecting like terms we find:

$$\left(\frac{1}{T^L}-\frac{1}{T^V}\right)dU^L+\left(\frac{P^R}{T^R}-\frac{P^V}{T^V}\right)dV^R-\left(\frac{\mu_1^L}{T^L}-\frac{\mu_1^V}{T^V}\right)dN_1^L+\left(\frac{1}{T^S}-\frac{1}{T^V}\right)dU^S$$

$$+\left(\frac{1}{T^{LV}}-\frac{1}{T^V}\right)dU^{LV}-\left(\frac{\mu_1^{LV}}{T^{LV}}-\frac{\mu_1^V}{T^V}\right)dN_1^{LV}+\left(\frac{1}{T^{SL}}-\frac{1}{T^V}\right)dU^{SL}-\left(\frac{\mu_1^{SL}}{T^{SL}}-\frac{\mu_1^V}{T^V}\right)dN_1^{SL}$$

$$+\left(\frac{1}{T^{SV}}-\frac{1}{T^V}\right)dU^{SV}-\left(\frac{\mu_1^{SV}}{T^{SV}}-\frac{\mu_1^V}{T^V}\right)dN_1^{SV}+\left(\frac{1}{T^R}-\frac{1}{T^V}\right)dU^R$$

$$+\left[\left(\frac{P^L}{T^L}-\frac{P^V}{T^V}\right)\left(2-\cos\theta\left(2+\sin^2\theta\right)\right)\pi R^2-\frac{\gamma^{LV}}{T^{LV}}(1-\cos\theta)4\pi R+\frac{(\gamma^{SV}-\gamma^{SL})}{T^{SL}}\left(2\pi R\sin^2\theta\right)\right]dR$$

$$+\left[\left(\frac{P^L}{T^L}-\frac{P^V}{T^V}\right)\left(\sin\theta\left(2+\sin^2\theta\right)-2\sin\theta\cos^2\theta\right)\frac{\pi R^3}{3}-\frac{\gamma^{LV}}{T^{LV}}2\pi R^2\sin\theta+\frac{(\gamma^{SV}-\gamma^{SL})}{T^{SL}}2\pi R^2\sin\theta\cos\theta\right]d\theta$$

$$=0 \qquad\qquad (2\text{-}13)$$

In order for the above expression to be valid for any arbitrary displacement about equilibrium, the coefficient of each independent variation may be set equal to zero. Consequently, the conditions for equilibrium are found to be as follows:

$$T^L=T^{LV}=T^{SL}=T^V=T^{SV}=T^S=T^R \qquad\qquad (2\text{-}14)$$

$$\mu_1^V=\mu_1^{LV}=\mu_1^{SV}=\mu_1^L=\mu_1^{SL} \qquad\qquad (2\text{-}15)$$

$$P^V=P^R \qquad\qquad (2\text{-}16)$$

$$P^L-P^V=\frac{2\gamma^{LV}}{R_c} \qquad\qquad (2\text{-}17)$$

$$\gamma^{SV}-\gamma^{SL}=\gamma^{LV}\cos\theta \qquad\qquad (2\text{-}18)$$

Equations (2-17) and (2-18) are the Laplace equation and Young equation, respectively, which come out of the derivation as conditions for equilibrium.

Considering the ideal gas for the vapor phase and incompressible fluid for the liquid phase, we will have:

$$\mu^V(T, P^V) = \mu^V(T, P_\infty) + \bar{R}T \ln\left(\frac{P^V}{P_\infty}\right) \tag{2-19}$$

$$\mu^L(T, P^L) = \mu^L(T, P_\infty) + v_\infty^L(P^L - P_\infty) \tag{2-20}$$

After combining conditions for equilibrium with equations of state (2-19) and (2-20), the following relation for equilibrium radii will be found:[26]

$$R_c = \frac{2\gamma^{LV}}{\left[\frac{\bar{R}T}{v_\infty^L}\ln\left(\frac{P^V}{P_\infty}\right) + P_\infty - P^V\right]} \tag{2-21}$$

In equation (2-21), P_∞, v_∞^L and $\bar{R}$ represent the saturation pressure, liquid molar volume at the saturation pressure, and the universal gas constant, respectively. Equation (2-21) is equivalent to what is commonly referred to as the Kelvin equation, which differs from the original Kelvin equation since it was corrected by Gibbs to be thermodynamically consistent.[27,28]

After performing the calculations[28,29] that determine which function acts as the free energy for this system, the following free energy,[25,29] B, is found:

$$\Delta B = \Delta(G^V + F^L + F^S + F^{SL} + F^{LV} + F^{SV} + P^V V^L) \leq 0 \tag{2-22}$$

where G is the Gibbs free energy and F is the Helmholtz free energy. B is a combination of Gibbs free energy for the vapour phase—due to the constant vapor phase pressure—and Helmholtz free energy for other subsystems except for the liquid phase. In the case of liquid phase, since neither the pressure nor the volume are constant the extra term of $P^V V^L$ appears in the free energy.

Since the energy should be computed with respect to a reference point, for convenience we choose the system of the solid and vapor phase without any drop in it to be a reference state; thus the potential function for the reference state is equal to:

$$B_0 = \mu_{10}^V N_{10}^V + \mu_{10}^{SV} N_{10}^{SV} + \gamma^{SV} A_0^{SV} + \mu_{20}^S N_{20}^S - P^S V^S \qquad (2\text{-}23)$$

Given that the total moles and container cross sectional area will not change from that of the reference state, and by assuming the reference state to be an equilibrium state, we will have:

$$B(R) - B_0 = N_1^V\left(\mu_1^V - \mu_1^{eq}\right) + N_1^L\left(\mu_1^L - \mu_1^{eq}\right) + N_1^{LV}\left(\mu_1^{LV} - \mu_1^{eq}\right) + N_1^{SV}\left(\mu_1^{SV} - \mu_1^{eq}\right)$$

$$+ N_1^{SL}\left(\mu_1^{SL} - \mu_1^{eq}\right) + N_2^S\left(\mu_2^S - \mu_2^{eq}\right) + (\gamma^{SL} - \gamma^{SV})A^{SL} + \gamma^{LV} A^{LV} + (P^V - P^L)V^L$$

$$(2\text{-}24)$$

Since equilibrium states are going to be investigated, the value of $B(R)$–B_0 in the limit of equilibrium is equal to:[25]

$$B(R) - B_0 = (\gamma^{SL} - \gamma^{SV})A^{SL} + \gamma^{LV} A^{LV} + (P^V - P^L)V^L \qquad (2\text{-}25)$$

We note that the above approach implicitly assumes that the values of the intensive parameters at equilibrium are the same as those of the hypothetical reference equilibrium state. Such a reference state need not physically exist.

2.3.2. Nucleation of a Sessile Drop on a Fluid Surface:

Figure 2-1b shows a sessile drop of one liquid, L, on another liquid, L', with contact angle β and deformation angle α surrounded by a reservoir at constant pressure, P^R, and constant temperature, T^R. Here, the L and V phases consist of component 1, and the L' phase consists of

component 2. We repeat the same procedure as for the nucleation on a rigid surface. The constraints are the same as for the rigid surface except for that, in the nucleation on a fluid surface, only the $L'V$ interface is flat, so based on the "Gibbs dividing surface" approach

$$N_2^{L'V} = 0 \tag{2-26}$$

Therefore, the conservation of moles for component 2 becomes

$$dN_2^{L'} = -dN_2^{LL'} \tag{2-27}$$

In addition, in this case, the constraint $dV^{L'} = 0$ is not imposed.

The drop volume and interfacial areas in this case are given by the relations for liquid lenses:[16]

$$V^L = \int_0^\beta \pi R_U^3 \sin^3\varphi \, d\varphi + \int_0^\alpha \pi R_L^3 \sin^3\varphi \, d\varphi$$

$$= \frac{\pi R_U^3}{3}[2 - \cos\beta(2 + \sin^2\beta)] + \frac{\pi R_L^3}{3}[2 - \cos\alpha(2 + \sin^2\alpha)] \tag{2-28}$$

$$A^{LV} = \int_0^\beta 2\pi R_U^2 \sin\varphi \, d\varphi = 2\pi R_U^2(1 - \cos\beta) \tag{2-29}$$

$$A^{LL'} = \int_0^\alpha 2\pi R_L^2 \sin\varphi \, d\varphi = 2\pi R_L^2(1 - \cos\alpha) \tag{2-30}$$

$$A^{L'V} = A_0^{L'V} - \pi R_U^2 \sin^2\beta = A_0^{L'V} - \pi R_L{}^2 \sin^2\alpha \tag{2-31}$$

In equation (2-31), $A_0^{L'V}$ is the initial $L'V$ interfacial area, before the liquid lens has formed. In addition, the following equation relates the geometrical variables:

$$R_U \sin\beta = R_L \sin\alpha \tag{2-32}$$

where R_U is the radius of curvature of the upper curved interface, LV, and R_L is the radius of curvature of the lower curved interface, LL'.

In order to find the derivatives of volume and areas, they should be differentiated with respect to three independent variables, which are any three variables out of R_U, R_L, α, and β.

Following a similar procedure to that used for nucleation on a rigid surface, the equilibrium conditions for a sessile drop on a fluid interface are found to be

$$T^L = T^{LV} = T^{LL'} = T^V = T^{L'V} = T^{L'} = T^R \tag{2-33}$$

$$\mu_1^V = \mu_1^{LV} = \mu_1^{L'V} = \mu_1^L = \mu_1^{LL'} \tag{2-34}$$

$$\mu_2^{L'} = \mu_2^{LL'} \tag{2-35}$$

$$P^V = P^R \tag{2-36}$$

$$P^V = P^{L'} \tag{2-37}$$

$$(P^L - P^V) = (P^L - P^{L'}) = \frac{2\gamma^{LL'}}{R_{Uc}(\frac{\sin\beta}{\sin\alpha})} = \frac{2\gamma^{LL'}}{R_{Lc}} \tag{2-38}$$

$$(P^L - P^V) = \frac{2\gamma^{LV}}{R_{Uc}} \tag{2-39}$$

$$\gamma^{LV}\cos\beta + \gamma^{LL'}\cos\alpha = \gamma^{L'V} \tag{2-40}$$

$$\gamma^{LV}\sin\beta = \gamma^{LL'}\sin\alpha \tag{2-41}$$

Equations (2-38) and (2-39) are the Laplace equations for the LL' and LV interfaces, respectively and equations (2-40) and (2-41) are the force balance of interfacial tensions at the

three phase contact line, in the horizontal and vertical directions; so they can be called Young equations. R_{Uc} and R_{Lc} in equations (2-38) and (2-39) are the equilibrium radii of upper curvature and lower curvature, respectively. The same free energy B is found for the fluid case as in the rigid case, but due to the differences in geometry, $B(R)–B_0$ is found to be:[16]

$$B(R) - B_0 = \gamma^{LL'}A^{LL'} + \gamma^{LV}A^{LV} - \gamma^{L'V}\pi R_U^2 sin^2\beta + (P^V - P^L)V^L \qquad (2\text{-}42)$$

2.4. Results and Discussion

2.4.1. Effect of Contact Angle on the Energy Barrier for Heterogeneous Nucleation on a Rigid Surface

First, we investigate the effect of contact angle of a drop on a rigid surface. We consider drops of water that are nucleated from their vapor at constant vapor phase pressure heterogeneously and on rigid solids on which they experience different equilibrium contact angles. By specifying the contact angles, we are considering different surfaces with different inherent surface tensions and adsorptive states that correspond to the chosen contact angle at the equilibrium state.

Figure 2-2 shows the potential function $B(R)–B_0$ versus the drop radius R for different contact angles for a drop of water on a rigid surface at $T = 22$ °C and $P^V = 2700$ Pa. The obtained equilibrium radius and liquid pressure are $R_c = 4.9072 \times 10^{-8}$ m and $P^L = 2.9547 \times 10^6$ Pa. From the extrema in Figure 2-2, an unstable equilibrium state is seen in the system. Thus, if a spontaneously formed drop has a radius smaller than the unstable equilibrium radius (the maxima in Figure 2-2) it will evaporate, but if its radius is larger than the equilibrium radius, the drop will grow larger, and since there is not any stable drop size in this case, the drop will grow until all the vapor has condensed. Figure 2-2 shows that as contact angle is increased, drop nucleation becomes harder since the barrier for nucleation becomes larger.
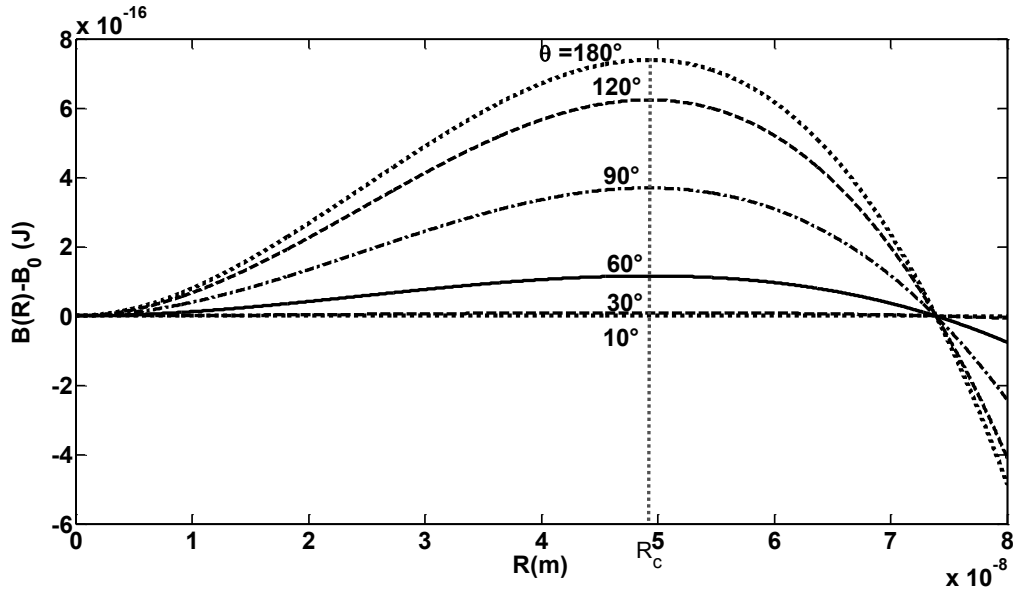
Figure 2-3 Free energy $B(R)-B_0$ versus the radius of the water drop on a rigid surface for different contact angles where T=22 °C, P^V=2700 Pa, and $\gamma^{LV} = \gamma^W$ =72.43 mN/m

2.4.2. Comparison of the Barrier for Heterogeneous Nucleation on a Rigid Surface with That for a Fluid Surface

In order to compare the energy barrier for heterogeneous nucleation on a rigid surface with that for a fluid surface, we choose two systems. In one case, we have a container of dodecane, and a drop of water from its vapor is nucleated on it at constant vapor phase pressure (Figure 2-1b). In the second case, we have a rigid solid with the same solid–liquid interfacial tension as dodecane–liquid water and the same solid–vapor surface tension as dodecane–water vapor, and then we nucleate a drop of water from its vapor phase on it (Figure 2-1a).

Therefore, by supposing fluids L and L' to be water and dodecane, at $T = 22$ °C the surface tension of dodecane–water vapor,[30] $\gamma^{L'V} = \gamma^d$, and water–dodecane[30], $\gamma^{LL'} = \gamma^{wd}$, can be taken to be 25.3 mN/m and 53.7 mN/m, respectively. Other properties are taken to be $\gamma^{LV} = \gamma^W =$ 72.43 mN/m and $P^V = 2700$ Pa. Since we have specified the interfacial tensions of this hypothetical case, and we, by definition, consider these to be the surface tensions at the

equilibrium state, the contact angle β and the deformation angle α that corresponds to these interfacial tensions follow from equations (2-40) and (2-41) in the fluid case and the contact angle, θ, follows from equation (2-18) in the rigid case. The contact angle (θ) in the rigid case is $\theta=113^{o,}$ while the contact angle (β) and the deformation angle (α) for the fluid surface are found to be $\beta=34.99^{o}$ and $\alpha=129.33^{o}$.

Figure 2-3 shows the plot of $B(R)-B_0$ versus R; it confirms that the free energy extremum in the fluid surface case is at the same critical radius as for the rigid surface, but due to the lower barrier for the fluid surface, nucleation is predicted to happen more easily.
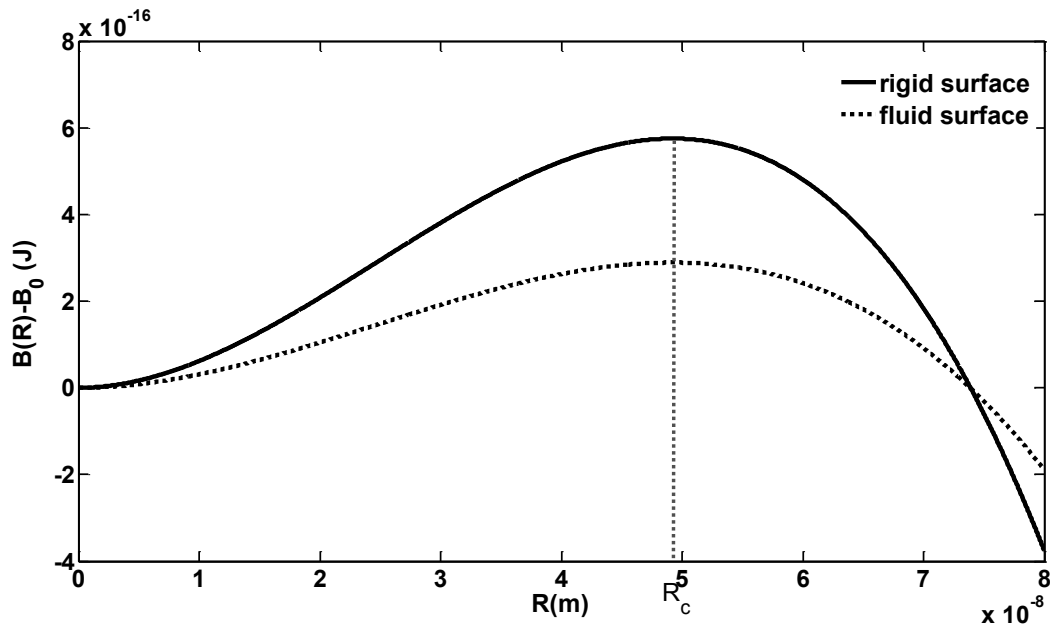
Figure 2-4 Free energy $B(R)-B_0$ versus radius of the water drop for fluid (dodecane) substrate and rigid substrate with the same interfacial tensions where $T=22$ °C, $P^V=2700$ Pa, $\gamma^{LV} = \gamma^w =72.43$ mN/m, $\gamma^{L'V} = \gamma^d =25.3$ mN/m and, $\gamma^{LL'} = \gamma^{wd} =53.7$ mN/m

39
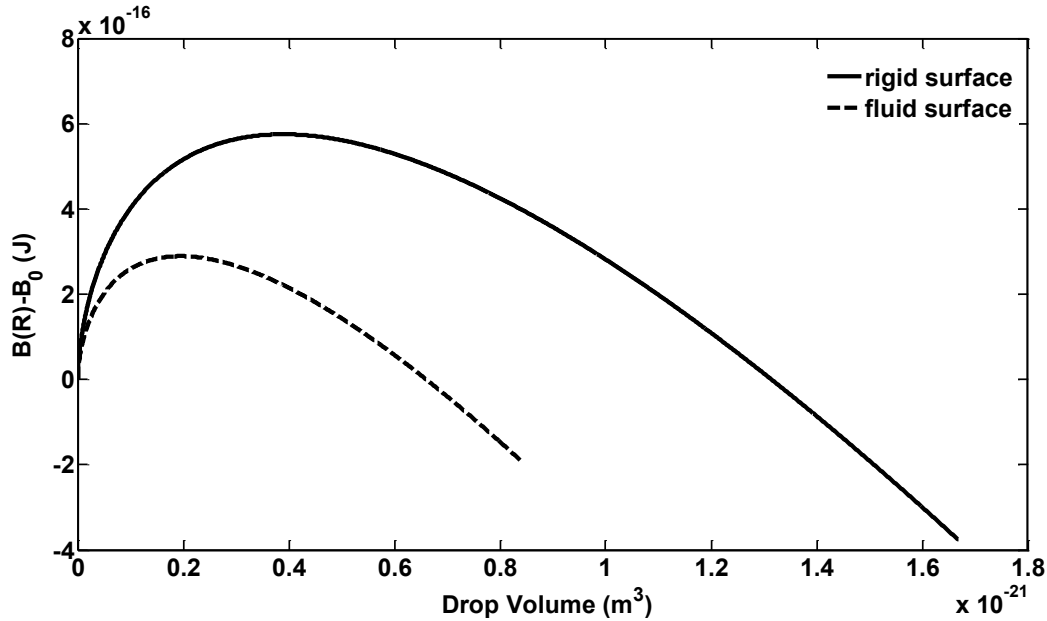
Figure 2-5 Free energy $B(R)-B_0$ versus water drop volume for fluid (dodecane) substrate and rigid substrate with the same interfacial tensions where T=22°C, P^V=2700 Pa, $\gamma^{LV} = \gamma^w$ =72.43 mN/m, $\gamma^{L'V} = \gamma^d$ =25.3 mN/m and, $\gamma^{LL'} = \gamma^{wd}$ =53.7 mN/m

In addition, a plot of $B(R)-B_0$ versus volume of the liquid phase (L) is given in Figure 2-4. It also demonstrates the ease of nucleation on a fluid surface in two ways. As can be seen, at equilibrium for the fluid surface case, not only is the barrier lower than for the rigid surface, but also the unstable equilibrium happens at a smaller drop volume.

On the basis of Figures 2-3 and 2-4, an explanation is provided for the experimental work of Sokuler et al.[2] which showed that nucleation is easier on soft surfaces. In order to further understand physically the reason for the lowered barrier for nucleation on fluid surfaces, we investigate the contribution of each term to the free energies in the rigid and fluid cases and plot each of these terms versus the radius of the drop for both cases. We name each of the terms as the following:

For the rigid surface:

$$B_{Laplace} = (P^V - P^L)V^L \tag{2-43}$$

$$B_{LV} = \gamma^{LV} A^{LV} \tag{2-44}$$

$$B_{SL} = \gamma^{SL} A^{SL} \tag{2-45}$$

$$B_{SV} = -\gamma^{SV} A^{SL} \tag{2-46}$$

For the fluid surface:

$$B_{Laplace} = (P^V - P^L)V^L \tag{2-47}$$

$$B_{LV} = \gamma^{LV} A^{LV} \tag{2-48}$$

$$B_{SL} = \gamma^{LL'} A^{LL'} \tag{2-49}$$

$$B_{SV} = -\gamma^{L'V} \pi R_U^2 sin^2\beta \tag{2-50}$$

As can be seen in Figure 2-5, all contributions lead to easier nucleation on rigid surfaces except for the role of B_{LV}. Actually, in nucleation on a fluid surface, due to the deformation of the surface beneath the drop, the area of the liquid–vapor interface decreases to such a degree that it overcomes the increases in every other term and affects the overall result. Therefore, on the whole, nucleation of a drop on a fluid surface results in a lower energy barrier in comparison with nucleation on a rigid surface.
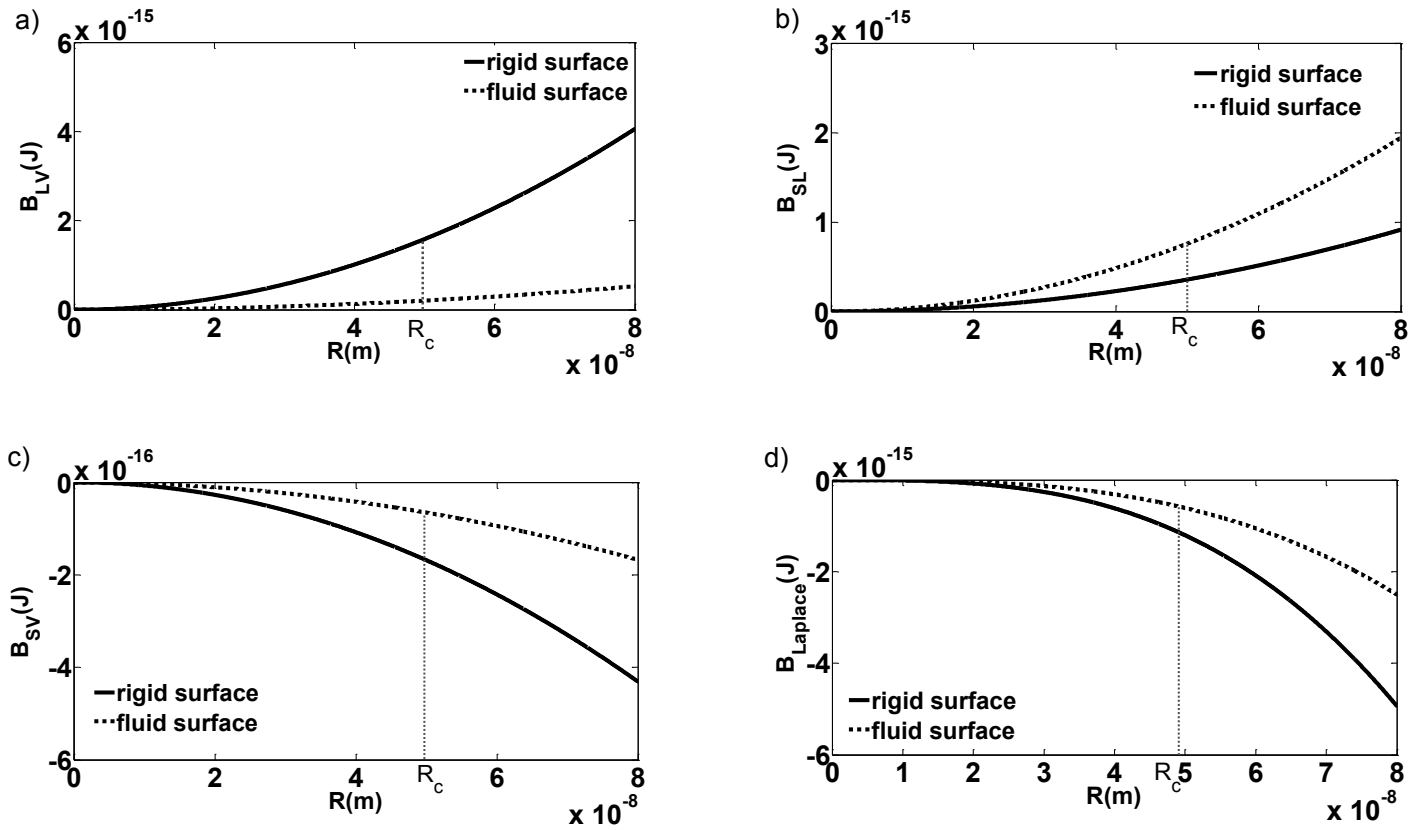
Figure 2-6 Contribution of each term in the free energy to the energy barrier for nucleation of a water droplet on fluid (dodecane) substrate and rigid substrate with the same values of the interfacial tensions where $T=22^{\circ C}$, $P^V=2700$ Pa, $\gamma^{LV} = \gamma^w =72.43$ mN/m, $\gamma^{L'V} = \gamma^d =25.3$ mN/m and, $\gamma^{LL'} = \gamma^{wd} =53.7$ mN/m: (a) B_{LV} vs. R, (b) B_{SL} vs. R, (c) B_{SV} vs. R, (d) $B_{Laplace}$ vs. R

42

2.5. Conclusions

We first explored the effect of contact angle on the barrier for nucleation on a rigid surface. It was found that the nucleation energy barrier increases with increasing contact angle. Next we considered two cases, one nucleation on a fluid surface and the other nucleation on a rigid surface with the same interfacial tensions as in the fluid case. It was shown that the energy barrier for heterogeneous nucleation on a fluid surface is lower than that for a rigid surface, so that heterogeneous nucleation will be easier on a fluid surface. In addition, by inspection of the contribution of different terms to the free energy, it was found that for nucleation on a fluid substrate the decrease in the liquid vapor area, A^{LV}, decreases the free energy to the extent that it more than compensates for the energy increase due to the higher substrate–drop area and lower drop volume. It should also be mentioned that these are general conclusions for heterogeneous nucleation and that the values of interfacial properties were chosen for illustration only.

2.6.   Appendix to Chapter 2

In order to find the criteria for surface and interfacial tensions so that the liquid lens can be formed, we use the contact angle and deformation angle relations which followed from solving equations (2-38) and (2-39) for $\cos\beta$ and $\cos\alpha$ or more directly from the cosine rule:[16]

$$\cos\alpha = \frac{\left(\gamma^{L'V}\right)^2 + \left(\gamma^{LL'}\right)^2 - \left(\gamma^{LV}\right)^2}{2\gamma^{LL'}\gamma^{L'V}} \tag{A1}$$

$$\cos\beta = \frac{\left(\gamma^{L'V}\right)^2 + \left(\gamma^{LV}\right)^2 - \left(\gamma^{LL'}\right)^2}{2\gamma^{LV}\gamma^{L'V}} \tag{A2}$$

We know that, $-1 < \cos\alpha < 1$ and $-1 < \cos\beta < 1$ should be met. By simplifying equations A1 and A2 and by keeping in mind that surface and interfacial tensions are always positive, the following criteria are found:

$$\left(\gamma^{L'V} - \gamma^{LL'} - \gamma^{LV}\right) < 0 \qquad \rightarrow \qquad \gamma^{LL'} > \gamma^{L'V} - \gamma^{LV} \qquad (A3)$$

$$\left(\gamma^{L'V} + \gamma^{LL'} - \gamma^{LV}\right) > 0 \qquad \rightarrow \qquad \gamma^{LL'} > \gamma^{LV} - \gamma^{L'V} \qquad (A4)$$

$$\left(\gamma^{L'V} - \gamma^{LL'} + \gamma^{LV}\right) > 0 \qquad \rightarrow \qquad \gamma^{LL'} < \gamma^{L'V} + \gamma^{LV} \qquad (A5)$$

The criteria A3 and A4 are the same as those given by Jarvis *et al.*,[18] and the criterion A5 is the same as that given by Nepomnyashchy *et al.*[16]

In our paper, we chose dodecane as a fluid substrate for nucleation of water on it. In fact, we chose water and dodecane so that heterogeneous nucleation takes place providing a good model for comparing the barrier for nucleation on a "rigid" versus a "soft" substrate.

In our sample case: $\gamma^{LV} = \gamma^{w} = 72.43$ mN/m, $\gamma^{L'V} = \gamma^{d} = 25.3$ mN/m, $\gamma^{LL'} = \gamma^{wd} = 53.7$ mN/m:

- Validation of criterion A3

$$\gamma^{L'V} - \gamma^{LV} = \gamma^{d} - \gamma^{w} = 25.3 - 72.43 = -47.13\frac{mN}{m} < \gamma^{LL'} = \gamma^{wd} = 53.7\frac{mN}{m}$$

- Validation of criterion A4

$$\gamma^{LV} - \gamma^{L'V} = \gamma^{w} - \gamma^{d} = 72.43 - 25.3 = 47.13\frac{mN}{m} < \gamma^{LL'} = \gamma^{wd} = 53.7\frac{mN}{m}$$

- Validation of criterion A5

$$\gamma^{LV} + \gamma^{L'V} = \gamma^W + \gamma^d = 72.43 + 25.3 = 97.73\frac{mN}{m} > \gamma^{LL'} = \gamma^{wd} = 53.7\frac{mN}{m}$$

In order to find the criteria for nucleation of a sessile drop on a rigid substrate, we use the Young equation (2-18). Noting that $-1 < cos\theta < 1$, the criteria would be

$$\gamma^{LV} > \gamma^{SV} - \gamma^{SL} \tag{A6}$$

$$\gamma^{LV} > \gamma^{SL} - \gamma^{SV} \tag{A7}$$

Since in the rigid case we have S instead of L', by substituting γ^{SV} =25.3 mN/m and γ^{SL} =53.7 mN/m we will have:

- Validation of criterion A6

$$\gamma^{SV} - \gamma^{SL} = 25.3 - 53.7 = -28.4\frac{mN}{m} < \gamma^{LV} = 72.43\frac{mN}{m}$$

- Validation of criterion A7

$$\gamma^{SL} - \gamma^{SV} = 53.7 - 25.3 = 28.4\frac{mN}{m} < \gamma^{LV} = 72.43\frac{mN}{m}$$

2.7. References

1. Debenedetti, Thermodynamics: When a Phase is Born. P. G. *Nature* **2006**, *441*, 168-169.

2. Sokuler, M.; Auernhammer, G. K.; Roth, M.; Liu, C.; Bonaccurso, E.; Butt, H. The Softer the Better: Fast Condensation on Soft Surfaces. *Langmuir* **2010**, *26*, 1544-1547.

3. Leach, R. N.; Stevens, F.; Langford, S. C.; Dickinson, J. T. Dropwise Condensation: Experiments and Simulations of Nucleation and Growth of Water Drops in a Cooling System. *Langmuir* **2006**, *22*, 8864-8872.

4. Family, F.; Meakin, P. Scaling of the Droplet-Size Distribution in Vapor-Deposited Thin-Films. *Phys. Rev. Lett.* **1988**, *61*, 428-431.

5. Pericet-Camara, R.; Best, A.; Butt, H.; Bonaccurso, E. Effect of Capillary Pressure and Surface Tension on the Deformation of Elastic Surfaces by Sessile Liquid Microdrops: An Experimental Investigation. *Langmuir* **2008***, 24*, 10565-10568.

6. Lester, G. R. Contact Angles of Liquids at Deformable Solid Surfaces. *J. Colloid Sci.* **1961***, 16*, 315-326.

7. Rusanov, A. I. Theory of Wetting of Elastically Deformed Bodies, 1. Deformation with a Finite Contact-Angle. *Colloid J. Ussr+* **1975***, 37*, 614-622.

8. Yu, Y.; Zhao, Y. Elastic Deformation of Soft Membrane with Finite Thickness Induced by a Sessile Liquid Droplet. *J. Colloid Interface Sci.* **2009***, 339*, 489-494.

9. Kern, R.; Muller, P. Deformation of an Elastic Thin Solid Induced by a Liquid Droplet. *Surf Sci.* **1992***, 264*, 467-494.

10. Shanahan, M. E. R. The Influence of Solid Micro-Deformation on Contact-Angle Equilibrium. *J. Phys. D. Appl. Phys.* **1987***, 20*, 945-950.

11. Shanahan, M. E. R.; de Genns, P. G. In *Adhesion 11;* Allen, K. W., Ed.; Elsevier Applied Science Publ: London, 1987; Vol. 11, pp 71-81.

12. White, L. R. The Contact Angle on an Elastic Substrate. 1. The Role of Disjoining Pressure in the Surface Mechanics. *J. Colloid Interface Sci.* **2003***, 258*, 82-96.

13. Shanahan, M. E. R. Contact-Angle Equilibrium on Thin Elastic Solids. *J. Adhesion* **1985***, 18*, 247-267.

14. Shanahan, M. E. R. Equilibrium of Liquid-Drops on Thin Plates - Plate Rigidity and Stability Considerations. *J. Adhesion* **1987***, 20*, 261-274.

15. Carre, A.; Gastel, J. C.; Shanahan, M. E. R. Viscoelastic Effects in the Spreading of Liquids. *Nature* **1996***, 379*, 432-434.

16. Nepomnyashchy, A. A.; Golovin, A. A.; Tikhomirova, A. E.; Volpert, V. A. Nucleation and Growth of Droplets at a Liquid-Gas Interface. *Phys. Rev. E.* **2006***, 74*, 021605.

17. Forest, T. W.; Ward, C. A. Homogeneous Nucleation of Bubbles in Solutions at Pressures Above Vapor-Pressure of Pure Liquid. *J. Chem. Phys.* **1978***, 69*, 2221-2230.

18. Jarvis, T. J.; Donohue, M. D.; Katz, J. L. Bubble Nucleation Mechanisms of Liquid Droplets Superheated in Other Liquids. *J. Colloid Interface Sci.* **1975***, 50*, 359-368.

19. McGaughey, A. J. H.; Ward, C. A. Droplet Stability in a Finite System: Consideration of the Solid-Vapor Interface. *J. Appl. Phys.* **2003***, 93*, 3619-3626.

20. Ward, C. A.; Johnson, W. R.; Venter, R. D.; Ho, S.; Forest, T. W.; Fraser, W. D. Heterogeneous Bubble Nucleation and Conditions for Growth in a Liquid Gas System of Constant Mass and Volume. *J. Appl. Phys.* **1983***, 54*, 1833-1843.

21. Ghasemi, H.; Ward, C. A. Sessile-Water-Droplet Contact Angle Dependence on Adsorption at the Solid-Liquid Interface. *J. Phys. Chem. C* **2010***, 114*, 5088-5100.

22. Toshev, B. V.; Avramov, M. Z. On the Thermodynamic Stability of Small Droplets at Positive Line Tension. *Colloid Surface A.* **1993***, 75*, 33-37.

23. Toshev, B. V. Equilibrium and Stability of Spherical Cap-Shaped Liquid Drops. *Colloid surface A.* **1996***, 108*, 133-135.

24. Attard, P. Thermodynamic Analysis of Bridging Bubbles and a Quantitative Comparison with the Measured Hydrophobic Attraction. *Langmuir* **2000***, 16*, 4455-4466.

25. Elliott, J. A. W.; Voitcu, O. On the Thermodynamic Stability of Liquid Capillary Bridges. *Can. J. Chem. Eng.* **2007***, 85*, 692-700.

26. Ward, C. A.; Sasges, M. R. Effect of Gravity on Contact Angle: A Theoretical Investigation. *J. Chem. Phys.* **1998***, 109*, 3651-3660.

27. Hunter, R. J. *Introduction to Modern Colloid Science;* Oxford University Press Inc.: New York, 1993.

28. Elliott, J. A. W. On the Complete Kelvin Equation. *Chem. Eng. Educ.* **2001***, 35*, 274-278.

29. Ward, C. A.; Levart, E. Conditions for Stability of Bubble Nuclei in Solid-Surfaces Contacting a Liquid-Gas Solution. *J. Appl. Phys.* **1984***, 56*, 491-500.

30. Goebel, A.; Lunkenheimer, K. Interfacial Tension of the Water/N-alkane Interface. *Langmuir* **1997***, 13*, 369-372.

Chapter 3: Design of Microdrop Concentrating Processes

3.1. Introduction

Due to the demand for the investigation of chemical composition of ultra-small structures including sub-cellular materials, droplets—as microscale reaction vessels—were one of the means that came into consideration in microfluidic systems.[1] In this regard, a drop which contains nanoscale materials provides a suitable vessel for them to be manipulated, controlled and measured more precisely.[2] Encapsulating[3] and concentrating[4-7] nanoparticles and solutes are two manipulations that can be done by means of microdrops. Due to the small solubility of water in some vegetable oils, by inserting aqueous drops containing solutes within that organic phase, the microdrops can isolate the solute in confined volumes. This isolation of solutes within the small volume stops their dilution and facilitates their measurement and control over their reaction.[3] However, this phenomenon can be exploited only for those kinds of solutes that have very small partition coefficients in the organic phase; fortunately this requirement is valid for most biological molecules.[4] It should be mentioned that the concentrating of solutes in an aqueous drop by this procedure is more effective for those kinds of organic phases into which water has slow dissolution—over minutes.[4]

In order to concentrate solutes within aqueous microdrops, He *et al*. did mass transport calculations and found that the rate of change in the concentration of solutes depends on the fifth power of surface-area-to-volume ratio of the drops.[4] Since this ratio is high enough for micro- or nanometer scales, they exploited this effect to concentrate solutes within aqueous microdrops. It

is known that the solubility of water in some organic phases increases with increasing temperature and it was found that this phenomenon has a noticeable effect when dealing with micro or nano scale drops.[6,8] Jeffries *et al*. exploited the temperature rise of about 1 K that accompanied using a laser for trapping and tracking microdrops.[5,8] They used an optical vortex trapping method for translating aqueous microdrops in oil phases and found that turning the laser on and off resulted in shrinkage and re-expansion of drops. When the laser is turned on, the surrounding organic phase's temperature increases which increases the solubility of water in it. Therefore, a driving force for mass transport is created and water leaves the drop phase and the drop shrinks. Whereas when the laser is turned off, the surrounding organic phase cools and becomes supersaturated with water and water returns to the drop making the drop expand again. Jeffries *et al*. performed mass and heat transfer calculations for drops of pure water in acetophenone and decanol, and by solving the corresponding equations simultaneously found the droplet radius, temperature and supersaturation concentration of water in the organic phase with respect to time.[8]

Bajpayee *et al*. exploited the influence of temperature on concentrating solutes within aqueous drops for cryopreservation applications.[6] In vitrification processes, which is one method of cryopreserving biological cells, very high cooling rates are required, (about 10^6 °C/s); using lower cooling rates is possible but requires high concentrations of cryoprotective agents. However, keeping cells in such a high concentration of cryoprotective agents for a long time is lethal to the cells. As a result Bajpayee *et al*. applied a 10 °C temperature differential for a short time of about two minutes in order to increase the concentration of cryoprotective agents within an aqueous microdrop while at the same time minimizing the time of exposure of cells to such a

high concentration. Bajpayee *et al*. have done some dynamic calculations and found concentration and shrinkage profiles for aqueous microdrops containing glycerol.[6]

Generally speaking, controlling mass transfer[9] in biochemical processes is one way to enhance the accuracy of experiments. Using droplets especially with micro- or nanometer sizes is one technique that can minimize the mass transfer of isolated solute and increase the control over it. In this regard, a large amount of research including preparing,[3] sizing[10] and tracking[5] of the drops and concentrating[4,8] of solutes has been done on femtoliter to picoliter drop volumes. Most of the work in this area has been experimental. However, some theoretical research has been performed from a dynamic point of view such as mass transfer and heat transfer analysis of concentrating solutes within microdrops.[4,5] But, to the best of our knowledge, thermodynamic contributions have not yet been made to the prediction of concentration or size of aqueous microdrops which contain solutes or nanoparticles. In addition, the difference in the behaviors of microdrops containing two different types of solutes—solutes with no solubility limit or solutes that have a solubility limit—has not been considered for these processes. As a result, in this work we have investigated, by means of thermodynamic calculations, the final equilibrium concentration of the solute and the equilibrium size of the microdrop in the process of concentrating solutes within aqueous microdrops which are surrounded by an organic phase. We have also analyzed the effects of temperature, organic phase volume and the type of solute (from the solubility limit point of view).

In order to do the thermodynamic calculations for concentrating solutes within an aqueous microdrop which is surrounded by an organic phase, we have chosen glycerol as an example of an unlimited solubility agent and sodium chloride as an example of a limited solubility agent. Both of these solutes have important roles in cryobiological and biological processes. The

organic phase is chosen to be soybean oil. Neither glycerol[6] nor sodium chloride[4] can dissolve into the soybean oil. Therefore by increasing the temperature of the system from 25 °C to 35 °C, a small amount of water dissolves into the oil phase increasing the concentration of the entrapped solute within the drop.

3.2. Governing Equations

3.2.1. Unlimited Solubility Agent

For performing thermodynamic derivations we define a constant volume system that includes a drop of aqueous solution which is surrounded by an oil phase (Figure 3-1). The drop phase and the oil phase are represented by superscripts D and L respectively. The drop consists of water and solute (glycerol in the case of an unlimited solubility solute), and the oil phase contains oil and water. Glycerol, oil and water components are denoted by subscripts g, o and w respectively.
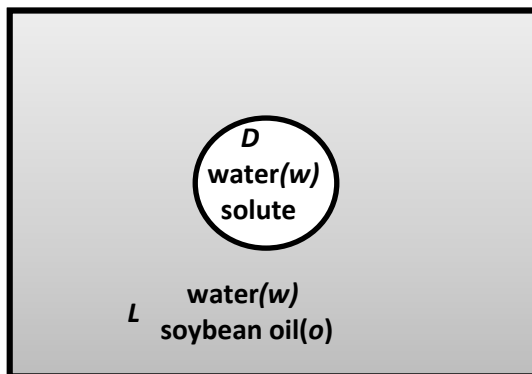
Figure 3-1 A drop of aqueous solution containing an unlimited solubility agent is placed within soybean oil

The requirements for equilibrium include equality of temperature, T,

$$T^D = T^L \tag{3-1}$$

and equality of chemical potential of the coexisting component—which is water here—in both phases, μ_w,

$$\mu_w^D(T, P^D, x_{solute}^D) = \mu_w^L(T, P^L, x_w^L) \qquad \text{(3-2)}$$

where we have indicated that chemical potential is a function of temperature, pressure, P and mole fraction, x. In addition, due to the curvature of the oil–drop interface, the Laplace equation should be satisfied at equilibrium.

$$P^D - P^L = \frac{2\sigma^{LD}}{R_{eq}} \qquad \text{(3-3)}$$

where σ and R are interfacial tension and drop radius, respectively, and the superscript LD denotes the oil–drop interface and subscript eq indicates the equilibrium state. To calculate the chemical potential of water in the oil phase we use the relationship between chemical potential and activity coefficient:

$$\mu_w^L(T, P^L, x_w^L) = \mu_w^{\circ}(T, P^L) + R_u T ln\,(\gamma_w^L x_w^L) \qquad \text{(3-4)}$$

where γ and R_u are activity coefficient and universal gas constant, respectively, and the superscript $^{\circ}$ indicates the pure state. For the activity coefficient of water in soybean oil, we use an empirical equation describing the activity coefficient of water in any edible oil as a function of temperature provided by Hilder.[11] Actually, Hilder measured the two-phase equilibrium of water vapor and water dissolved in some edible oils at several temperatures. Then he gathered and correlated the existing data of two-phase equilibria (water vapor–water in edible oil) and three-phase equilibria (water vapor–water in edible oil–liquid water) in the following format:

$$ln\,\gamma_w^{edible\;oil} = \frac{\alpha}{T} + \beta \qquad \text{(3-5)}$$

where α and β are reported by Hilder[11] to be 1600±40 °K and −2.5±0.5 respectively and T is temperature in Kelvin. In order to use a more precise activity coefficient of water in soybean oil, we adjusted the quantities in equation (3-5) with Bajpayee et al.'s experimental data.[6] More details about this adjustment are given in the "Results and Discussion" section.

To calculate the chemical potential of water in a glycerol solution we used the single-solute osmotic virial equation[12] on a mole fraction basis which is extensively applicable for a variety of solutes in aqueous solutions:[13]

$$\mu_w^D(T, P^D, x_i^D) = \overset{\circ}{\mu}_w(T, P^D) - R_u T[x_i^D + B_i^*(x_i^D)^2 + C_i^*(x_i^D)^3 + \cdots] \qquad (3\text{-}6)$$

In equation (3-6),[‡] B_i^* and C_i^* are the second and third osmotic virial coefficients of solute i in terms of mole fraction and x_i^D is the mole fraction of solute i in the drop phase. The function in the square brackets is known as osmole fraction ($\tilde{\pi}$) which is approximated by polynomials in mole fraction with solute-specific coefficients for second and higher order terms. Substituting equations (3-4) and (3-6) into equation (3-2) yields the following relation:

$$\overset{\circ}{\mu}_w(T, P^D) - R_u T[x_i^D + B_i^*(x_i^D)^2 + C_i^*(x_i^D)^3 + \cdots] = \overset{\circ}{\mu}_w(T, P^L) + R_u T ln\,(\gamma_w^L x_w^L) \qquad (3\text{-}7)$$

Assuming the incompressibility of water, the pressure dependence of the chemical potential of pure water is given by:

$$\overset{\circ}{\mu}_w(T, P^D) = \overset{\circ}{\mu}_w(T, P^L) + \overset{\circ}{v}_w(P^D - P^L) \qquad (3\text{-}8)$$

[‡] This equation differs slightly from that in reference 12. In that reference, the osmole fraction ($\tilde{\pi}$) had been mistakenly multiplied by $\frac{1}{x_w^D}$ which we have corrected here.

where v is molar volume. Substituting equations (3-8) and (3-3) into equation (3-7) and rearranging yields:

$$-v_w^\circ \left(\frac{2\sigma^{LD}}{R_{eq}}\right) + R_u T[x_i^D + B_i^*(x_i^D)^2 + C_i^*(x_i^D)^3 + \cdots] + R_u T ln\,(\gamma_w^L x_w^L) = 0 \qquad (3\text{-}9)$$

In addition to equation (3-9), which is related to the equilibrium conditions, mass or mole conservation equations are required to find the equilibrium mole fractions of components in each phase. Since the initial diameter (a_{init}) and molarity of the drop (C_{init}^D) are known, the total moles of solute i (N_i^t) in the system can be calculated:

$$N_i^t = \frac{\pi a_{init}^3}{6} C_{init}^D \qquad (3\text{-}10)$$

where superscript t denotes total. The other known quantities of this problem are the volume of pre-saturated oil at the initial temperature which is 25 °C (V_{satoil}) and the solubility of water in soybean oil on a mole fraction basis at this temperature (x_w^{sat}). As a result, using the initial density of the oil/water mixture (ρ_{init}^L), the initial density of the solute solution (ρ_{init}^D) and the initial molar mass of the oil/water mixture (M_{init}^L) the total moles of oil (N_o^t) and the total moles of water (N_w^t) can be calculated:

$$N_o^t = \frac{(1 - x_w^{sat})}{M_{init}^L} V_{satoil} \rho_{init}^L \qquad (3\text{-}11)$$

$$N_w^t = \frac{x_w^{sat}}{M_{init}^L} V_{satoil}\,\rho_{init}^L + \frac{\pi a_{init}^3}{6} \rho_{init}^D \left(1 - C_{init}^D \frac{M_i}{\rho_{init}^D}\right) \frac{1}{M_w} \qquad (3\text{-}12)$$

where M_i denotes the molar mass of component i. The first and the second terms in equation (3-12) are the numbers of water moles which were brought into the system by the pre-saturated oil and the initial drop, respectively. After calculating the total moles of each constituent in the

system we turn to the mole fraction relations at equilibrium. The mole fraction of water in the oil phase (x_w^L) is given by:

$$x_w^L = \frac{N_w^L}{N_w^L + N_o^t} \tag{3-13}$$

where N_w^L is the number of moles of water in the oil phase at equilibrium and the oil component is just present in the oil phase which means that $N_o^L = N_o^t$. Rearranging equation (3-13) gives:

$$N_w^L = \frac{x_w^L N_o^t}{1 - x_w^L} \tag{3-14}$$

Therefore the mole fractions of water and solute in the drop phase and the mole fraction of oil in the oil phase are given by the following relations:

$$x_w^D = \frac{N_w^D}{N_w^D + N_i^D} = \frac{N_w^t - N_w^L}{N_w^t - N_w^L + N_i^D} = \frac{N_w^t - \frac{x_w^L N_o^t}{1 - x_w^L}}{N_w^t - \frac{x_w^L N_o^t}{1 - x_w^L} + N_i^D} \tag{3-15}$$

$$x_i^D = 1 - x_w^D \tag{3-16}$$

$$x_o^L = 1 - x_w^L \tag{3-17}$$

where N_w^D is the number of moles of water in the drop phase at equilibrium and the solute i is just present in the drop phase which means that $N_i^D = N_i^t$.

In addition, since in the first term of equation (3-9), the size of the drop at equilibrium (R_{eq}) plays a role in the calculations, it should be found as well. Therefore, by means of drop mass (m^D) at equilibrium—which is equal to the sum of the masses of its constituents (water, m_w^D, and solute i, m_i^D)—and drop density (ρ^D) we can find the size of the drop at equilibrium:

$$m^D = m_w^D + m_i^D = m_w^t - m_w^L + m_i^D \tag{3-18}$$

$$R_{eq} = \left(\frac{3}{4\pi} \frac{m^D}{\rho^D} \right)^{\frac{1}{3}}$$ (3-19)

where m_w^t is the total mass of water in the system. Note that we consider the solute i, water and soybean oil to be incompressible liquids and by further assuming zero volume of mixing, we assume that the densities of their mixtures can be calculated by the following relations:

$$\rho^L = \frac{1}{\frac{w_o^L}{\rho_o} + \frac{w_w^L}{\rho_w}}$$ (3-20)

$$\rho^D = \frac{1}{\frac{w_i^D}{\rho_i} + \frac{w_w^D}{\rho_w}}$$ (3-21)

where w represents the weight fraction and can be converted into mole fraction by means of molar mass of the components and solutions. An example of this conversion is given for mole fraction of water in the drop phase:

$$x_w^D = w_w^D \frac{M^D}{M_w}$$ (3-22)

where M^D is the molar mass of the drop phase and can be found by following relation:

$$M^D = x_w^D M_w + x_i^D M_i = \frac{1}{\frac{w_w^D}{M_w} + \frac{w_i^D}{M_i}}$$ (3-23)

Now, by simultaneously solving equations (3-9), (3-15) to (3-17) and (3-19) for unknowns x_w^L, x_i^D, x_w^D, x_o^L and R_{eq} and making use of equations (3-5), (3-10) to (3-12), (3-18), (3-20) to (3-23) we can find the equilibrium concentration and size of the drop.

3.2.2. Limited Solubility Agent

As mentioned previously, some materials have a specific solubility limit in water such that when their solubility reaches the saturation value they will start to precipitate as a solid (S). Here, since we are interested in the behaviour of the aqueous solution in the microdrop, we have assumed that the precipitated solutes leave the drop in the solid form. As an example of limited solubility solutes we choose sodium chloride for investigation. Figure 3-2 shows this system schematically.
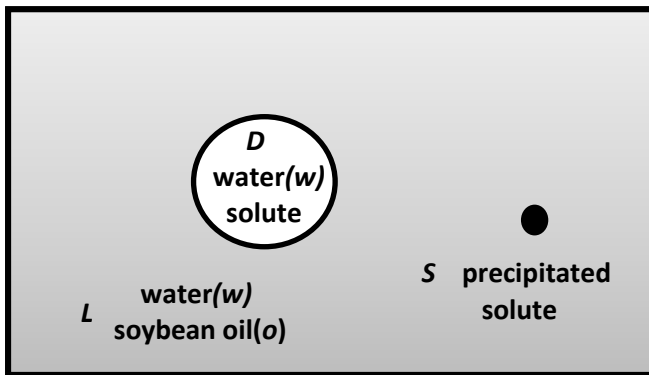
Figure 3-2 A drop of aqueous solution containing a limited solubility agent is placed within soybean oil

The procedure for calculating the equilibrium mole fractions of solute, water and oil in both phases is the same as for the unlimited-solubility agents, up to the solubility threshold. But after reaching that limit, since the chemical potential of solute in the solid phase has to be equal to the chemical potential of solute in the drop phase, the mole fraction of the limited-solubility solute in the drop will remain constant and equal to the saturation concentration. Due to the conservation of mass and moles for all the components, when the solute reaches the saturation concentration all the mole fractions in the liquid portion of the drop will remain constant. But since the solute starts precipitating and—as we assumed—leaving the drop, the drop starts to shrink more considerably.

To find the solubility limit of the solute i, $\left(x_i^{limit}\right)$, the chemical potential of the solute as a pure solid should be equal to the chemical potential of that solute in the drop phase:

$$\mu_i^{Solid}(T, P^S) = \mu_i^D(T, P^D, x_i^{limit}) \tag{3-24}$$

For the sake of simplicity, we ignore the effect of pressure difference between the solid phase and the drop phase in this equation and by setting the solid–liquid surface tension equal to zero (this assumption is relaxed in Chapter 5). As a result, the solubility limit of the solute would depend only on temperature and would not depend on the details of solid precipitation such as solid shape. For many solutes, such as sodium chloride, solubility calculations have been done, or experimental measurements have been made, so that the solubility limits of solutes are tabulated[14] at different temperatures and we have used these data as well.

In order to investigate the equilibrium concentration of sodium chloride inside the aqueous drop surrounded by the soybean oil we need the chemical potential of water in the sodium chloride aqueous phase. Sodium chloride aqueous solution is an electrolyte solution and an appropriate model for predicting the chemical potential of water in the solution is required. It was demonstrated by Prickett *et al.* that the osmotic virial equation, with the inclusion of an empirical "dissociation constant", can describe the chemical potential of water in electrolyte solution using less parameters than the Pitzer–Debye–Huckel equation but with the same accuracy.[15] Therefore, we applied this model for calculating the chemical potential of water in sodium chloride aqueous solution by using the following equation in place of equation (3-6):

$$\mu_w^D(T, P^D, x_i^D) = \mu_w^\circ(T, P^D) - R_u T \left[k_{diss,i}^* x_i^D + B_i^* \left(k_{diss,i}^* x_i^D \right)^2 + C_i^* \left(k_{diss,i}^* x_i^D \right)^3 + \cdots \right] \tag{3-25}$$

where $k_{diss,i}^*$ is the dissociation constant for the solute i for use on a mole fraction basis which captures non-idealities in the solution including dissociation of the electrolyte into ions, among others.

Here we summarize the required equations to find the equilibrium concentration and size of the drop containing the limited solubility solute: By substituting equations (3-4) and (3-25) into equation (3-2) and by making use of equations (3-3) and (3-8) we will find equation (3-26) as the main equilibrium equation:

$$-v_w^\circ \left(\frac{2\sigma^{LD}}{R_{eq}}\right) + R_u T \left[k_{diss,i}^* x_i^D + B_i^* \left(k_{diss,i}^* x_i^D\right)^2 + C_i^* \left(k_{diss,i}^* x_i^D\right)^3 + \cdots \right] + R_u T ln\left(\gamma_w^L x_w^L\right) = 0$$

$$(3\text{-}26)$$

Before reaching the solubility limit, by simultaneously solving equations (3-15) to (3-17), (3-19) and (3-26) for unknowns x_w^L, x_i^D, x_w^D, x_o^L and R_{eq} and making use of equations (3-5), (3-10) to (3-12), (3-18), (3-20) to (3-23) the equilibrium concentration and size of the drop can be found. However, after reaching the solubility limit, x_i^D and x_w^D will remain constant and solute i will leave the drop and precipitate in the solid form; so in this case:

$$x_i^D = x_i^{limit} \tag{3-27}$$

$$x_w^D = 1 - x_i^{limit} \tag{3-28}$$

$$N_i^S = N_i^t - N_i^D \tag{3-29}$$

Now, by simultaneously solving equations (3-17), (3-19), (3-26) and (3-29) for unknowns x_w^L, x_o^L, R_{eq} and N_i^S and making use of equations (3-5), (3-10) to (3-12), (3-18), (3-20) to (3-23), (3-27) to (3-28) the equilibrium concentration and size of the drop can be found.

3.3. Results and Discussion

In order to investigate the equilibrium size and concentration of solutes in an aqueous microdrop within an organic phase, and for the sake of comparison, we have chosen the same system as Bajpayee et al.[6] for the solute with no solubility limit. They made glycerol solutions of 1 M and 2 M and then prepared polydisperse emulsions of these glycerol solutions in pre-saturated (with water) soybean oil at 25 °C at a 1000:1 (oil : glycerol drop solution) volume ratio. They then pipetted a certain amount of this emulsion onto a hydrophobic surface and heated the surface from 25 °C to 35 °C. Finally, they monitored the size and concentration of drops with diameters in the range of 13-18 μm to see the effect of temperature on these features. Here we consider a single drop with initial diameter of 18 μm and different initial glycerol concentrations (i.e., 1 M or 2 M) within pre-saturated soybean oil at 25 °C. While Bajpayee et al. had investigated just the effect of temperature at a single oil-to-drop-volume ratio (1000:1), we studied both the effect of temperature and different oil: initial drop volume ratios to find the effect of oil availability for dissolution as well. To calculate the pre-saturation of oil with water at 25 °C, the solubility of water in soybean oil is needed. Based on the calculation of He et al. [4] the saturation concentration of water in soybean oil is reported to be 0.3% volume fraction which is equivalent to 14% mole fraction. However this value is not consistent with the available data[11, 16-18] for the solubility of water in soybean oil. Therefore, we have linearly correlated the available solubility data with temperature. Actually, Perkins[16] has mentioned that the resemblance of the constituent fatty acids of cottonseed oil and soybean oil leads to the similarity of the solubility of water in these oils. So, due to lack of enough data for the solubility of water in soybean oil we have correlated the solubility data of water in both of these oils and we have found a water solubility of 0.0546 mole fraction at 25 °C. However, using just the soybean oil–

water data results in a saturation mole fraction of 0.0537 at this temperature which shows that considering both oils for finding the saturation mole fraction of water in soybean oil is acceptable. Figure 3-3 shows the available data[11] for saturation mole fraction of water in cottonseed oil and soybean oil, along with the linear correlation of the entire data in terms of temperature as given by equation (3-30).
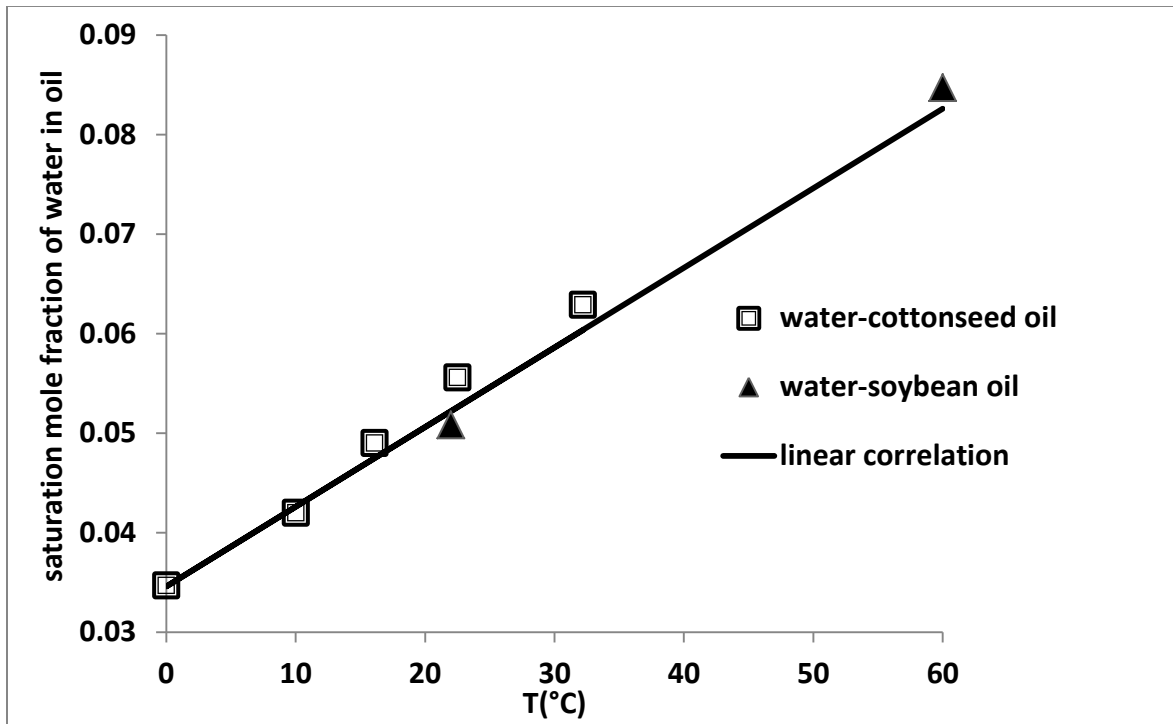
Figure 3-3 Linear correlation of saturation mole fraction of water in soybean oil versus temperature. [Data from reference 11]. Regression statistics are given in the Appendix.

$$x_w^{sat} = 0.0008T + 0.0346 \qquad (3\text{-}30)$$

where x_w^{sat} is the saturation mole fraction of water in soybean oil and T is temperature in °C.

Bajpayee et al.[6] report the final volumes of drops with initial concentrations of 1 M and 2 M glycerol to be 28% ± 4.5% and 38% ± 6.2% of their initial volumes, respectively, at 35 °C and

$\frac{V_{oil}}{V_{init}} = 1000$. To arrive at more precise values of α and β in the empirical equation (3-5), we have adjusted α and β (but still within the range given by Hilder[11]) by minimizing the following objective function.

$$f^V = \left(\frac{V_{eq}}{V_{init}}\bigg]_{C=1M} - 0.28\right)^2 + \left(\frac{V_{eq}}{V_{init}}\bigg]_{C=2M} - 0.38\right)^2 \tag{3-31}$$

As a result of minimizing this objective function, α and β in equation (3-5) are found to be equal to 1617 and –2.9 respectively.[§] Therefore, for calculating the activity coefficient of water in soybean oil as a function of temperature the following equation is used:

$$\ln \gamma_w^L = \frac{1617}{T} - 2.9 \tag{3-32}$$

Figure 3-4 shows the experimental equilibrium size range and calculated equilibrium size based on adjusted α and β for aqueous drops of 1 and 2 molar glycerol.

[§] It should be mentioned that by adjusting α and β to find the proper γ_w^L, the saturation mole fraction of water in oil x_w^{sat} will not satisfy $\gamma_w^L x_w^{sat} = 1$ as is suggested it should in Hilder's[11] paper. However, this is the best match that is consistent with the experimental work of Bajpayee[6] *et al.* despite the inconsistencies in x_w^{sat} at 25 °C.
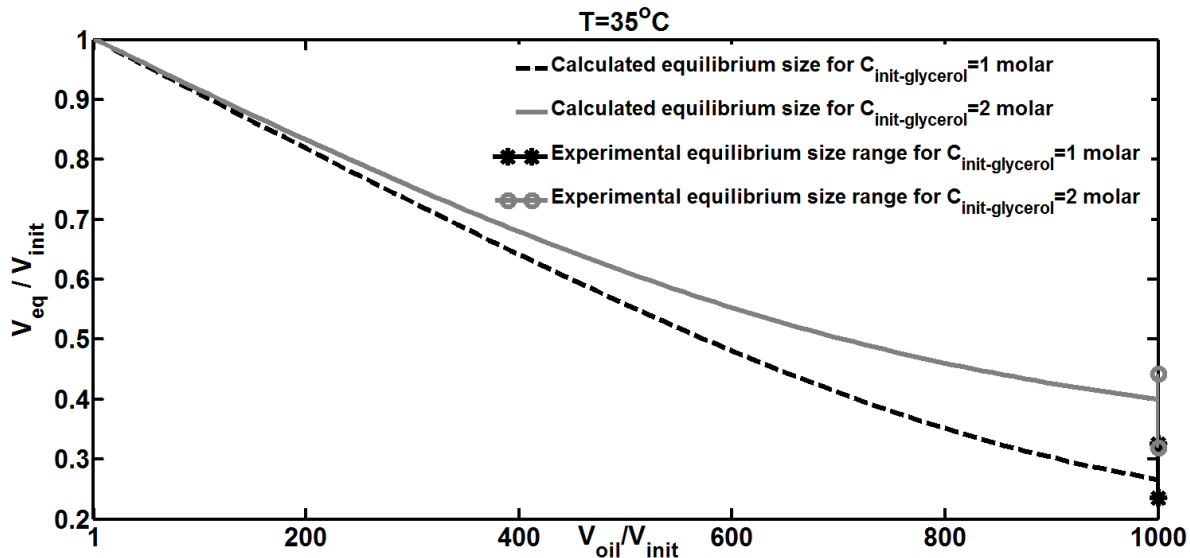
Figure 3-4 The equilibrium size of the drop containing glycerol per its initial size versus the oil-volume-to-initial-drop-volume ratio after adjusting α and β. The experimental final size with error bounds at $\frac{V_{oil}}{V_{init}} = 1000$, from Bajpayee et al.'s work,[6] is shown.

In order to calculate the chemical potential of water in the glycerol solution or in the sodium chloride solution, we have used the osmotic virial equation. The third osmotic virial coefficients for both glycerol and NaCl are taken to be zero.[12] For the second osmotic virial coefficients for use with mole fraction, B_i^*, we used 3.169 for glycerol and 3.8 for NaCl, and for the dissociation constant for NaCl for use with mole fraction, $k_{diss,i}^*$, we used 1.644.[**] In addition, the density, ρ, in kg/m^3 for NaCl solution[19] as a function of temperature, T, in °C and molarity of NaCl, c, is taken to be:

[**] The second osmotic virial coefficients for glycerol and NaCl and the dissociation constant for NaCl that are used in this work are different from those in reference 12. The values used here are updated coefficients provided by Michal Zielinski (unpublished at the time this Chapter was published but now published, reference 30 in Chapter 4). See footnote 1. We note that using the original coefficients from reference 12 does not lead to any substantive difference in this work.

$$\rho_{NaCl\,solution} = \rho_{water} + 44.85c - 0.09634cT + 0.6136 \times 10^{-3}cT^2 - 2.712c^{1.5} +$$

$$1.009 \times 10^{-2}c^{1.5}T \tag{3-33}$$

The glycerol[20] density, ρ, in kg/m³ as a function of temperature in K is taken to be:

$$\rho_{glycerol} = \frac{0.92382}{0.24386^{\left(1+\left(1-\frac{T}{850}\right)^{0.22114}\right)}} \times M_g \tag{3-34}$$

Furthermore, the saturation solubility data[14] of NaCl and the density data[16] of soybean oil have been correlated as functions of temperature as follows:

$$w_{NaCl}^{limit} = 1.374 \times 10^{-6}T^2 - 6.899 \times 10^{-4}T + 0.3484 \qquad\qquad ,T \text{ in K} \tag{3-35}$$

$$\rho_{soybean\,oil} = 934.43 - 0.6781T \qquad\qquad ,T \text{ in °C} \tag{3-36}$$

where w_{NaCl}^{limit} is the saturated mass fraction of NaCl in water and ρ is in kg/m³. Additionally, the molar mass of soybean oil[11] is taken to be 876 g/mol.

Another physical property which is needed in these calculations is the oil-drop interfacial tension (σ^{LD}). Since the Laplace pressure term which includes the interfacial tension does not affect the equilibrium results for drops of micrometer size or larger, we have chosen water–soybean oil interfacial tension[3] (22.8 mN/m) for the oil–drop interfacial tension (noting that we would have to choose a more accurate interfacial tension—which would depend on both temperature and the mole fractions of components in both phases—in the case of dealing with smaller drops such as those with nanometer size diameters).

By means of these physical properties and the governing equations described in the previous section, the designing parameters including the equilibrium concentration of the solutes and the

equilibrium size of the drops are calculated. The results of these calculations are presented in the following sections.

3.3.1. Equilibrium Concentration of the Drop

Figure 3-5 shows the plot of predicted equilibrium concentration of glycerol or NaCl (which are the examples for unlimited solubility solutes and limited solubility solutes respectively) versus the oil: initial drop volume ratio at a constant temperature of 35 °C. As Figure 3-5 demonstrates, increasing the availability of oil results in a higher equilibrium concentration of the solute within the drop. But this feature is not valid for solutes which reach their solubility limit. Furthermore, the trends of increasing the equilibrium drop concentration by increasing the availability of oil show within which range of oil volume the solute can be concentrated more efficiently. For example, for an initial concentration of glycerol of 1 M in Figure 3-5, the inflection point (maximum slope) happens at $\frac{V_{oil}}{V_{init}}$ of about 1000. In addition, Figure 3-5 illustrates that the sodium chloride solution reaches its solubility limit at different oil volumes depending on its initial concentration.
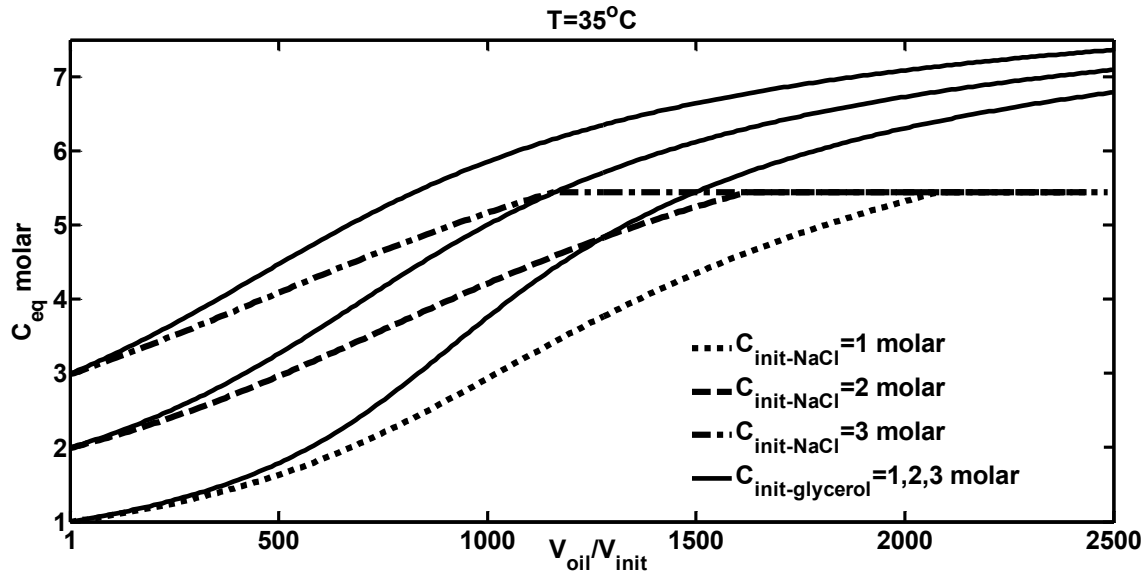
Figure 3-5 Equilibrium concentration of the solutes (glycerol and NaCl) within the drop phase versus the oil-volume-to-initial-drop-volume ratio at different initial concentrations of the solutions at a constant temperature of 35 °C

3.3.2. Equilibrium Size of the Drop

Figures 3-6 and 3-7 show the ratio of equilibrium volume of the drop to its initial volume versus the oil-to-initial-drop-volume ratio at a constant temperature of 35 °C for glycerol and NaCl solutions, respectively, at three different initial concentrations of the solutes. Figure 3-6 indicates that, for glycerol solutions, the equilibrium size of the drop decreases significantly with oil: initial drop volume ratio at lower oil-to-initial-drop-volume ratios. But as the availability of oil increases, the size of the drop appears to reach an asymptote for unlimited solubility agents. This characteristic is completely different for solutes that have a solubility limit (see Figure 3-7). Limited solubility solutes have a similar trend to unlimited solubility agents before reaching their solubility limit. But after the solubility limit is reached, the amount of solute in the liquid drop cannot exceed the saturation amount. So, the solute mole fraction in the drop remains constant while some solute has to leave the drop in solid form. As a result, a certain amount of water also

66
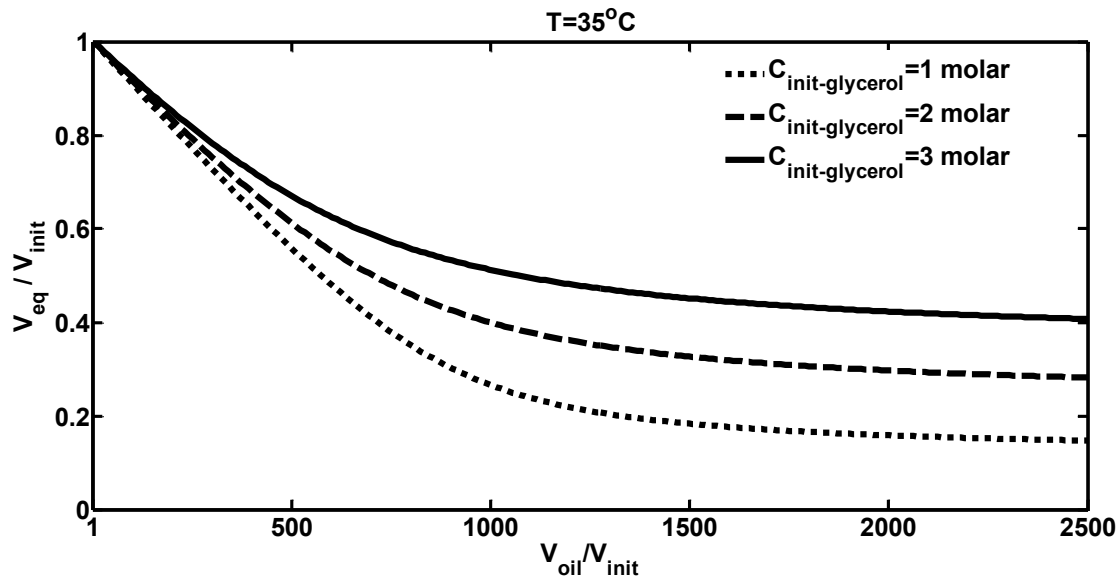
Figure 3-6 Equilibrium volume of the drop (which contains glycerol) per its initial volume versus the oil-volume-to-initial-drop-volume ratio for different initial concentrations of the glycerol solutions at a constant temperature of 35 °C
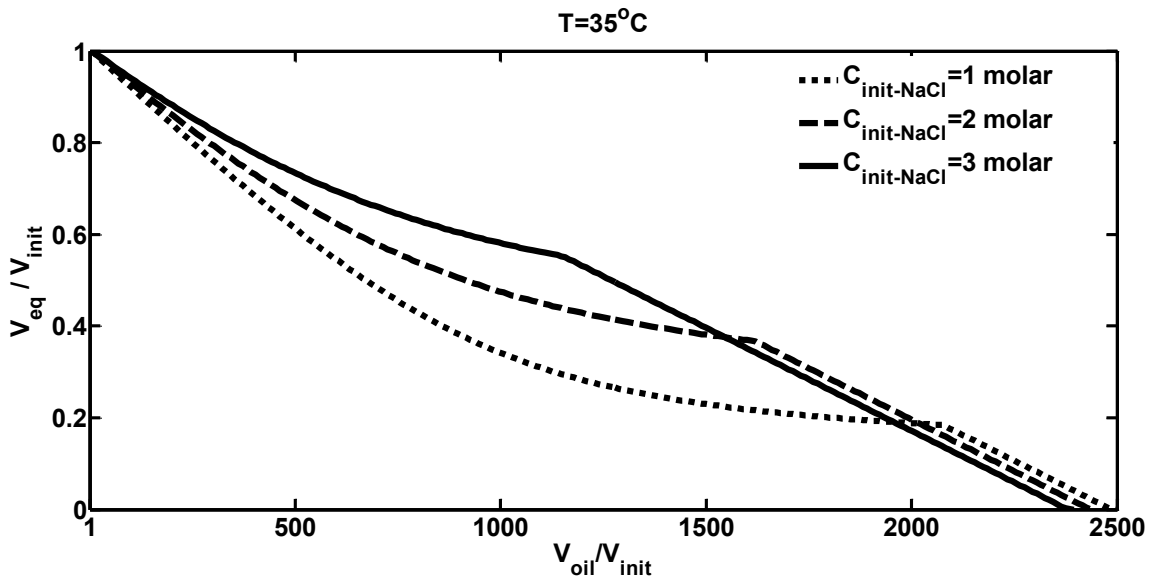
Figure 3-7 Equilibrium volume of the drop (which contains NaCl) per its initial volume versus the oil-volume-to-initial-drop-volume ratio for different initial concentrations of the sodium chloride solutions at a constant temperature of 35 °C

has to leave the drop to keep the chemical potential of water in both phases equal. Consequently, the equilibrium drop volume decreases considerably with oil: initial drop volume ratio after its

saturation limit and the drop can disappear completely if enough oil is available. From Figure 3-6, it can be seen that complete dissolution of drops which contain unlimited solubility agents is not expected even when sufficient oil is present.

In Figure 3-8, the equilibrium volume of the drop containing glycerol is plotted versus the amount of encapsulated solute (the *x*-axis is on a logarithmic scale). Each point on the graph corresponds to a different initial concentration of the solute within the drop. The shape of this curve is very similar to the experimental data obtained by Wu *et al.*[7] for the kinetic concentrating of dextran in aqueous microdrops and similarly plotted. The resemblance of our results with this previous independent experimental work leads to further confidence in our predictions.
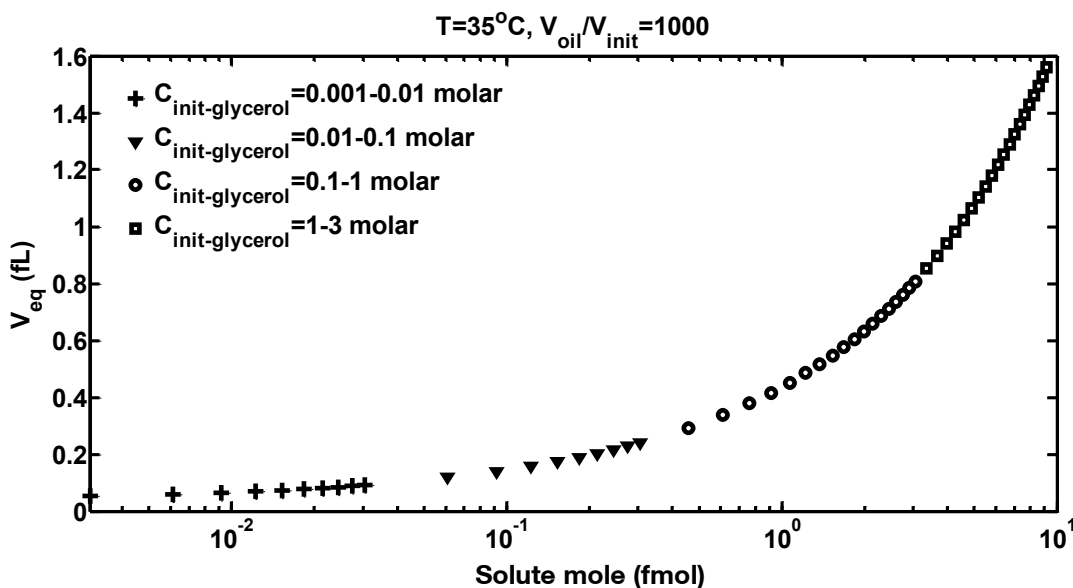
Figure 3-8 Equilibrium volume of the drop (which contains glycerol) versus the number of moles of encapsulated solute at a constant temperature of 35 °C and oil-volume-to-initial-drop-volume ratio of 1000. Each point on the graph corresponds to a different initial concentration of glycerol.

3.3.3. Effect of Temperature

Figures 3-9 and 3-10 show the effect of temperature on the equilibrium concentration at different oil-to-initial-drop-volume ratios for glycerol and sodium chloride solutions respectively. These figures illustrate that increasing the temperature will result in higher equilibrium concentrations in the drops. However, this feature is not valid for limited solubility solutes after reaching their solubility threshold. Although it is difficult to distinguish in Figure 3-10, solubility limit is a function of temperature and these solutes reach slightly different saturation values at different temperatures.
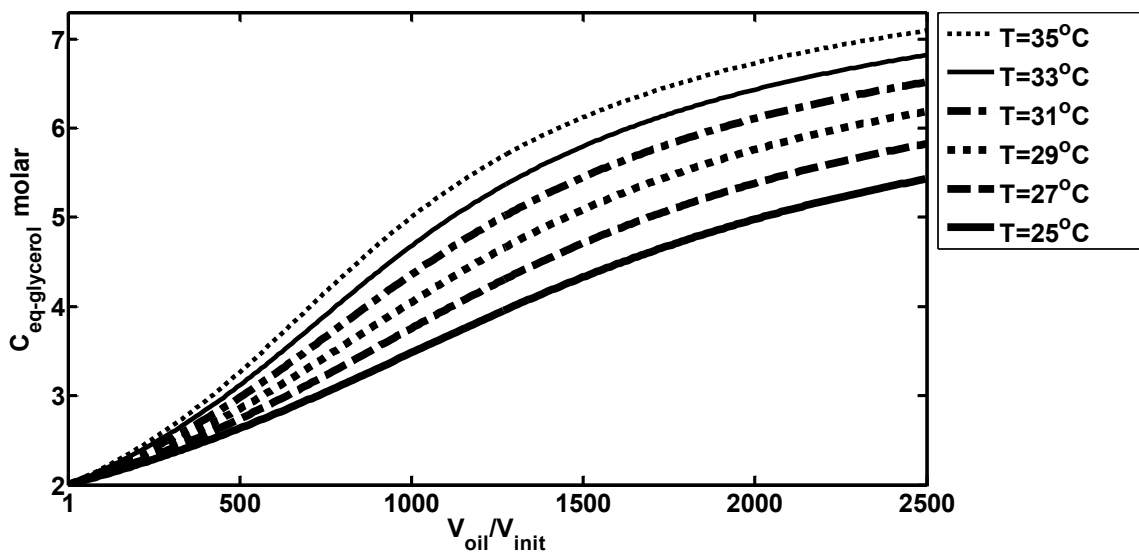
Figure 3-9 Equilibrium concentration of a glycerol aqueous drop versus the oil-volume-to-initial-drop-volume ratio at different temperatures
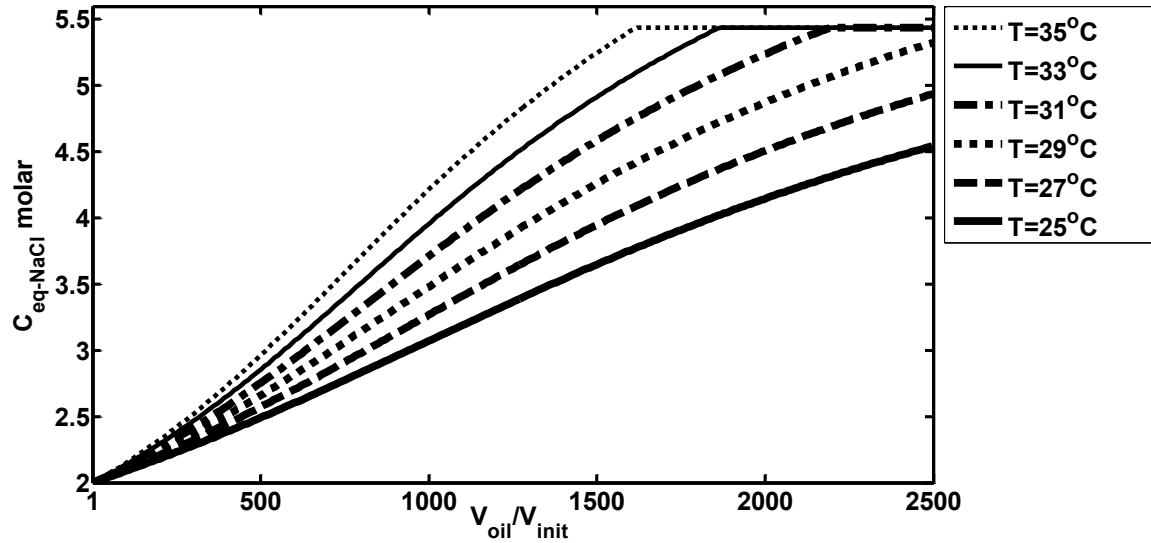
Figure 3-10 Equilibrium concentration of a sodium chloride aqueous drop versus the oil-volume-to-initial-drop-volume ratio at different temperatures

Figures 3-11 and 3-12 show the effect of temperature on the equilibrium size of the drop at various oil-to-initial-drop-volume ratios for glycerol and sodium chloride solutions, respectively. These figures point out that increasing the temperature leads to lower equilibrium size of the drop. This characteristic is more severe for sodium chloride solution since the drop will completely disappear at higher temperatures.
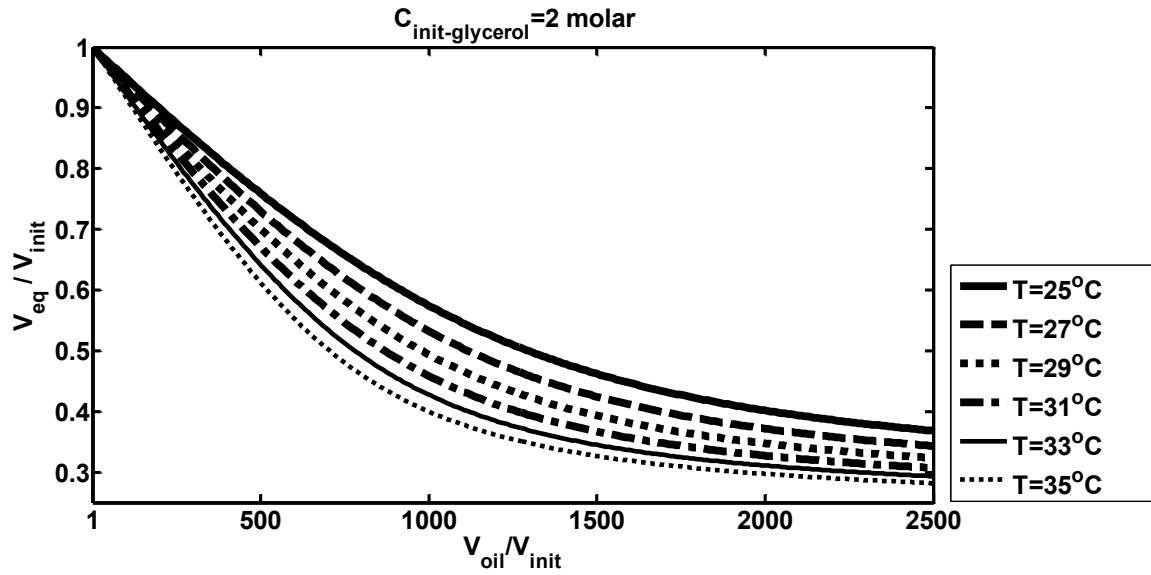
Figure 3-11 Equilibrium volume of the drop (which contains glycerol) per its initial volume versus the oil-volume-to-initial-drop-volume ratio at different temperatures
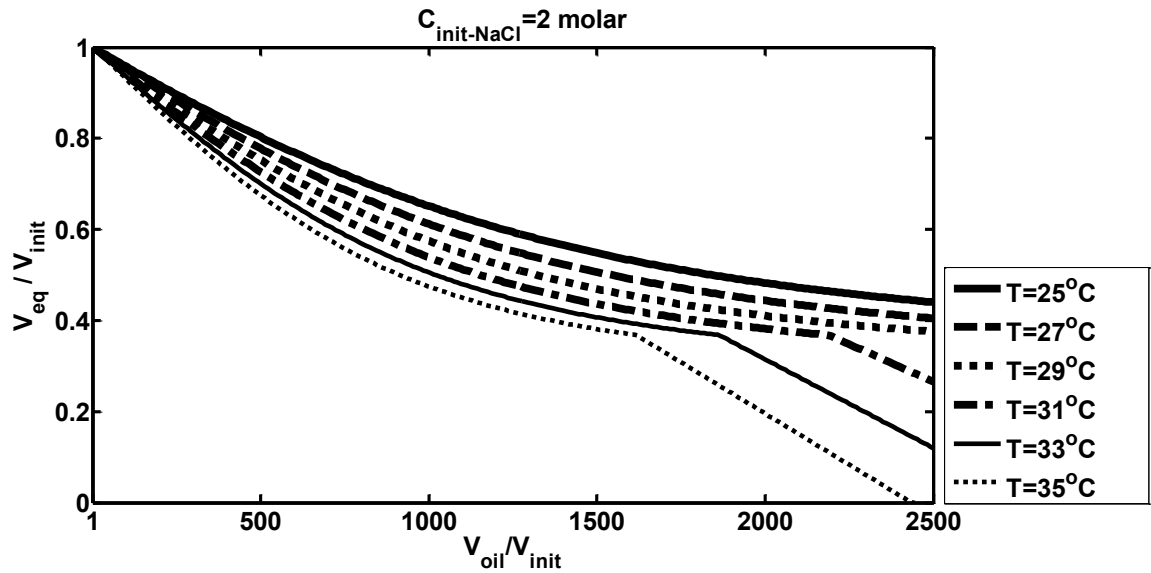
Figure 3-12 Equilibrium volume of the drop (which contains NaCl) per its initial volume versus the oil-volume-to-initial-drop-volume ratio at different temperatures

3.3.4. Precipitated Solute

Figure 3-13 shows the precipitated mass of NaCl per total mass of NaCl at various oil-to-initial-drop-volume ratios for three different initial concentrations of the drop at a constant temperature of 35 °C. This figure clearly shows that precipitation starts and terminates at different amounts of available oil for different initial concentrations of the drop. In addition, by increasing the initial concentration of the solute within the drop, the slope of solute precipitation with respect to availability of the oil in the system decreases.
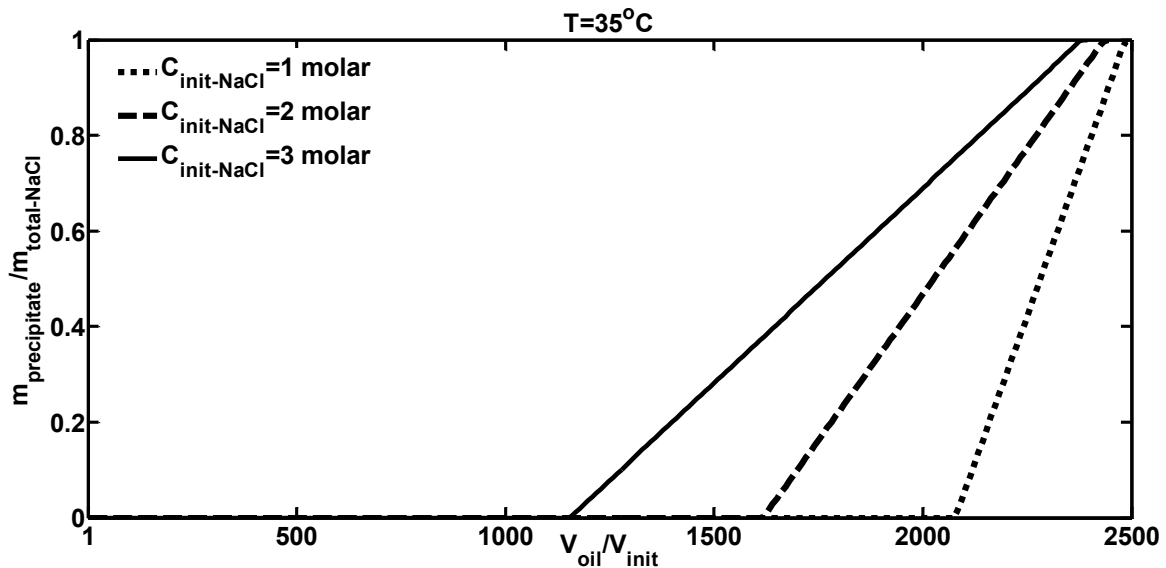
Figure 3-13 Precipitated mass of NaCl per total mass of NaCl at various oil-to-initial-drop-volume ratios for three different initial concentrations of the drop at a constant temperature of 35 °C

3.4. Conclusions

Equilibrium thermodynamic analysis has been done for the process of concentrating solutes within aqueous microdrops for two types of solutes—with and without solubility limits—and the influence of temperature and oil volume on the equilibrium drop volumes and concentrations has been investigated. It is found that by increasing the temperature and volume of the oil in the

system, the equilibrium drop concentrations of both types of solutes will increase. However, for the limited solubility agent this trend is only valid up to its saturation concentration at each temperature, and after reaching that limit the solute concentration in the drop remains constant with the volume of oil in the system and at the saturation concentration as a function of temperature. In addition, based on Figure 3-5, the trend of solute equilibrium concentration with oil volume shows that at a certain amount of oil volume a maximum in the slope of the curve exists. So, in this way, the most effective amount of oil for concentrating process can be found.

Furthermore, the equilibrium size of the drop decreases with increasing oil volume for both types of solutes. However, the decreasing trend is completely altered after reaching the solubility limit. After reaching the saturation limit, the solute starts precipitating in a solid form (and for the sake of simplicity we assumed that it leaves the drop) and the concentration of the solute within the drop has to remain constant at the saturation value. As a result, the solute has to leave the drop in a solid form and water has to leave the drop to equilibrate the water chemical potential between the drop and the oil. Therefore, the equilibrium drop size decreases more significantly with respect to the oil volume so that, in the case of availability of enough oil, the drop will disappear completely.

The insights demonstrated in this paper can be used to more effectively design microdrop concentrating processes of interest in emerging microfluidic technologies.

3.5. References

1. Chiu, D. T. Micro- and Nano-Scale Chemical Analysis of Individual Sub-Cellular Compartments. *TrAC - Trend Anal. Chem.* **2003***, 22*, 528-536.

2. Sgro, A. E.; Allen, P. B.; Chiu, D. T. Thermoelectric Manipulation of Aqueous Droplets in Microfluidic Devices. *Anal. Chem.* **2007***, 79*, 4845-4851.

3. He, M.; Edgar, J. S.; Jeffries, G. D. M.; Lorenz, R. M.; Shelby, J. P.; Chiu, D. T. Selective Encapsulation of Single Cells and Subcellular Organelles into Picoliter- and Femtoliter- Volume Droplets. *Anal. Chem.* **2005***, 77*, 1539-1544.

4. He, M.; Sun, C.; Chiu, D. T. Concentrating Solutes and Nanoparticles within Individual Aqueous Microdroplets. *Anal. Chem.* **2004***, 76*, 1222-1227.

5. Jeffries, G. D. M.; Kuo, J. S.; Chiu, D. T. Dynamic Modulation of Chemical Concentration in an Aqueous Droplet. *Angew. Chem. Int. Ed.* **2007***, 46*, 1326-1328.

6. Bajpayee, A.; Edd, J. F.; Chang, A.; Toner, M. Concentration of Glycerol in Aqueous Microdroplets by Selective Removal of Water. *Anal. Chem.* **2010***, 82*, 1288-1291.

7. Wu, T.; Hirata, K.; Suzuki, H.; Xiang, R.; Tang, Z.; Yomo, T. Shrunk to Femtolitre: Tuning High-Throughput Monodisperse Water-In-Oil Droplet Arrays for Ultra-Small Micro- Reactors. *Appl. Phys. Lett.* **2012***, 101*, 074108.

8. Jeffries, G. D. M.; Kuo, J. S.; Chiu, D. T. Controlled Shrinkage and Re-Expansion of a Single Aqueous Droplet inside an Optical Vortex Trap. *J. Phys.Chem. B.* **2007***, 111*, 2806-2812.

9. Kuo, J. S.; Chiu, D. T. Controlling Mass Transport in Microfluidic Devices. *Annu. Rev. Anal. Chem.* **2011***, 4*, 275-296.

10. Gadd, J. C.; Kuyper, C. L.; Fujimoto, B. S.; Allen, R. W.; Chiu, D. T. Sizing Subcellular Organelles and Nanoparticles Confined within Aqueous Droplets. *Anal. Chem.* **2008***, 80*, 3450-3457.

11. Hilder, M. H. The Solubility of Water in Edible Oils and Fats. *J. Am. Oil Chem. Soc.* **1968***, 45*, 703-707.

12. Prickett, R. C.; Elliott, J. A. W.; McGann, L. E. Application of the Osmotic Virial Equation in Cryobiology. *Cryobiology* **2010***, 60*, 30-42.

13. Elliott, J. A. W.; Prickett, R. C.; Elmoazzen, H. Y.; Porter, K. R.; McGann, L. E. A Multisolute Osmotic Virial Equation for Solutions of Interest in Biology. *J. Phys. Chem. B.* **2007***, 111*, 1775-1785.

14. Pinho, S. P.; Macedo, E. A. Solubility of NaCl, NaBr, and KCl in Water, Methanol, Ethanol, and their Mixed Solvents. *J. Chem. Eng. Data* **2005***, 50*, 29-32.

15. Prickett, R. C.; Elliott, J. A. W.; McGann, L. E. Application of the Multisolute Osmotic Virial Equation to Solutions Containing Electrolytes. *J. Phys. Chem. B.* **2011***, 115*, 14531-14543.

16. Perkins, E. G. In *Physical Properties of Soybeans;* Erickson, D. R., Ed.; Practical Handbook of Soybean Processing and Utilization; AOCS Press: Champaign,IL, 1995; pp 29-38.

17. Wang, T. In *Soybean Oil;* Gunstone, F. D., Ed.; Vegetable Oils in Food Technology : Composition, Properties, and Uses; Blackwell ; CRC Press: Osney Mead, Oxford; Boca Raton, 2002; pp 90-103.

18. Hammond, E. G.; Johnson, L. A.; White, P. J.; Wang, T.; Su, C. In *Soybean Oil;* Shahidi, F., Ed.; Bailey's Industrial Oil and Fat Products; Wiley: New York, 1979; pp 577-653.

19. Novotny, P.; Sohnel, O. Densities of Binary Aqueous Solutions of 306 Inorganic Substances. *J. Chem. Eng. Data* **1988**, *33*, 49-55.

20. Design Institute for Physical Properties, Sponsored,by AIChE DIPPR Project 801 - Full Version.

Chapter 4: Stability Analysis of Microdrops during Concentrating Processes

4.1. Introduction

   Microfluidic technologies are one of the great tools for understanding and exploiting the behavior of a variety of systems by means of micrometer sized fluids. Among these technologies, droplet-based microfluidics—containing micrometer sized droplets of one fluid dispersed in an immiscible continuous phase—provide remarkable features including the compartmentalization of chemical reactions in the closed volume of the droplets, consumption of very small amounts of reagents in drops, high throughput due to formation of a large number of droplets in a short time, formation of monodisperse and miniaturized droplets, higher quantitative control over the reaction and concentration of solutes, and higher mass or heat transfer due to the high surface-to-volume ratio of the droplets.[1-4] Concentrating of solutes and nanoparticles within aqueous microdrops is one of the processes that make use of a drop-based microfluidic platform[5-9] by mass transfer of water between an aqueous drop phase which contains the solutes and a surrounding oil phase which has a minor solubility of water. Therefore, when the water leaves the drop, the drop shrinks and the solute which cannot dissolve into the oil phase is concentrated. Manipulating the concentration and size[10] of the microdrops is very important especially in some biological and cryobiological applications where the solute of interest within the drop is too small to be detected[6] or where time-sensitive preservation of cells[5] at a specific concentration of solute is needed. In addition, in cases where control over the concentration of a tiny amount of materials in two-phase systems is required, this concentration process via dehydration of microdrops is applicable: such as in protein crystallization[11] or in finding the binodal curves[12] of

aqueous two-phase systems. In the case of non-aqueous droplets, such as polymer solution microdroplets, concentrating the polymer via solvent dissolution into the continuous phase may lead to fabrication of toroidal particles.[13] Another application of microdrop concentrating processes is the desalination of water with an energy-efficient method; Bajpayee *et al*.[14] applied dehydration of microdrops to salt solutions in order to precipitate the sodium chloride and extract pure water in water-oil emulsions. Although several dynamic investigations have been done for microdrop concentrating systems,[5-8,12,15,16] to the best of our knowledge we have not found any thermodynamic study of this issue.

In our previous work,[9] we developed a thermodynamic equilibrium description of microdrop concentrating processes which allowed us to investigate the effect of different parameters such as temperature, amount of available oil, initial concentration of the solute, and the solute type from a solubility limit standpoint, providing a basis for the design of microdrop systems. In the previous work, we considered only sets of controlling parameters that corresponded to a single equilibrium state. However, as we shall fully explore here, we find that for certain amounts of available oil in the system more than one equilibrium state can exist. This issue becomes more important for smaller initial sizes of the drop since the different equilibrium states are of more comparable size. If more than one equilibrium state exists for a given set of controlling parameters, then the question arises as to which of these equilibrium states the system will physically adopt in an experimental circumstance. This matter motivates us to perform a free energy analysis of microdrop states during concentrating processes and thereby investigate the thermodynamic stability of different equilibrium states in order to understand which equilibrium state the system will physically adopt and predict the behavior of the system.

Gibbs[17] was the first to perform thermodynamic stability analysis for a one-component single droplet in the constant pressure system of its vapor and found that the system has an unstable equilibrium. From that time onward, several investigations on the stability of heterogeneous[18,19] and homogeneous[20,21] nucleation of droplets or bubbles at different conditions[22-26] have been done. It was found that during nucleation of a drop in the case of constant volume systems,[18,20,27] or addition of a second non-volatile component to the droplets, or nucleation of a bubble out of liquid–gas solution, that stable equilibrium in addition to unstable equilibrium can take place. Actually, in finite volume systems, a small variation of the drop size around the equilibrium affects the vapor phase pressure and the equilibrium state. Similarly, addition of a solute decreases the chemical potential of the liquid and affects the equilibrium states.[27] Knowing the free energy as a function of microdrop size identifies the number of equilibrium states and their stabilities enabling prediction of the physical behavior of the system. This knowledge allows design of microdrop systems more wisely with awareness of the influence of different controlling variables on the final system state.

Therefore, using Gibbs' surface thermodynamics, we have done the free energy analysis for aqueous microdrops containing either glycerol or sodium chloride as examples of unlimited and limited solubility solutes respectively since both of these solutes have been used for previous applications.[5,14] This work is completely theoretical; we have used existing experimental data for the physical and thermodynamic properties of the system wherever needed.

4.2. Governing Equations

Consider a system which includes an aqueous drop that contains a solute, with the drop being placed within soybean oil which is presaturated with water at 25 °C. It has been shown[9] that by

increasing either the temperature or the amount of oil in the system, more water will dissolve into the oil. Hence, the size of the drop will decrease and the solute within the drop will be concentrated. Herein, we analyze the system from the free energy point of view and inspect the stability behavior of different equilibrium states at different available amounts of oil in the system at 35 °C.

We have categorized our work into two parts: first, when the solutes completely dissolve in the water and second, when the solute cannot completely dissolve in the water and some solid precipitate exists in the system. As was mentioned before, we have chosen glycerol and sodium chloride as solutes to be investigated which dissolve completely and partially in the water respectively. Therefore, the first category includes both glycerol and sodium chloride up to its solubility limit in water, and the second category includes sodium chloride after it reaches its solubility limit.

4.2.1. Cases where the Solute Completely Dissolves in Water

4.2.1.1. Solute: Glycerol

Figure 4-1 shows the system schematically. In this case, two phases exist: the drop phase, D, and the liquid phase, L. The drop phase contains water and the solute and the liquid phase includes water and oil. Since the volume of the system is constant, the free energy of each subsystem is considered to be the Helmholtz free energy, F. The free energy of the system is the sum of the free energies of its subsystems:
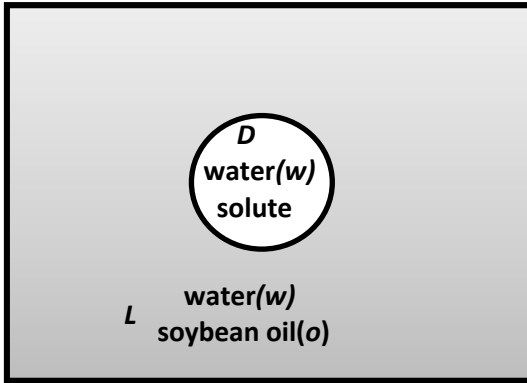
Figure 4-1 Drop of aqueous solution containing an unlimited solubility agent placed within soybean oil

$$F = F^D + F^L + F^{LD} \tag{4-1}$$

where the superscript LD indicates the liquid–drop interface. Substituting the definition of Helmholtz free energy in terms of extensive and intensive parameters into equation (4-1) yields:

$$F = -P^D V^D + \mu_g^D N_g^D + \mu_w^D N_w^D - P^L V^L + \mu_o^L N_o^L + \mu_w^L N_w^L + \sigma^{LD} A^{LD} + \mu_o^{LD} N_o^{LD} + \mu_w^{LD} N_w^{LD} +$$

$$\mu_g^{LD} N_g^{LD} \tag{4-2}$$

where N, V, A, P, μ_i and σ represent the number of moles, volume, area, pressure, chemical potential of component i and surface tension of a phase and subscripts g, w and o denote the glycerol, water and oil components. The constraints on the system can be summarized by the following equations:

$$V^D + V^L = V^t = V_0^D + V_0^L \tag{4-3}$$

$$N_w^D + N_w^L + N_w^{LD} = N_w^t = N_{w,0}^D + N_{w,0}^L + N_{w,0}^{LD} \tag{4-4}$$

$$N_o^L + N_o^{LD} = N_o^t = N_{o,0}^L + N_{o,0}^{LD} \tag{4-5}$$

80

$$N_g^D + N_g^{LD} = N_g^t = N_{g,0}^D + N_{g,0}^{LD} \tag{4-6}$$

where superscript t indicates the total quantity. Since the energy has to be computed with respect to a reference, we have chosen one of the equilibrium states to be the reference point and denote the reference state with subscript 0.

$F - F_0$ can be found by evaluating equation (4-2) at the reference state and subtracting it from equation (4-2) evaluated in any other state. After substituting the constraints of the system, equations (4-3) to (4-6), $F - F_0$ becomes:

$$F - F_0 = -P^D V^D + \mu_g^D N_g^D + \mu_w^D N_w^D - P^L(V_0^D + V_0^L - V^D) + \mu_o^L N_o^L + \mu_w^L N_w^L + \sigma^{LD} A^{LD} +$$

$$\mu_o^{LD}\left(N_{o,0}^L + N_{o,0}^{LD} - N_o^L\right) + \mu_w^{LD}\left(N_{w,0}^D + N_{w,0}^L + N_{w,0}^{LD} - N_w^D - N_w^L\right) + \mu_g^{LD}\left(N_{g,0}^D + N_{g,0}^{LD} - N_g^D\right) +$$

$$P_0^D V_0^D - \mu_{g,0}^D N_{g,0}^D - \mu_{w,0}^D N_{w,0}^D + P_0^L V_0^L - \mu_{o,0}^L N_{o,0}^L - \mu_{w,0}^L N_{w,0}^L - \sigma_0^{LD} A_0^{LD} - \mu_{o,0}^{LD} N_{o,0}^{LD} - \mu_{w,0}^{LD} N_{w,0}^{LD} -$$

$$\mu_{g,0}^{LD} N_{g,0}^{LD} \tag{4-7}$$

where R_0 is the radius of the drop at the reference point. We further assume that:

$$P_0^L = P^L \tag{4-8}$$

$$\sigma_0^{LD} = \sigma^{LD} \tag{4-9}$$

Since both the drop phase and the liquid phase are incompressible liquids it is acceptable to assume that the liquid phase pressure is constant. By substituting equations (4-8) and (4-9) into equation (4-7), the expression for $F - F_0$ becomes:

$$F - F_0 = -(P^D - P^L)V^D + \left(\mu_g^D - \mu_g^{LD}\right)N_g^D + \left(\mu_w^D - \mu_w^{LD}\right)N_w^D + \left(\mu_o^L - \mu_o^{LD}\right)N_o^L + \left(\mu_w^L -\right.$$

$$\left.\mu_w^{LD}\right)N_w^L + \sigma^{LD}\left(A^{LD} - A_0^{LD}\right) + \left(\mu_o^{LD} - \mu_{o,0}^{LD}\right)N_{o,0}^{LD} + \left(\mu_w^{LD} - \mu_{w,0}^{LD}\right)N_{w,0}^{LD} + \left(\mu_g^{LD} - \mu_{g,0}^{LD}\right)N_{g,0}^{LD} +$$

$$(P_0^D - P_0^L)V_0^D + (\mu_g^{LD} - \mu_{g,0}^D)N_{g,0}^D + (\mu_w^{LD} - \mu_{w,0}^D)N_{w,0}^D + (\mu_o^{LD} - \mu_{o,0}^L)N_{o,0}^L + (\mu_w^{LD} - \mu_{w,0}^L)N_{w,0}^L$$

$$(4\text{-}10)$$

In addition, since we have chosen the reference state to be an equilibrium state, the following relations are valid for the reference state:

$$\mu_{w,0}^D = \mu_{w,0}^L = \mu_{w,0}^{LD} = \mu_{w,0}^{eq} \tag{4-11}$$

$$\mu_{o,0}^L = \mu_{o,0}^{LD} = \mu_{o,0}^{eq} \tag{4-12}$$

$$\mu_{g,0}^D = \mu_{g,0}^{LD} = \mu_{g,0}^{eq} \tag{4-13}$$

$$P_0^D - P_0^L = \frac{2\sigma^{LD}}{R_0} \tag{4-14}$$

Since we are going to investigate the free energy around the equilibrium states, the conditions for equilibrium on intensive properties should be substituted in the free energy. The equilibrium conditions are:

$$\mu_w^D = \mu_w^L = \mu_w^{LD} = \mu_w^{eq} \tag{4-15}$$

$$\mu_o^L = \mu_o^{LD} = \mu_o^{eq} \tag{4-16}$$

$$\mu_g^D = \mu_g^{LD} = \mu_g^{eq} \tag{4-17}$$

$$P^D - P^L = \frac{2\sigma^{LD}}{R_c} \tag{4-18}$$

where R_c is the Kelvin radius. Now by inserting the reference point equilibrium conditions, equations (4-11) to (4-14), and the equilibrium conditions, equations (4-15) to (4-18), into equation (4-10) we find:

$$F - F_0 = -\left(\frac{2\sigma^{LD}}{R_c}\right)(V^D) + \sigma^{LD}(A^{LD} - A_0^{LD}) + \left(\mu_o^{eq} - \mu_{o,0}^{eq}\right)\left(N_{o,0}^{LD} + N_{o,0}^{L}\right) + \left(\mu_w^{eq} - \right.$$

$$\left. \mu_{w,0}^{eq}\right)\left(N_{w,0}^{L} + N_{w,0}^{D} + N_{w,0}^{LD}\right) + \left(\mu_g^{eq} - \mu_{g,0}^{eq}\right)\left(N_{g,0}^{LD} + N_{g,0}^{D}\right) + \left(\frac{2\sigma^{LD}}{R_0}\right)(V_0^D) \qquad (4\text{-}19)$$

Considering the drop to be a sphere, by substituting the volume and area of the sphere for V^D and A^{LD} and by making use of equations (4-4) to (4-6) the free energy relation is equal to:

$$F - F_0 = -\left(\frac{2\sigma^{LD}}{R_c}\right)\left(\frac{4}{3}\pi R^3\right) + \sigma^{LD}(4\pi R^2 - 4\pi R_0^2) + N_o^t\left(\mu_o^{eq} - \mu_{o,0}^{eq}\right) + N_w^t\left(\mu_w^{eq} - \mu_{w,0}^{eq}\right) +$$

$$N_g^t\left(\mu_g^{eq} - \mu_{g,0}^{eq}\right) + \left(\frac{2\sigma^{LD}}{R_0}\right)\left(\frac{4}{3}\pi R_0^3\right) \qquad (4\text{-}20)$$

It should be noted that although both μ_i^{eq} and $\mu_{i,0}^{eq}$ for the component i, are at equilibrium states, we have assumed them not to be the same. This means that in the case of more than one equilibrium state, $\mu_i^{eq} - \mu_{i,0}^{eq}$ has a definite value and in the case of just one equilibrium state this difference would be equal to zero. In addition, for the sake of simplification we ignore the presence of each of the components at the interfaces, which means: $N_w^{LD} = N_g^{LD} = N_o^{LD} = 0$

The chemical potentials of water and oil in the liquid phase are given by the following equations:

$$\mu_w^L(T, P^L, x_w^L) = \mu_w^0(T, P^L) + R_u T ln(\gamma_w^L x_w^L) \qquad (4\text{-}21)$$

$$\mu_o^L(T, P^L, x_o^L) = \mu_o^0(T, P^L) + R_u T ln(\gamma_o^L x_o^L) \qquad (4\text{-}22)$$

where R_u, T, x and γ are universal gas constant, temperature, mole fraction and activity coefficient. The activity coefficient of water in soybean oil is given by the following equation:[9,28]

$$\gamma_w^L = \frac{1617}{T} - 2.9 \tag{4-23}$$

Since the activity coefficient of water in soybean oil depends only on temperature, based on the Gibbs–Duhem relation, the activity coefficient of soybean oil in the liquid phase will also depend only on temperature. The chemical potentials of water and glycerol in the drop phase are defined based on osmotic virial equations as follows:

$$\mu_w^D(T, P^D, x_g^D) = \mu_w^0(T, P^L) + v_w(P^D - P^L) - R_u T \left[x_g^D + B_g^*(x_g^D)^2 + \cdots \right] \tag{4-24}$$

$$\mu_g^D(T, P^D, x_g^D) = \mu_g^D(T, P^L) + v_g(P^D - P^L) + R_u T \left(1 - B_g^* + \ln(x_g^D) - x_g^D + 2B_g^* \left(x_g^D - \right. \right.$$
$$\left. \left. \frac{1}{2}(x_g^D)^2 \right) + \cdots \right) \tag{4-25}$$

where equation (4-25) is found based on the Gibbs–Duhem relation and B^* is the second osmotic virial coefficient on a mole fraction basis; we used the value of 3.169 for B_g^*.[9,29,30]

Since the oil is present only in the L phase, the oil component chemical potential difference between the two equilibrium states is given by:

$$\mu_o^{eq} - \mu_{o,0}^{eq} = \mu_o^L - \mu_{o,0}^L = R_u T \ln \left(\frac{x_o^L}{x_{o,0}^L} \right) \tag{4-26}$$

Since water is present in both D and L phases, the water chemical potential difference between the two equilibrium states can be evaluated by either of the following equations:

$$\mu_w^{eq} - \mu_{w,0}^{eq} = \mu_w^L - \mu_{w,0}^L = R_u T ln\left(\frac{x_w^L}{x_{w,0}^L}\right) \tag{4-27}$$

$$\mu_w^{eq} - \mu_{w,0}^{eq} = \mu_w^D - \mu_{w,0}^D = v_w(P^D - P_0^D) - R_u T\left(x_g^D - x_{g,0}^D + B_g^*\left(x_g^{D^2} - x_{g,0}^{D^2}\right)\right) \tag{4-28}$$

The first term on the right hand side of equation (4-28) is due to the difference in pressure within the drop at two different equilibrium states. It can be simplified by first subtracting and adding P^L:

$$v_w(P^D - P_0^D) = v_w(P^D - P^L + P^L - P_0^D) = v_w\left(\frac{2\sigma^{LD}}{R_c} - \frac{2\sigma^{LD}}{R_0}\right) \tag{4-29}$$

where the second equality comes from the equality of P^L and P_0^L and using the Laplace equation. Using equation (4-29), we can simplify equation (4-28) to the following:

$$\mu_w^{eq} - \mu_{w,0}^{eq} = \mu_w^D - \mu_{w,0}^D = v_w\left(\frac{2\sigma^{LD}}{R_c} - \frac{2\sigma^{LD}}{R_0}\right) - R_u T\left(x_g^D - x_{g,0}^D + B_g^*\left(x_g^{D^2} - x_{g,0}^{D^2}\right)\right) \tag{4-30}$$

The chemical potential difference between the two equilibrium states in the case of glycerol, since it is present only in the drop phase, is given by:

$$\mu_g^{eq} - \mu_{g,0}^{eq} = \mu_g^D - \mu_{g,0}^D = v_g\left(\frac{2\sigma^{LD}}{R_c} - \frac{2\sigma^{LD}}{R_0}\right) + R_u T\left[\left(ln\left(\frac{x_g^D}{x_{g,0}^D}\right) - x_g^D + x_{g,0}^D\right) + 2B_g^*\left(x_g^D - x_{g,0}^D - \right.\right.$$

$$\left.\left.\frac{x_g^{D^2}}{2} + \frac{x_{g,0}^{D^2}}{2}\right)\right] \tag{4-31}$$

where again the first term on the right hand side of equation (4-31) is due to the pressure difference within the drop for two different equilibrium states.

The Kelvin radius, R_c can be found by simultaneously solving the Laplace equation and the equality of chemical potentials of water in the oil and the drop phase. As a result, R_c is given by:

$$R_c = \frac{2\sigma^{LD} v_w}{R_u T \left(x_g^D + B_g^* x_g^{D^2} + ln(\gamma_w^L x_w^L) \right)} \tag{4-32}$$

Since we are going to plot $F(R) - F_0$ versus R, we have to substitute R_c as a function of R. In order to find the dependence of R_c on R, we have to consider a drop with radius R, which is not necessarily in an equilibrium state, and define the mole fractions of components in terms of R. Since both solutes, glycerol and sodium chloride, have a very small partition coefficient in soybean oil the solutes cannot leave the drop. Therefore, we can find the mole fraction of glycerol within the drop at each R by equating equations (4-33) and (4-34):

$$N_w^D = N_g^{init} \frac{(1 - x_g^D)}{x_g^D} \tag{4-33}$$

$$N_w^D = \left(\frac{4}{3} \pi R^3 \rho^D - N_g^{init} M_g \right) \frac{1}{M_w} \tag{4-34}$$

where N and M represent the number of moles and molar mass, respectively, and superscript *init* denotes initial. The density of the drop, ρ^D, is given by:

$$\rho^D = \frac{1}{\frac{w_g^D}{\rho_g} + \frac{w_w^D}{\rho_w}} = \frac{1}{\frac{x_g^D \frac{M_g}{M^D}}{\rho_g} + \frac{\left(1 - x_g^D \frac{M_g}{M^D}\right)}{\rho_w}} \tag{4-35}$$

where w is the mass fraction. The right hand side of equation (4-35) is found by definition of mass fraction in terms of mole fraction $w_g^D = x_g^D \frac{M_g}{M^D}$. In addition the molar mass of the drop is equal to:

$$M^D = x_g^D M_g + x_w^D M_w = x_g^D M_g + (1 - x_g^D) M_w \tag{4-36}$$

By equating equations (4-33) and (4-34) and substituting equations (4-35) and (4-36) into them, the following relation is found which gives x_g^D for each radius of the drop, R:

$$N_g^{init} \frac{(1-x_g^D)}{x_g^D} - \left(\frac{4}{3}\pi R^3 \frac{1}{\dfrac{x_g^D \frac{M_g}{\left(x_g^D M_g + (1-x_g^D)M_w\right)}}{\rho_g} + \dfrac{\left(1-x_g^D \frac{M_g}{\left(x_g^D M_g + (1-x_g^D)M_w\right)}\right)}{\rho_w}} - N_g^{init} M_g \right) \frac{1}{M_w} = 0 \tag{4-37}$$

Since the total moles of water, N_w^t, and the initial moles of oil, N_o^{init}, in the system are known and water can be either in the drop phase or the liquid phase, the mole fraction of water within the liquid phase can be calculated using the following relations:

$$N_w^L = N_w^t - N_w^D = N_w^t - N_g^{init} \frac{(1-x_g^D)}{x_g^D} \tag{4-38}$$

$$x_w^L = \frac{N_w^L}{N_w^L + N_o^{init}} = \frac{N_w^t - N_g^{init}\frac{(1-x_g^D)}{x_g^D}}{N_w^t - N_g^{init}\frac{(1-x_g^D)}{x_g^D} + N_o^{init}} \tag{4-39}$$

So by substituting the x_g^D obtained from solving equation (4-37) into equation (4-39), x_w^L is found. In addition, the dependencies of x_w^D and x_o^L on R are then found via the following relations:

$$x_w^D = 1 - x_g^D \tag{4-40}$$

$$x_o^L = 1 - x_w^L \tag{4-41}$$

Looking back to equation (4-20), it can be seen that all the variables are now defined completely except for R_0 and the related parameters such as $x^L_{w,0}$, $x^D_{w,0}$, $x^D_{g,0}$ and $x^L_{o,0}$. As was mentioned earlier, R_0 is the radius of one of the equilibrium states of the system. In order to find the equilibrium size of the system we have to plot the curve of R_c (equation (4-32)) versus R.[20,27] The intersections of this curve with the 45° line (where R_c=R) determine the equilibrium sizes of the system. We choose one of these equilibrium sizes as R_0 and by substituting this size in equations (4-37) and (4-39) to (4-41) the corresponding $x^D_{g,0}$, $x^L_{w,0}$, $x^D_{w,0}$ and $x^L_{o,0}$ would be obtained. Hence, by having all the variables we can draw $F(R) - F_0$ versus R and analyze the stability of the equilibrium states.

4.2.1.2. Solute: NaCl (Before Precipitation, *i.e.*, when NaCl Is Completely Dissolved in Water)

When the drop contains a limited solubility solute, the solute starts to precipitate after reaching its saturation solubility. So before reaching the solubility limit, since NaCl completely dissolves in water, its free energy calculation is similar to the case of glycerol as a solute within the drop. Therefore, equation (4-20) may be written for the case of sodium chloride:

$$F - F_0 = -\left(\frac{2\sigma^{LD}}{R_c}\right)\left(\frac{4}{3}\pi R^3\right) + \sigma^{LD}(4\pi R^2 - 4\pi R_0^2) + N^t_o\left(\mu^{eq}_o - \mu^{eq}_{o,0}\right) + N^t_w\left(\mu^{eq}_w - \mu^{eq}_{w,0}\right) +$$

$$N^t_{NaCl}\left(\mu^{eq}_{NaCl} - \mu^{eq}_{NaCl,0}\right) + \left(\frac{2\sigma^{LD}}{R_0}\right)\left(\frac{4}{3}\pi R_0^3\right) \tag{4-42}$$

The chemical potentials of water and sodium chloride in the drop phase are given in terms of osmotic virial equations as follows respectively:

$$\mu^D_w(T, P^D, x^D_{NaCl}) =$$

$$\mu^0_w(T, P^L) + v_w(P^D - P^L) - R_u T\left[k^*_{diss,NaCl}x^D_{NaCl} + B^*_{NaCl}\left(k^*_{diss,NaCl}x^D_{NaCl}\right)^2 + \cdots\right] \tag{4-43}$$

$$\mu_{NaCl}^D(T, P^D, x_{NaCl}^D) = \mu_{NaCl}^D(T, P^L) + v_{NaCl}(P^D - P^L) + R_u T \left[k_{diss,NaCl}^* - B_{NaCl}^* k_{diss,NaCl}^{*}{}^2 + \right.$$

$$\left. k_{diss,NaCl}^* \ln(x_{NaCl}^D) - k_{diss,NaCl}^* x_{NaCl}^D + 2 B_{NaCl}^* k_{diss,NaCl}^{*}{}^2 \left(x_{NaCl}^D - \frac{1}{2} x_{NaCl}^{D}{}^2 \right) + \cdots \right] \quad (4\text{-}44)$$

where k_{diss}^* is an empirical electrolyte constant; we used the values of 3.8 and 1.644 for B_{NaCl}^*

and $k_{diss,NaCl}^*$ respectively.[9,29-31] All the terms in equation (4-42) are similar to equation (4-20)

except for $\left(\mu_w^{eq} - \mu_{w,0}^{eq} \right)$ and $\left(\mu_{NaCl}^{eq} - \mu_{NaCl,0}^{eq} \right)$. The former one in terms of the water in the drop

phase is given by:

$$\mu_w^D - \mu_{w,0}^D = v_w \left(\frac{2\sigma^{LD}}{R_c} - \frac{2\sigma^{LD}}{R_0} \right) - R_u T \left(k_{diss,NaCl}^* \left(x_{NaCl}^D - x_{NaCl,0}^D \right) + \right.$$

$$\left. B_{NaCl}^* k_{diss,NaCl}^{*}{}^2 \left(x_{NaCl}^{D}{}^2 - x_{NaCl,0}^{D}{}^2 \right) \right) \quad (4\text{-}45)$$

and the latter one is given by:

$$\mu_{NaCl}^D - \mu_{NaCl,0}^D = v_{NaCl} \left(\frac{2\sigma^{LD}}{R_c} - \frac{2\sigma^{LD}}{R_0} \right) + R_u T \left[k_{diss,NaCl}^* \left(\ln \left(\frac{x_{NaCl}^D}{x_{NaCl,0}^D} \right) - x_{NaCl}^D + x_{NaCl,0}^D \right) + \right.$$

$$\left. 2 B_{NaCl}^* k_{diss,NaCl}^{*}{}^2 \left(x_{NaCl}^D - x_{NaCl,0}^D - \frac{x_{NaCl}^{D}{}^2}{2} + \frac{x_{NaCl,0}^{D}{}^2}{2} \right) \right] \quad (4\text{-}46)$$

In addition, the density of the drop, ρ^D, in the case of sodium chloride solution is given by:[32]

$$\rho^D = \rho_{water} + 44.85c - 0.09634cT + 0.6136 \times 10^{-3} cT^2 - 2.712 c^{1.5} + 1.009 \times 10^{-2} c^{1.5} T$$

$$(4\text{-}47)$$

The Kelvin radius, which comes from solving simultaneously the Laplace equation and the

equality of the chemical potentials of water within the drop and within the liquid phase, would be

equal to:

$$R_c = \frac{2\sigma^{LD}v_w}{R_uT\left(k^*_{diss,NaCl}x^D_{NaCl}+B^*_{NaCl}k^{*}_{diss,NaCl}{}^2 x^D_{NaCl}{}^2 +ln(\gamma^L_w x^L_w)\right)} \tag{4-48}$$

In order to find the x^D_{NaCl} at each R, similar to what we have done for glycerol, we equate equations (4-33) and (4-34) except that we replace subscript g with NaCl which means:

$$N^D_w = N^{init}_{NaCl}\frac{(1-x^D_{NaCl})}{x^D_{NaCl}} \tag{4-49}$$

$$N^D_w = \left(\frac{4}{3}\pi R^3\rho^D - N^{init}_{NaCl}M_{NaCl}\right)\frac{1}{M_w} \tag{4-50}$$

Equating equation (4-49) with (4-50) yields:

$$N^{init}_{NaCl}\frac{(1-x^D_{NaCl})}{x^D_{NaCl}} - \left(\frac{4}{3}\pi R^3\rho^D - N^{init}_{NaCl}M_{NaCl}\right)\frac{1}{M_w} = 0 \tag{4-51}$$

In the case of sodium chloride solution ρ^D is governed by equation (4-47), so that x^D_{NaCl} must be found by solving equation (4-51) by trial and error. For the rest of the required relations, we can replace g with NaCl. Then, we can analyze the stability of the microdrop containing NaCl before its precipitation by drawing $F(R) - F_0$, equation (4-42), versus the size of the drop.

4.2.2. Cases where the Solute Cannot Completely Dissolve in Water and Some Solid Precipitate Exists in the System

4.2.2.1. Solute: NaCl (After it Reaches its Solubility Limit in Water)

When the drop contains a limited solubility solute such as sodium chloride, after the solubility limit is reached the solute starts to precipitate in solid form.
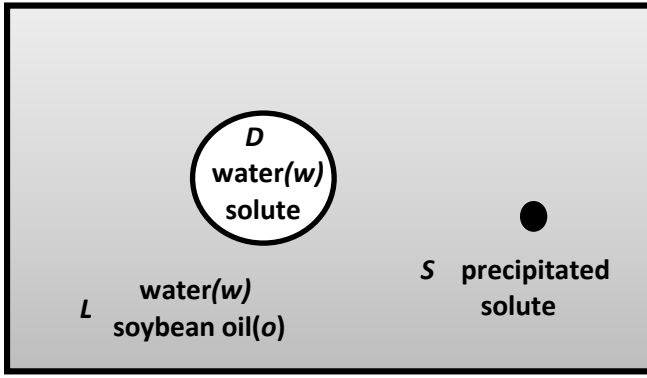
Figure 4-2 Drop of aqueous solution containing a limited solubility agent placed within soybean oil.

After precipitation of the solute, the solid phase is present in the system. The free energy of the system is thus:

$$F = F^D + F^L + F^{LD} + F^S + F^{SL} \tag{4-52}$$

where superscripts S and SL represent the solid phase and the solid–liquid interface, respectively. Substituting the definition of Helmholtz free energy in terms of extensive and intensive parameters into equation (4-52) yields:

$$F = -P^D V^D + \mu_{NaCl}^D N_{NaCl}^D + \mu_w^D N_w^D - P^L V^L + \mu_o^L N_o^L + \mu_w^L N_w^L + \sigma^{LD} A^{LD} + \mu_o^{LD} N_o^{LD} +$$

$$\mu_w^{LD} N_w^{LD} + \mu_{NaCl}^{LD} N_{NaCl}^{LD} - P^S V^S + \mu_{NaCl}^S N_{NaCl}^S + \sigma^{SL} A^{SL} + \mu_o^{SL} N_o^{SL} + \mu_w^{SL} N_w^{SL} + \mu_{NaCl}^{SL} N_{NaCl}^{SL}$$

$$\tag{4-53}$$

The constraints are similar to equations (4-3) to (4-6) except that there is a solid phase in addition to liquid and drop phases in the system:

$$V^D + V^L + V^S = V^t = V_0^D + V_0^L + V_0^S \tag{4-54}$$

$$N_w^D + N_w^L + N_w^{LD} + N_w^{SL} = N_w^t = N_{w,0}^D + N_{w,0}^L + N_{w,0}^{LD} + N_{w,0}^{SL} \tag{4-55}$$

$$N_o^L + N_o^{LD} + N_o^{SL} = N_o^t = N_{o,0}^L + N_{o,0}^{LD} + N_{o,0}^{SL} \tag{4-56}$$

$$N_{NaCl}^D + N_{NaCl}^{LD} + N_{NaCl}^S + N_{NaCl}^{SL} = N_{NaCl}^t = N_{NaCl,0}^D + N_{NaCl,0}^{LD} + N_{NaCl,0}^S + N_{NaCl,0}^{SL} \tag{4-57}$$

Again, the reference state is chosen as one of the equilibrium states. So, the reference point properties are similar to equations (4-11) to (4-14) except that solid phase is present in the system in addition to liquid and drop phases:

$$\mu_{w,0}^D = \mu_{w,0}^L = \mu_{w,0}^{LD} = \mu_{w,0}^{SL} = \mu_{w,0}^{eq} \tag{4-58}$$

$$\mu_{o,0}^L = \mu_{o,0}^{LD} = \mu_{o,0}^{SL} = \mu_{o,0}^{eq} \tag{4-59}$$

$$\mu_{NaCl,0}^D = \mu_{NaCl,0}^{LD} = \mu_{NaCl,0}^{SL} = \mu_{NaCl,0}^S = \mu_{NaCl,0}^{eq} \tag{4-60}$$

$$P_0^D - P_0^L = \frac{2\sigma^{LD}}{R_0} \tag{4-61}$$

$$P_0^S - P_0^L = \frac{2\sigma^{LD}}{R_{so}} \tag{4-62}$$

where R_{so} is the radius of the solid at the reference point. We further assume that:

$$\sigma_0^{SL} = \sigma^{SL} \tag{4-63}$$

In addition, at equilibrium the following relations are valid which are similar to equations (4-15) to (4-18) while the solid phase is present:

$$\mu_w^D = \mu_w^L = \mu_w^{LD} = \mu_w^{SL} = \mu_w^{eq} \tag{4-64}$$

$$\mu_o^L = \mu_o^{LD} = \mu_o^{SL} = \mu_o^{eq} \tag{4-65}$$

$$\mu_{NaCl}^D = \mu_{Nacl}^{LD} = \mu_{Nacl}^{SL} = \mu_{Nacl}^S = \mu_{NaCl}^{eq} \tag{4-66}$$

$$P^S - P^L = \frac{2\sigma^{SL}}{R_{Sc}} \tag{4-67}$$

where R_{Sc} is the Kelvin radius for the solid phase. Now by subtracting F_0 from F we find:

$$F - F_0 = -\left(\frac{2\sigma^{LD}}{R_c}\right)\left(\frac{4}{3}\pi R^3\right) + \sigma^{LD}(4\pi R^2 - 4\pi R_0^2) + N_o^t\left(\mu_o^{eq} - \mu_{o,0}^{eq}\right) + N_w^t\left(\mu_w^{eq} - \mu_{w,0}^{eq}\right) +$$

$$N_{NaCl}^t\left(\mu_{NaCl}^{eq} - \mu_{NaCl,0}^{eq}\right) + \left(\frac{2\sigma^{LD}}{R_0}\right)\left(\frac{4}{3}\pi R_0^3\right) - \left(\frac{2\sigma^{SL}}{R_{Sc}}\right)\left(\frac{4}{3}\pi R_S^3\right) + \sigma^{SL}(4\pi R_S^2 - 4\pi R_{S0}^2) +$$

$$\left(\frac{2\sigma^{SL}}{R_{S0}}\right)\left(\frac{4}{3}\pi R_{S0}^3\right) \tag{4-68}$$

Here, for the sake of simplicity, we have assumed that solid–liquid interfacial tension has no role in the precipitation process, accomplished by setting $\sigma^{SL} = 0$; we are going to consider this role in future work. Actually, by assuming $\sigma^{SL} = 0$, the solid pressure and the liquid pressure are equal and since we have assumed $P^L = P_0^L$, it leads to the equality of P^S and P_0^S. We have also neglected the role of pressure on the solubility limit of the salt within the drop. Thus, we assume that after precipitation at each temperature x_{NaCl}^D is constant and equal to the saturation mole fraction and would not be found by equating chemical potentials in a solid–liquid equilibrium calculation. (These assumptions affect the minima of the free energy diagrams a small amount but they do not change the results qualitatively). Therefore, the solubility limit only depends on temperature and this dependency was found by curve fitting experimental data[33] and is equal to:

$$w_{NaCl}^{limit} = 1.374 \times 10^{-6}T^2 - 6.899 \times 10^{-4}T + 0.3484 \qquad ,T \text{ in K} \tag{4-69}$$

where w_{NaCl}^{limit} is the saturation weight fraction of sodium chloride in solution with water. So after precipitation x_{NaCl}^D is constant and is equal to x_{NaCl}^{limit} for any R which is such that precipitation results. Since after precipitation both x_{NaCl}^D and $x_{NaCl,0}^D$ are equal to x_{NaCl}^{limit} and we have neglected

the role of pressure difference between the solid and the drop phase on the solubility limit, we

have $\mu_{NaCl}^{eq} - \mu_{NaCl,0}^{eq} = 0$. By considering these assumptions, the equation (4-68) will simplify

to:

$$F - F_0 = -\left(\frac{2\sigma^{LD}}{R_c}\right)\left(\frac{4}{3}\pi R^3\right) + \sigma^{LD}(4\pi R^2 - 4\pi R_0^2) + N_o^t\left(\mu_o^{eq} - \mu_{o,0}^{eq}\right) + N_w^t\left(\mu_w^{eq} - \mu_{w,0}^{eq}\right) +$$

$$\left(\frac{2\sigma^{LD}}{R_0}\right)\left(\frac{4}{3}\pi R_0^3\right) \tag{4-70}$$

As a result, if solving equation (4-51) results in $x_{NaCl}^D > x_{NaCl}^{limit}$, we should substitute x_{NaCl}^D

with x_{NaCl}^{limit} in all the relations and then we can find the free energy of the system after the

precipitation occurred.

4.3. Results and Discussion

We choose two different initial diameters for the drop ($a_1 = 18 \times 10^{-6}$ m and $a_2 = 18 \times 10^{-8}$ m) and

an initial temperature and concentration of the solute of 25 °C and 2 molar and investigate the

role of available oil and initial size of the drop on the behavior of the system with respect to

stability of equilibrium drops at constant temperature of 35 °C.

4.3.1. Cases where the Solute Completely Dissolves in Water

4.3.1.1. Solute: Glycerol

Here we are going to plot $F - F_0$ for an unlimited solubility solute such as glycerol. As was

mentioned previously, the first step in plotting the free energy is to find the reference equilibrium

size of the drop, R_0. Therefore, we have to plot two curves of $Y_1 = R_c$ (equation (4-32)) and $Y_2 = R$

versus R to find R_0 which is one of the intersections of these two curves; recall that intersections

indicate equilibrium states. In order to draw $Y_1 = R_c$, equation (4-32), we need to have x_g^D at each

R. Changing the radius of the drop from zero to its initial radius; we solve equation (4-37) for x_g^D at each specific *R*. It was found that for drop sizes smaller than a specific size of the drop x_g^D becomes negative which means that the drop cannot be smaller than a specific size and never shrinks completely.

Figure 4-3 shows these curves ($Y_1=R_c$ and $Y_2=R$) for two different volumes of oil per initial volume of the drop when the initial drop diameters are 18×10^{-6} m and 18×10^{-8} m. As can be seen in Figure 4-3, the curves do not exist for drop sizes smaller than about 4.7×10^{-6} m and 4.7×10^{-8} m respectively, since at these ranges the mole fraction of the glycerol within the drop, x_g^D, would be negative. It should be mentioned that, as is clear from equation (4-37), the ranges of the drop size that would correspond to negative x_g^D depend only on the initial number of moles of glycerol within the drop (N_g^{init}). In addition, Figure 4-3 shows that the intersection of $Y_1=R_c$ and $Y_2=R$ happens just once which means that there is only a single equilibrium state for these systems and thus this single equilibrium state is used as the reference state giving the value of R_0.
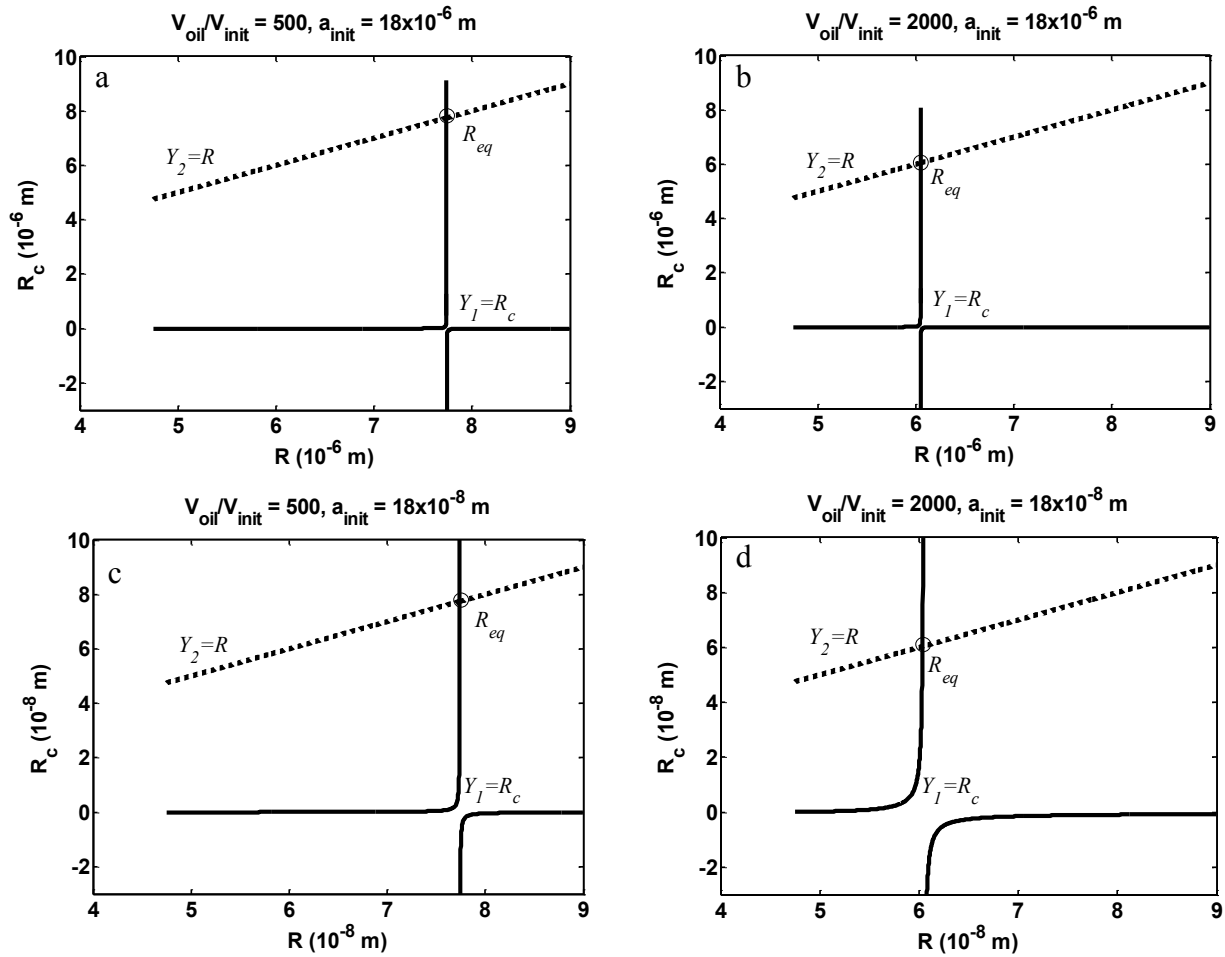
Figure 4-3 Kelvin radius versus radius of the drop for a drop containing glycerol with initial concentration of 2 M, and initial drop sizes of 18×10^{-6} m and 18×10^{-8} m for two different volumes of oil per initiasl volume of the drop. Intersections of the Kelvin radius curve with the 45° dashed line indicate equilibrium states where the drop size R equals the Kelvin radius R_c.

Figure 4-4 shows a similar figure to Figure 4-3 but for four different volumes of oil per initial volume of the drop in the system when the initial size of the drop is 18×10^{-8} m. It shows that there is a definite volume of oil in the system that if the amount of oil is increased beyond that definite volume, only a very small change in the equilibrium size of the drop will happen. In addition, it shows that for any amount of oil in the system curves of $Y_1 = R_c$ and $Y_2 = R$ will always intersect and the equilibrium size will never be outside the meaningful region for x_g^D and the

drops will never shrink completely
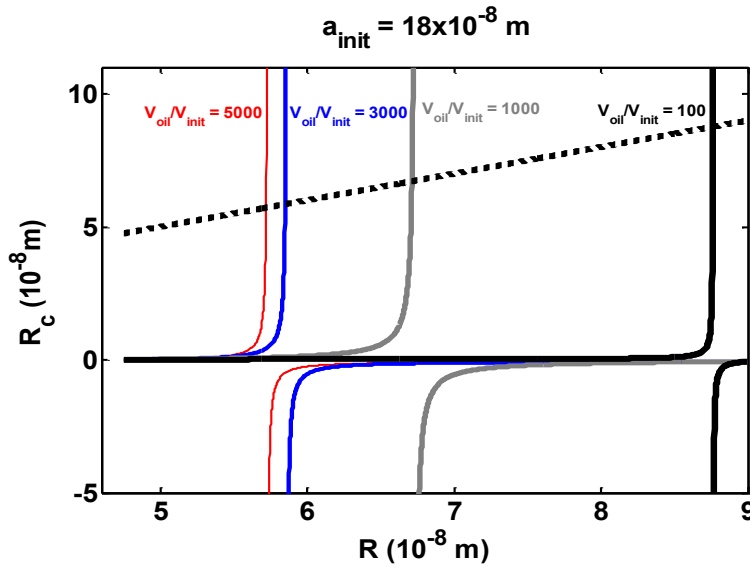
$$a_{init} = 18 \times 10^{-8} \text{ m}$$

Figure 4-4 Kelvin radius versus radius of the drop for a drop containing glycerol with initial concentration of 2 M, and initial drop size of 18×10^{-8} m for four different volumes of oil per initial volume of the drop. The intersections with the 45° line show the equilibrium sizes for each case.

To do the stability analysis we use equation (4-20) to draw the free energy versus the size of the drop. By finding the value R_0 by the procedure above and substituting equations (4-26) and (4-27) or (4-30), (4-31) and (4-32) into equation (4-20) and by making use of equations (4-37) and (4-40) to (4-41) we plot $F - F_0$ versus the size of the drop for glycerol.

Figure 4-5 shows the free energy of the system versus the size of the drop which contains glycerol for oil volumes of 2000 and 500 times the initial drop volume and for two initial sizes of the drop of 18×10^{-6} m and 18×10^{-8} m in parts a and b respectively. As a minimum in free energy corresponds to a stable equilibrium state, it is shown that the free energy diagram has only one stable equilibrium state. In addition, since we have chosen the reference state to be an equilibrium state the amount of $F - F_0$ at the equilibrium state should be equal to zero. In all

curves of Figure 4-5 we can see that the positions of the minima of the curves correspond well to the calculated equilibrium radii in Figure 4-3.
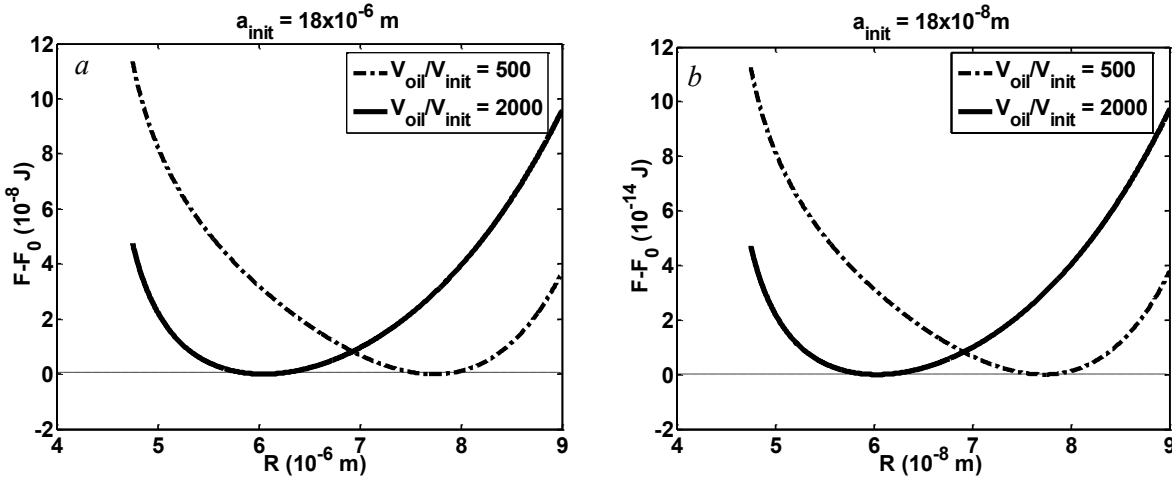
Figure 4-5 Free energy versus the size of the drop for a drop containing glycerol with initial concentration of 2 M, and initial drop sizes of 18×10^{-6} m and 18×10^{-8} m for two different volumes of oil per initial volume of the drop

4.3.1.2. Solute: NaCl (Before Precipitation, *i.e.*, when NaCl Is Completely Dissolved in Water)

Here we do the stability analysis of a drop which contains a limited solubility solute such as sodium chloride up to its solubility limit in water which means before the precipitation occurs. The procedure is similar to what we have done for glycerol, which means we first find R_0, the drop radius at the equilibrium reference state, by finding the intersection of curves $Y_1 = R_c$ and $Y_2 = R$ versus R and then in order to find $F - F_0$ we substitute equations (4-26) and (4-27) or (4-45), (4-46) and (4-48) into equation (4-42) and make use of equation (4-51) and (4-39) to (4-41) (replacing subscript g with *NaCl* in equations (4-39) to (4-41)). In this case, we have only accepted those drop sizes that correspond to the region before precipitation. The only important difference in the case of limited solubility solutes is that we should check that the R_0 does not

correspond to the range for which $x_{NaCl}^D > x_{NaCl}^{limit}$ because then we would no longer be in the region before precipitation of the solutes, and a different calculation procedure would be required as described below. For example, when the solute is sodium chloride, solute will have precipitated at the equilibrium state when oil volumes are 2000 times the initial drop volume or larger, in which case the effect of precipitation has to be explored as in in the next section, where solid precipitate is present in the system.
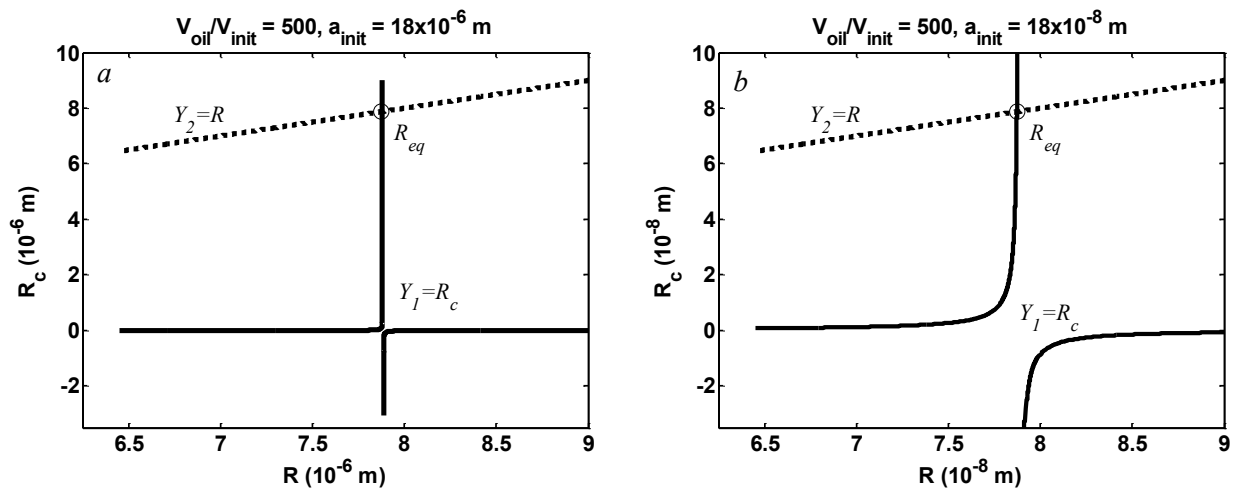
Figure 4-6 Kelvin radius versus radius of the drop for a drop containing NaCl at specific volumes of oil per initial volume of the drop for initial drop sizes of 18×10^{-6} m and 18×10^{-8} m. Intersections with the 45° line show the equilibrium sizes for each case.

Figure 4-6 shows the plots of two curves of $Y_1=R_c$ and $Y_2=R$ versus R when the oil volume is 500 times the initial drop volume for a drop which contains sodium chloride with initial diameters of 18×10^{-6} m and 18×10^{-8} m respectively in parts a and b. Figure 4-7 shows the free energies of these systems versus the size of the drop. Both figures show that in the region before precipitation for limited solubility solutes there is only one stable equilibrium state (similar to the case for the unlimited solubility solute) and the minima in Figure 4-7 correspond very well to the calculated equilibrium points in Figure 4-6.
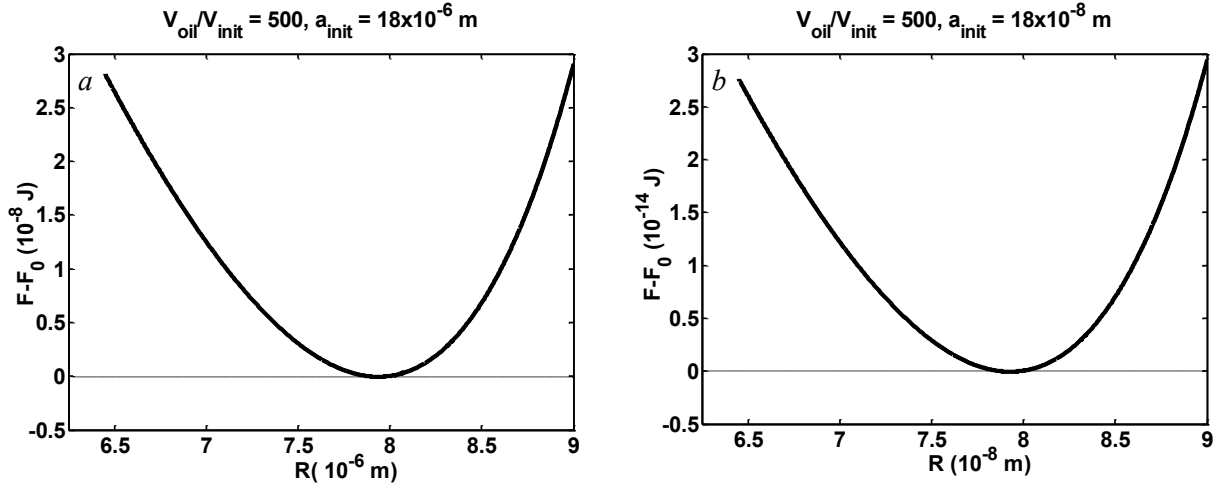
Figure 4-7 Free energy versus the size of the drop for a drop containing NaCl with initial drop sizes of 18×10^{-6} m and 18×10^{-8} m for a specific volume of oil per initial volume of the drop before precipitation has occurred

Generally speaking, it was found that as long as the solute completely dissolves in water, even if it is a limited solubility solute, there is only one equilibrium state which corresponds to the stable state. Therefore, concentrating the drop will result in a stable concentrated drop but it will never shrink completely and disappear in the system.

4.3.2. Cases where the Solute Cannot Completely Dissolve in Water and Some Solid Precipitates in the System

4.3.2.1. Solute: NaCl (After it Reaches its Solubility Limit in Water)

In this section we explore the behavior of the equilibrium states when a solute, such as NaCl, starts to precipitate in solid form. As was mentioned, when two curves of $Y_1=R_c$ and $Y_2=R$ are plotted versus the size of the drop which contains sodium chloride, we found that at higher than a specific amount of available oil in the system the intersection of these curves corresponds to $x^D_{NaCl} > x^{limit}_{NaCl}$. The relationship between x^D_{NaCl} and R can be found by solving equation (4-51) which gives the equivalent mole fraction of salt within the drop at each size of the drop. So

whenever $x_{NaCl}^D > x_{NaCl}^{limit}$ we are in the region of solute having precipitated. Therefore, in this region, instead of solving equation (4-51) we set the mole fraction of the solute at $x_{NaCl}^D = x_{NaCl}^{limit}$. In these cases, as will be shown below, $Y_1=R_c$ and $Y_2=R$ may intersect twice and we may have two equilibrium states and by means of free energy analysis we are going to find the nature of each equilibrium state from the stability point of view. It is for this more complex case of microdrop concentrating including precipitation, that the free energy analysis becomes essential in understanding the complex predicted behavior of the system.

Figure 4-8, shows the plot of $Y_1=R_c$ and $Y_2=R$ for drops with initial diameters of 18×10^{-6} m and 18×10^{-8} m and for three different amounts of oil in the system. Each of these conditions has been selected so as to be in the precipitation region. In parts a and d, the Kelvin radius curve intersects the 45° line, indicating equilibrium radii where $R_c = R$, at two points (R_{eq_1}, R_{eq_2}) which means that the system has two equilibrium states and one of them is chosen to be the reference size of the drop, R_0. By increasing the amount of oil in the system, these two equilibrium points become closer and closer until at a certain amount of oil there exists only one equilibrium state. Therefore, as can be seen in Figure 4-8 parts b and e, at that certain amount of oil (which depends on the initial size of the drop in addition to the initial concentration of the solute) $Y_1=R_c$ and $Y_2=R$ touch each other at a single point so the system has one equilibrium state. In parts c and f, by furthur increasing the amount of oil $Y_1=R_c$ and $Y_2=R$ do not intersect at all, and thus for these volumes of oil, no equilibrium state exists in which the drop is present at all.
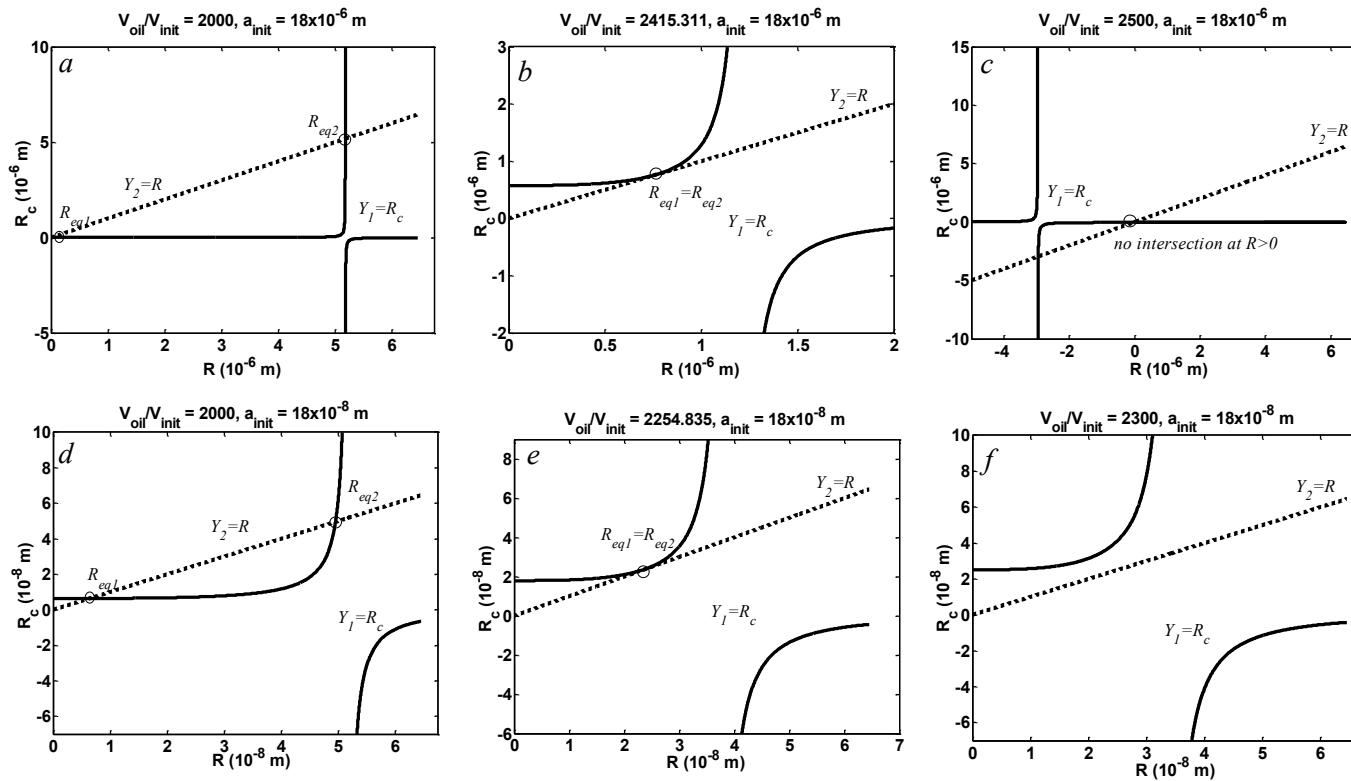
Figure 4-8 Kelvin radius versus radius of the drop for a drop containing NaCl with initial concentration of 2 M, and initial drop sizes of 18×10^{-6} m and 18×10^{-8} m for different volumes of oil per initial volume of the drop. Intersections of the Kelvin radius curve with the 45° dashed line indicate equilibrium states where the drop size R equals the Kelvin radius R_c.

Figure 4-9 shows the free energies of the system for drops with initial diameters of 18×10^{-6} m and 18×10^{-8} m for different oil volumes with respect to the free energy at the reference point which is arbitrarily chosen to be R_{eq2}. All systems have an additional minimum in free energy when $R_{eq0}=0$, which means that complete disappearance of the drop satisfies the equilibrium equations. However, instersecting $Y_1=R_c$ and $Y_2=R$ in Figure 4-8 does not show R_{eq0} to be one of the equilibrium states. This is because the method of calculation in Figure 4-8 (finding intersections of the Kelvin radius with the 45° line, *i.e.*, finding radii for which $R_c=R$) presupposes a drop to be present and thus can only find equilibrium states for which a drop is present. In addition to R_{eq0}, the free energy diagram for an oil volume of 2000 times the initial drop volume shows a maximum at a smaller equlibrium size, R_{eq1}, which corresponds to the unstable equilibrium state and a minimum at a larger equilibrium size, R_{eq2}, which corresponds to the stable equilibrium state. The maxima in parts *a* and *b* have very small energy levels and are hardly visible in the main figures; however they have been expanded to show the maxima.

As was mentioned previously, we are considering a system which already contains a drop with a specific initial diameter as would be purposefully formed in a microfluidic device and due to the water migration between the drop and oil phase at a specific amount of oil in the system, the drop shrinks until it reaches a new condition, stopping at a stable equilibrium. So, here we do not investigate the formation of a new drop (as is the case of free energy analysis used to understand nucleation phenomena[18,24,27]), but rather we are looking for shrinkage of the existing drop. As a result, we analyze the free energy diagrams from right to left of the diagram (from the larger size of the drop to the lower size).Thus, since the stable equilibrium happens at a larger drop size, the drop will remain in that stable equilibrium state and would not reach the unstable equilibrium
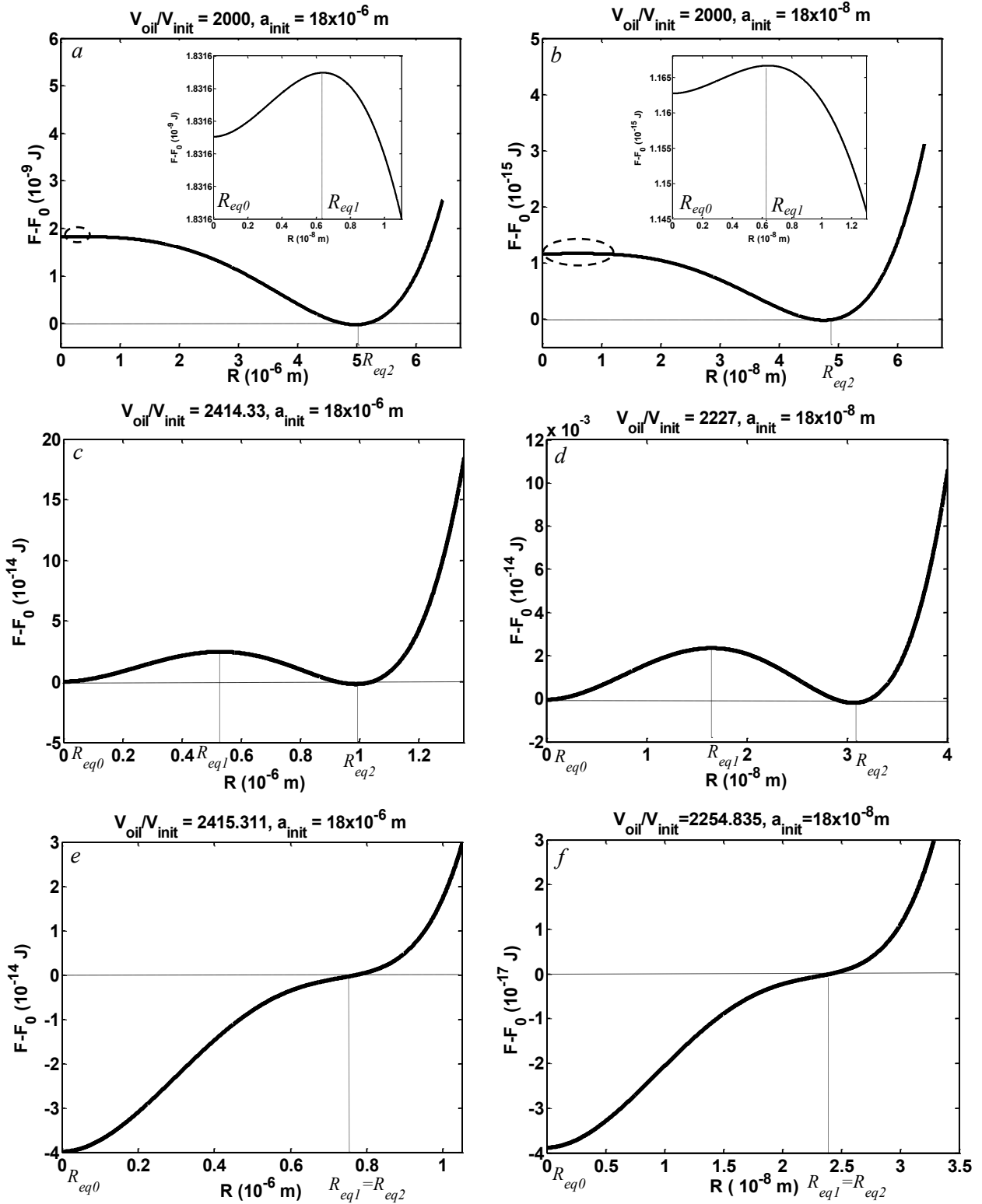
Figure 4-9 Free energy versus the radius of the drop which contains NaCl for different oil volume to the initial drop volume for drops with initial diameter of 18×10^{-6} m and 18×10^{-8} m after precipitation has occurred.

one which happens at lower size unless the difference of energy levels for these equilibrium states is comparable to the extent of molecular fluctuation.[26] Since we have chosen R_{eq2} to be the reference R_0, the energy of R_{eq2} states are equal to zero and for increasing amounts of oil the energy level of the unstable equilibrium states and also the energy level at R_{eq0} decrease and the difference in energy level between the stable and unstable equilibrium states decreases. In parts *c* and *d*, increasing the amount of oil leads to the condition that the energy levels of the minima of the diagram at both R_{eq0} and R_{eq2} become equal. In this condition, we have two equally stable equilibrium states. Upon further increasing the oil in the system, the energy level of R_{eq0} decreases even further and the state with no drop present becomes the global minimum of the
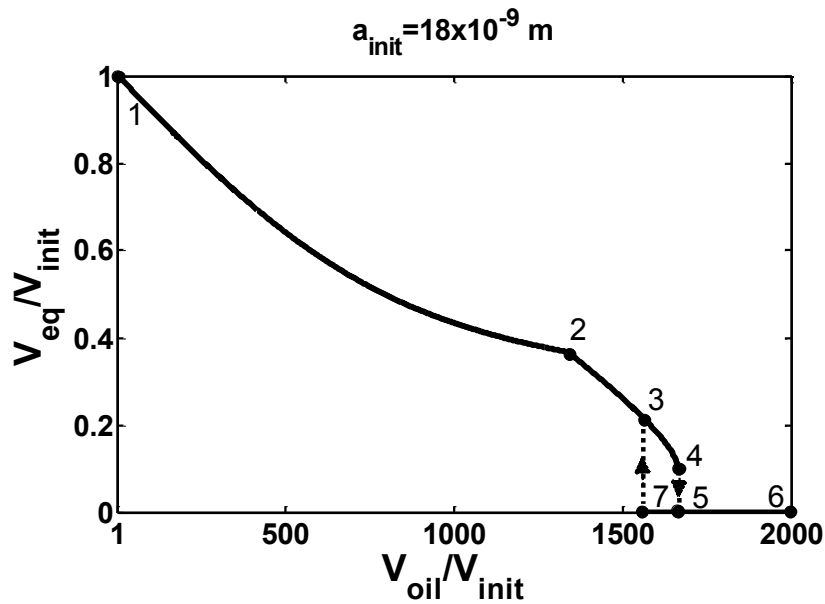
Figure 4-10 Equilibrium volume of the drop per initial drop volume versus the oil volume per initial drop volume for an initial diameter of 18×10^{-9} m of a drop which contains sodium chloride with different stability ranges: (1–2) before precipitation, (2–3) after precipitation, where R_{eq2} is the most stable equilibrium, (3–4) after precipitation, where R_{eq2} is metastable, (5–6) after precipitation, where R_{eq0} *is* the only stable equilibrium, (5–7) after precipitation, where R_{eq0} is the most stable equilibrium.

free energy and the stable equilbrium of the system and the energy levels of R_{eq1} and R_{eq2} become closer and closer until in parts *e* and *f* their energy levels become the same and instead of a maximum and minimum we find an inflection point in the free energy diagram. It is clear that in this case the stable equilibrium state is R_{eq0} which means disappearance of the drop in the system, and increasing the oil in the system will lead to complete disappearance of the drop at once without even facing any energy barrier to be overcome.

We have summarized the results schematically in Figure 4-10. It shows the equilibrium volume of the drop per initial drop volume versus the oil volume per initial drop volume for a drop which contains sodium chloride with initial drop diameter of 18×10^{-9} m for different stability regions. By increasing the amount of oil in the system the equilibrium size of the drop decreases according to the curve from point 1 to point 2, without any precipitation happening. This region pertains to the condition where the solute completely dissolves in the water and only one equilibrium state exists. At point 2 precipitaton begins and increases as the drop proceeds through points 2 through 6. Thus, due to the presence of the new solid phase we found different equilibrum states in this region. From 2 to 3, R_{eq2} is the most stable equilibrium state and at point 3 both R_{eq2} and R_{eq0} have the same amount of energy. As a result, between points 3 and 4 R_{eq2} is a metastable equilibrium and R_{eq0} is the most stable one. By increasing the amount of oil, at point 4 R_{eq1} and R_{eq2} become equal and between points 5 and 6 R_{eq0} is the only equilibrium state in the system. If, once the system were to reach point 6, the amount of oil in the system were to be decreased some hysteresis will happen and the drop will follow the different path 6–5–7–3–2–1. Thus, if the amount of oil in the system were to be changed continually which is a possibility in microfluidic systems, the equilibrium size that drops in the system would adopt would depend on the history of the system. In the forward direction, in which oil is being increased in the system,
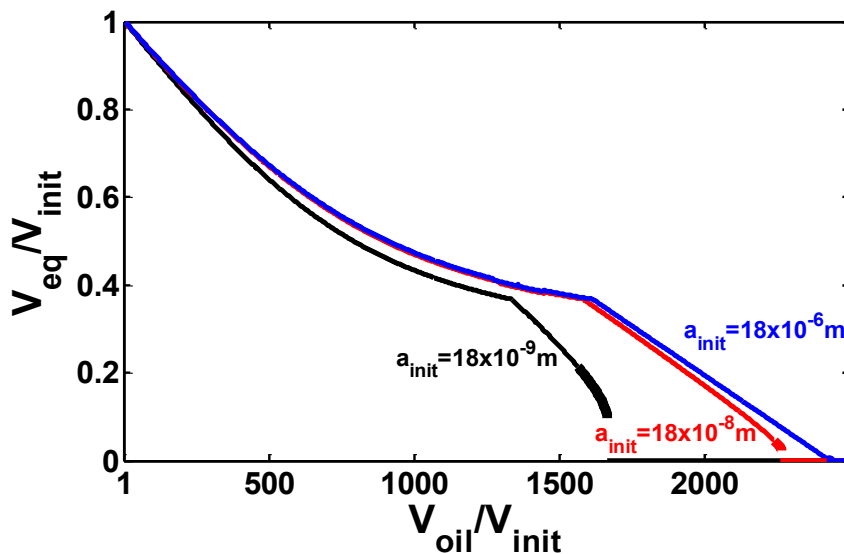
Figure 4-11 Equilibrium volume of the drop per initial drop volume versus the oil volume per initial drop volume for a drop containing NaCl at different initial drop diameters with different stability ranges. The metastable regions for the drops are shown with thicker lines.

since prior to entering this region R_{eq2} was the stable equilibrium, the equilibrium size of the drop will be R_{eq2} and the drop will follow the path 3–4. But in the backwards direction in which oil is decreased in the system, since prior to entering this region $R_{eq0}=0$ was the stable equilibrium, the equilibrium size of the drop will be R_{eq0} and the drop will follow the path 5–7.

To compare different initial size of the drops, in Figure 4-11 we plot equilibrium volume of the drop per initial drop volume versus the oil volume per initial drop volume for different initial drop diameters with different stability ranges. It is illustrated that a larger initial size of the drop has a wider range of stability and a narrower range of metastability for R_{eq2}. Also, by decreasing the initial size of the drop, the drop will disappear completely at a smaller amount of available oil in the system. In addition, as can be seen in parts *a* and *b* of Figure 4-9, a larger initial size of the drop has a more stable equilibrium state due to the deeper energy difference with respect to the

original points at R_{eq2}. However, the differences in energy between the unstable equilibrium at R_{eq1} and the stable equilibrium at R_{eq2} are of the same order of magnitude for different initial sizes of the drop.

4.4. Conclusion

In order to investigate the detailed equilibrium behavior of microdrops during concentrating processes, stability analysis for two types of solute from a solubility limit standpoint (glycerol and sodium chloride) has been done. It was found that when the solute completely dissolves in water and no solid exists in the system—either in the case of an unlimited solubility solute or a limited solubility solute before its saturation limit is reached—the system has only one stable equilibrium state. However, when solid precipitate exists in the system in the case of a limited solubility solute, different equilibrium behavior may be encountered depending on the amount of available oil or initial size of the drop in the system: it was found that in this case disappearance of the drop ($R_{eq0}=0$) is always one of the equilibrium states which corresponds to a minimum of the free energy diagram. Beside R_{eq0}, the system may have two other equilibrium states: one of them a smaller drop that corresponds to a maximum in the free energy diagram and hence it is an unstable equilibrium state, R_{eq1}, and the other equilibrium state is a larger drop that corresponds to a minimum in the free energy diagram, R_{eq2}. For a specific initial size of the drop, by increasing the amount of oil in the precipitation region, first R_{eq2} corresponds to the global minimum in free energy of the system; hence it is the stable equilibrium. By further increasing the oil in the system, the energy levels at R_{eq0} and R_{eq1} decrease until, at a certain amount of oil, R_{eq2} is no more the global free energy minimum of the system, but rather R_{eq0} is the stable equilibrium state. Finally, by furthur increasing the amount of oil, both R_{eq1} and R_{eq2} become the same and we have R_{eq0} as the only equilibrium state in the system which means no more drop

can exist in the system. Here we have only shown the effect of oil amount on the stability of the system, but changing the temperature of the system has a similar effect on the stability of the microdrops. The implication of this study is that more caution is needed in designing microdrop concentrating process where formation of precipitate outside the drop is probable. Although continuous drop size change by changing the amount of oil or temperature in these systems is expected, an abrupt change may happen in microdrop size due to the change in thermodynamic stability of different equilibrium states as explored in this paper.

4.5. References

1. Theberge, A. B.; Courtois, F.; Schaerli, Y.; Fischlechner, M.; Abell, C.; Hollfelder, F.; Huck, W. T. S. Microdroplets in Microfluidics: An Evolving Platform for Discoveries in Chemistry and Biology. *Angew. Chem. int. Edit.* **2010**, *49*, 5846-5868.

2. Joensson, H. N.; Svahn, H. A. Droplet Microfluidics-A Tool for Single-Cell Analysis. *Angew. Chem. int. Edit.* **2012**, *51*, 12176-12192.

3. Bremond, N.; Bibette, J. Exploring Emulsion Science with Microfluidics. *Soft Matter* **2012**, *8*, 10549-10559.

4. Lagus, T. P.; Edd, J. F. A eview of the Theory, Methods and Recent Applications of High-Throughput Single-Cell Droplet Microfluidics. *J. Phys. D. Appl. Phys.* **2013**, *46*, 114005.

5. Bajpayee, A.; Edd, J. F.; Chang, A.; Toner, M. Concentration of Glycerol in Aqueous Microdroplets by Selective Removal of Water. *Anal. Chem.* **2010**, *82*, 1288-1291.

6. He, M.; Sun, C.; Chiu, D. T. Concentrating Solutes and Nanoparticles within Individual Aqueous Microdroplets. *Anal. Chem.* **2004**, *76*, 1222-1227.

7. Jeffries, G. D. M.; Kuo, J. S.; Chiu, D. T. Dynamic Modulation of Chemical Concentration in an Aqueous Droplet. *Angew. Chem. int. Edit.* **2007**, *46*, 1326-1328.

8. Jeffries, G. D. M.; Kuo, J. S.; Chiu, D. T. Controlled Shrinkage and Re-Expansion of a Single Aqueous Droplet inside an Optical Vortex Trap. *J. Phys. Chem. B.* **2007**, *111*, 2806-2812.

9. Eslami, F.; Elliott, J. A. W. Design of Microdrop Concentrating Processes. *J. Phys. Chem. B.* **2013**, *117*, 2205-2214.

10. Wu, T.; Hirata, K.; Suzuki, H.; Xiang, R.; Tang, Z.; Yomo, T. Shrunk to Femtolitre: Tuning High-Throughput Monodisperse Water-In-Oil Droplet Arrays for Ultra-Small Micro-Reactors. *Appl. Phys. Lett.* **2012***, 101*, 074108.

11. Shim, J.; Cristobal, G.; Link, D. R.; Thorsen, T.; Jia, Y.; Piattelli, K.; Fraden, S. Control and Measurement of the Phase Behavior of Aqueous Solutions Using Microfluidics. *J. Am. Chem. Soc.* **2007***, 129*, 8825-8835.

12. Kojima, T.; Takayama, S. Microscale Determination of Aqueous Two Phase System Binodals by Droplet Dehydration in Oil. *Anal. Chem.* **2013***, 85*, 5213-5218.

13. Wang, B.; Shum, H. C.; Weitz, D. A. Fabrication of Monodisperse Toroidal Particles by Polymer Solidification in Microfluidics. *Chemphyschem* **2009***, 10*, 641-645.

14. Bajpayee, A.; Luo, T.; Muto, A.; Chen, G. Very Low Temperature Membrane-Free Desalination by Directional Solvent Extraction. *Energy Environ. Sci.* **2011***, 4*, 1672-1675.

15. Ji, J.; Nie, L.; Li, Y.; Yang, P.; Liu, B. Simultaneous Online Enrichment and Identification of Trace Species Based on Microfluidic Droplets. *Anal. Chem.* **2013***, 85*, 9617-9622.

16. Shen, A. Q.; Wang, D.; Spicer, P. T. Kinetics of Colloidal Templating Using Emulsion Drop Consolidation. *Langmuir* **2007***, 23*, 12821-12826.

17. Gibbs, J. W. On the Equilibrium of Heterogeneous Substances. *Trans. Conn. Acad. Arts Sci.3* **1876**, 108–248 ; **1878**, 343–524, in "The Scientific Papers of J. Willard Gibbs," Ox Bow, Woodridge, CT (1993), Vol. I, pp. 55–353.

18. Ward, C. A.; Johnson, W. R.; Venter, R. D.; Ho, S.; Forest, T. W.; Fraser, W. D. Heterogeneous Bubble Nucleation and Conditions for Growth in a Liquid Gas System of Constant Mass and Volume. *J. Appl. Phys.* **1983***, 54*, 1833-1843.

19. Ward, C. A.; Levart, E. Conditions for Stability of Bubble Nuclei in Solid-Surfaces Contacting a Liquid-Gas Solution. *J. Appl. Phys.* **1984***, 56*, 491-500.

20. Ward, C. A.; Tikuisis, P.; Venter, R. D. Stability of Bubbles in a Closed Volume of Liquid-Gas Solution. *J. Appl. Phys.* **1982***, 53*, 6076-6084.

21. Forest, T. W.; Ward, C. A. Homogeneous Nucleation of Bubbles in Solutions at Pressures Above Vapor-Pressure of Pure Liquid. *J. Chem. Phys.* **1978***, 69*, 2221-2230.

22. Vogelsberger, W. Use of Chemical-Potentials in the Condensation of a Pure Vapor. *Chem. Phy. Lett.* **1979***, 64*, 601-604.

23. Zargarzadeh, L.; Elliott, J. A. W. Comparative Surface Thermodynamic Analysis of New Fluid Phase Formation between a Sphere and a Flat Plate. *Langmuir* **2013***, 29*, 3610-3627.

24. Eslami, F.; Elliott, J. A. W. Thermodynamic Investigation of the Barrier for Heterogeneous Nucleation on a Fluid Surface in Comparison with a Rigid Surface. *J. Phys. Chem. B*. **2011***, 115*, 10646-10653.

25. Zargarzadeh, L.; Elliott, J. A. W. Surface Thermodynamic Analysis of Fluid Confined in a Cone and Comparison with the Sphere-Plate and Plate-Plate Geometries. *Langmuir* **2013***, 29*, 12950-12958.

26. Elliott, J. A. W.; Voitcu, O. On the Thermodynamic Stability of Liquid Capillary Bridges. *Can. J. Chem. Eng.* **2007***, 85*, 692-700.

27. McGaughey, A. J. H.; Ward, C. A. Droplet Stability in a Finite System: Consideration of the Solid-Vapor Interface. *J. Appl. Phys.* **2003***, 93*, 3619-3626.

28. Hilder, M. H. The Solubility of Water in Edible Oils and Fats. *J. Am. Oil Chem. Soc.* **1968***, 45*, 703-707.

29. Prickett, R. C.; Elliott, J. A. W.; McGann, L. E. Application of the Osmotic Virial Equation in Cryobiology. *Cryobiology* **2010***, 60*, 30-42.

30. Zielinski, M. W.; McGann, L. E.; Nychka, J. A.; Elliott, J. A. W. Comparison of Non-Ideal Solution Theories for Multi-Solute Solutions in Cryobiology and Tabulation of Required Coefficients. In Press *Cryobiology,* Accepted August 13, **2014**.

31. Prickett, R. C.; Elliott, J. A. W.; McGann, L. E. Application of the Multisolute Osmotic Virial Equation to Solutions Containing Electrolytes. *J. Phys. Chem. B*. **2011***, 115*, 14531-14543.

32. Novotny, P.; Sohnel, O. Densities of Binary Aqueous Solutions of 306 Inorganic Substances. *J. Chem. Eng.Data* **1988***, 33*, 49-55.

33. Pinho, S. P.; Macedo, E. A. Solubility of NaCl, NaBr, and KCl in Water, Methanol, Ethanol, and Their Mixed Solvents. *J. Chem. Eng. Data* **2005***, 50*, 29-32.

Chapter 5: Role of Precipitating Solute Curvature on Microdrops during Concentrating Processes: The Non-Ideal Ostwald–Freundlich Equation

5.1. Introduction

The microdrop concentrating process[1-6] is an important technique which is mainly used in microfluidic technologies and has many applications.[1,4,7-10] This process takes place mainly in water-in-oil emulsions where the oil phase has a slight solubility of water and the droplets include a solute which cannot dissolve in the oil phase and is planned to be concentrated. Increasing the temperature increases the solubility of water in the oil phase and dehydration of the microdrops leads to concentrating of the solute. These micro or nano sized droplets act as a confined reactor vessel and due to their ultra-small volume they let the minute amount of solute concentrate highly and be controlled and detected with high sensitivity. This process also provides appropriate conditions for protein crystallization,[8] cryopreservation of cells[4] and energy-efficient desalination of water.[10]

Previously, we have explored the thermodynamic description[5] of aqueous microdrop concentrating processes for limited and unlimited solubility solutes and performed a thermodynamic stability analysis[6] by means of free energy calculation which is a relevant approach[11-17] to find the behaviour of the system at each equilibrium state. In the case of a limited solubility solute, when the solute concentration reaches the solubility limit it starts to precipitate, and in our previous work we studied the situation where the solute precipitated

outside of the droplet and simplified our analysis by not considering the role of solid–drop interfacial tension which results in solubility being dependent only on temperature.

Actually, solubility of solids in liquids is a thermodynamic characteristic that can be predicted by means of melting point or water–oil partition coefficient of the compound.[18] However, as the size of the solids is reduced to the nanometer scale, the solubility is no longer a thermodynamic property and will depend on the size and shape of the solid.[19] Ostwald was the first person to present a relation for this dependency for spherical particles and his relation was later corrected by Freundlich which is then called the Ostwald–Freundlich equation[20] (the original Ostwald[21] and Freundlich[22] papers are written in German):

$$x_\alpha = x_\alpha^\infty exp\left(\frac{2\, v_\alpha^S \sigma^{SD}}{R_u T R_{seq}}\right)$$

(5-1)

which relates the solubility in mole fraction, x_α, of solute α to the equilibrium solid radius, R_{seq}, where x, v, σ, R_u, and T, are mole fraction, molar volume, interfacial tension, universal gas constant, and temperature, respectively, and superscripts S and SD indicate the solid phase, and the solid–drop interface, respectively. x_α^∞ denotes the solute solubility when the solid radius is infinity, *i.e.* for a flat interface.

Based on this equation, decreasing the size of the solid particle leads to an exponential increase in its solubility and this feature becomes more important for nanometer sizes. This phenomenon is widely used in pharmaceutical nanotechnology to increase the solubility of poorly soluble drugs[23,24] and in the physics of soluble nanoparticles in the atmosphere.[25,26] Furthermore, the dependence of solubility on the particle size produces the Ostwald ripening phenomenon;[24] in a system in which small and large particles coexist, when the system reaches the solubility of the

113

large particles, the smaller particles dissolve further and get smaller since the smaller particles have higher solubility, but the larger ones have reached their solubility limit and continue to grow.

Exploring the validity of the Ostwald–Freundlich equation, Knapp considered the electric tension—that acts against the surface tension—in the equation and demonstrated that the solubility meets a maximum instead of going to infinity at very small sizes.[18] In addition, some attempts have been made to apply the Ostwald–Freundlich equation for irregular surfaces by introduction of fractal dimension[18] or a non-extensive thermodynamic approach.[23] Experiments verify[24,27] the validity of this equation; however the ambiguous value of solid–liquid surface tension produces some inaccuracies in the results.

In contrast to liquid–vapor interfacial tension, direct measurement of saturated solution–crystal interfacial tension is not well-established. As a result, homogeneous nucleation theory is one method to find an experimental value of this parameter.[28] However, since preparing suitable conditions for homogeneous nucleation is tedious and time-consuming, researchers[28-30] try to find empirical or theoretical relations between σ^{SL} and other physical properties of the solution. Therefore, they found a linear relation between σ^{SL} and dissolution enthalpy or σ^{SL} and the natural logarithm of the equilibrium concentration of the solute in solution. These relations have been verified by means of surface nucleation[31] and regular solution[30] theories. Mersmann[32] used fundamental thermodynamic relations with the Guggenheim approach and found a simple relation for saturated solution–crystal interfacial tension. Sangwal[33] used the relation between surface entropy factor and surface tension and by applying some simplifications submitted the following equation:

$$\sigma^{SL} = \frac{kT}{8a^2}\left(3 - ln(x_\alpha)\right)$$

(5-2)

where k and a are Boltzmann constant and crystallographic interionic distance. Sangwal mentioned that this equation is very good for compounds with higher symmetry such as alkali halides. Since, here we explore the precipitation of sodium chloride as a solute and the input parameters of equation (5-2) are similar to our work, we have chosen this equation to represent the solid–drop interfacial tension.

Generally speaking, as the objectives of the present work, we investigate the role of the Ostwald–Freundlich equation in microdrop concentrating process for a limited solubility solute thermodynamically and then provide the stability analysis of the system. This includes the overall thermodynamic description of the system at its equilibrium states and finding the nature of the equilibrium states—whether they are stable, unstable or metastable. In this work, as in our previous ones,[5,6] solute precipitates after reaching its solubility limit. In addition, and new to this work, since the role of solid–drop interfacial tension is to be considered, we assumed the precipitate to remain within the drop and allow the solubility limit of the solute to depend on both temperature and σ^{SL}. This study also provides better understanding of the behaviour of complex multiphase systems with precipitating solutes such as might occur for the salts in water-in-oil emulsions,[10,34] or asphaltenes in multi-phase oil systems in oil industry processes.[35]

5.2. Governing Equations

Here, we are going to consider the role of solid–drop interfacial tension on microdrop concentrating processes. Therefore, we consider an aqueous drop which contains a limited solubility solute, such as sodium chloride, which precipitates inside the drop. The drop with
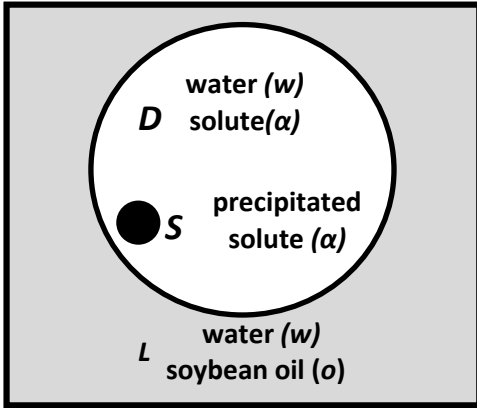
Figure 5-1 A drop of aqueous solution containing a limited solubility solute is placed within soybean oil

known initial concentration of the solute is placed within an oil phase presaturated with water at 25 °C. The system is then heated and allowed to reach equilibrium. At equilibrium, at each temperature and amount of oil in the system, the following relations (5-3) to (5-6) should be valid. There will be equality of the chemical potentials of each phase-boundary crossing component (water, subscript w, and solute, subscript α) in the coexisting phases:

$$\mu_w^D(T, P^D, x_w^D) = \mu_w^L(T, P^L, x_w^L) \tag{5-3}$$

$$\mu_\alpha^D(T, P^D, x_\alpha^{limit}) = \mu_\alpha^S(T, P^S) \tag{5-4}$$

where μ and P are chemical potential and pressure and superscripts D, L and $limit$ indicate the drop phase, the surrounding oil phase and the saturation point, respectively. We have assumed that the precipitate is in the form of a sphere with radius R_s. Therefore, the Laplace equations for the curved interfaces are:

$$P^D - P^L = \frac{2\sigma^{LD}}{R_{eq}} \tag{5-5}$$

$$P^S - P^D = \frac{2\sigma^{SD}}{R_{seq}}$$

(5-6)

where R_{eq} is the equilibrium aqueous drop radius, and superscript LD indicates the liquid–drop interface. In our previous works,[5,6] we investigated microdrop concentrating processes thermodynamically and found the final concentration and size of the drops, and the role of: i) initial concentration and drop size, ii) temperature, iii) oil volume and iv) type of solute from the solubility limit point of view, on the equilibrium condition. We also analyzed the stability of the system for both limited and unlimited solubility solutes. However, in case of the limited solubility solute we considered that the solid precipitated outside of the drop, and the solid–liquid interfacial tension was set to zero and the solubility limit depended only on temperature. Therefore, instead of solving equation (5-4) we used a correlation based on available experimental data for solubility as a function of temperature only. Here, in order to find the solubility limit of the solute including the effect of the solid–drop interfacial tension after the solid precipitates in a spherical format with radius R_s we should solve equation (5-4). Due to the presence of solid curvature and the non-negligible role of solid–drop interfacial tension, the solid and the drop phases have different pressures and the following equation shows the effect of this pressure difference on the chemical potential of the solid phase:

$$\mu_\alpha^S(T, P^S) = \mu_\alpha^S(T, P^D) + v_\alpha^S(P^S - P^D)$$

(5-7)

where v is the molar volume. The chemical potential of the solute in the drop phase can be found by any activity equation:

$$\mu_\alpha^D(T, P^D, x_\alpha^{limit}) = \mu_\alpha^D(T, P^D, x_\alpha^{ref}) + R_u T\, ln(a_\alpha) = \mu_\alpha^D(T, P^D, x_\alpha^{ref}) + R_u T\, f(x_\alpha^{limit})$$

(5-8)

where a is the activity. Since the activity models mostly depend on the composition, we have

substituted the natural logarithm of activity with a function of saturation composition, $f\left(x_\alpha^{limit}\right)$.

Equating equations (5-7) and (5-8), according to equation (5-4), and rearranging yields:

$$\mu_\alpha^S(T, P^D) - \mu_\alpha^D\left(T, P^D, x_\alpha^{ref}\right) = -v_\alpha^S(P^S - P^D) + R_u T f\left(x_\alpha^{limit}\right) \tag{5-9}$$

The left side of equation (5-9) can be found by considering a case where a flat surface exists

between a drop phase and a solid phase. In this case, since no curvature exists between the drop

phase and the solid phase, they both have the same pressure of P^D and the solubility limit only

depends on temperature (x_α^∞). In this case, equating the chemical potentials of the solute in the

drop phase and solid phase yields:

$$\mu_\alpha^S(T, P^D) = \mu_\alpha^D(T, P^D, x_\alpha^\infty) = \mu_\alpha^D\left(T, P^D, x_\alpha^{ref}\right) + R_u T f(x_\alpha^\infty) \tag{5-10}$$

where superscript ∞ indicates the flat surface. Substituting equation (5-10) into equation (5-9)

yields:

$$v_\alpha^S(P^S - P^D) = R_u T f\left(x_\alpha^{limit}\right) - R_u T f(x_\alpha^\infty) \tag{5-11}$$

The left side of equation (5-11) can be rewritten in terms of solid–drop interfacial tension by

means of the Laplace equation, equation (5-6), resulting in:

$$v_\alpha^S \frac{2\sigma^{SD}}{R_s} = R_u T f\left(x_\alpha^{limit}\right) - R_u T f(x_\alpha^\infty) \tag{5-12}$$

Rearranging equation (5-12) yields:

$$f\left(x_\alpha^{limit}\right) - f(x_\alpha^\infty) = \frac{2 v_\alpha^S \sigma^{SD}}{R_u T R_{seq}} \tag{5-13}$$

Equation (5-13) is a more general form of an equation which is well known as the Ostwald–Freundlich equation (OFE):

$$x_\alpha^{limit} = x_\alpha^\infty exp\left(\frac{2\, v_\alpha^S \sigma^{SD}}{R_u T R_{seq}}\right)$$

(5-14)

which results from equation (5-13) if an ideal, dilute solution assumption is made.

If the osmotic virial equation[36] is used to represent the activity of the solute within the drop phase, we will have the following relation for the activity of the solute:[6]

$$ln(a_\alpha) = f(x_\alpha^D) = \left[k_{diss,\alpha}^* - B_\alpha^* k_{diss,\alpha}^{*2} + k_{diss,\alpha}^* ln(x_\alpha^D) - k_{diss,\alpha}^* x_\alpha^D + 2B_\alpha^* k_{diss,\alpha}^{*2}\left(x_\alpha^D - \right.\right.$$
$$\left.\left.\frac{1}{2}x_\alpha^{D2}\right)\right]$$

(5-15)

where k_{diss}^* and B^* are an empirical electrolyte constant and second osmotic virial coefficient respectively. Substituting equation (5-15) into equation (5-13) yields:

$$k_{diss,\alpha}^* ln\left(\frac{x_\alpha^{limit}}{x_\alpha^\infty}\right) - k_{diss,\alpha}^*\left(x_\alpha^{limit} - x_\alpha^\infty\right) + 2B_\alpha^* k_{diss,\alpha}^{*2}\left[\left(x_\alpha^{limit} - x_\alpha^\infty\right) - \frac{1}{2}\left(x_\alpha^{limit\,2} - x_\alpha^{\infty 2}\right)\right] =$$
$$\frac{2v_\alpha^S \sigma^{SD}}{R_u T R_{seq}}$$

(5-16)

Equation (5-16) is the governing equation to find the solubility of the solute at each size of the solid solute sphere.

Here, we choose the solute to be sodium chloride. Therefore, we use the values of 3.8 and 1.644 for B_{NaCl}^* and $k_{diss,NaCl}^*$ respectively.[37] The solid–drop interfacial tension is considered to be dependent on the solubility limit and follows the Sangwal equation (5-2), using the value of 2.81×10^{-10} m for crystallographic interionic distance.[38] For the saturation mole fraction in the

case of the flat interface, x_α^∞, we used a correlation based on available experimental data where it is assumed to depend only on temperature:[5,39]

$$x_{NaCl}^\infty = (1.374 \times 10^{-6}T^2 - 6.899 \times 10^{-4}T + 0.3484)\frac{M^D}{M_{NaCl}} \qquad ,T \text{ in K} \qquad (5\text{-}17)$$

where M is the molar mass. Now that we have a relation for the solubility limit of the solute (equation (5-16)), we can find the equilibrium properties of the process. Before the precipitation happens, only equations (5-3) and (5-5) should be simultaneously satisfied as explained and explored in our previous paper.[5] As in that paper, we use the osmotic virial equation for the chemical potential of water in the drop phase:

$$\mu_w^D(T, P^D, x_\alpha^D) = \mu_w^0(T, P^L) + v_w(P^D - P^L) - R_u T\left[k_{diss,\alpha}^* x_\alpha^D + B_\alpha^*\left(k_{diss,\alpha}^* x_\alpha^D\right)^2\right] \quad (5\text{-}18)$$

where μ_w^0 is the chemical potential of pure water, and an empirical equation for the chemical potential of water in the liquid oil phase:

$$\mu_w^L(T, P^L, x_w^L) = \mu_w^0(T, P^L) + R_u T ln(\gamma_w^L x_w^L) \qquad (5\text{-}19)$$

where $\gamma_w^L = \frac{1617}{T} - 2.9$ is an empirical activity coefficient of water in soybean oil.[5,40] Substituting equations (5-18) and (5-19) into equation (5-3) and making use of equation (5-5) results in:

$$R_u T\left(ln(\gamma_w^L x_w^L) + k_{diss,\alpha}^* x_\alpha^D + B_\alpha^*\left(k_{diss,\alpha}^* x_\alpha^D\right)^2\right) = v_w\frac{2\sigma^{LD}}{R_{eq}} \qquad (5\text{-}20)$$

After the precipitation occurs, x_α^D would be constant and equal to x_α^{limit} and at equilibrium equations (5-3) to (5-6) should be satisfied simultaneously. Therefore equation (5-20) should be rewritten in terms of x_α^{limit}:

$$R_u T \left(ln(\gamma_w^L x_w^L) + k_{diss,\alpha}^* x_\alpha^{limit} + B_\alpha^* \left(k_{diss,\alpha}^* x_\alpha^{limit}\right)^2\right) = v_w \frac{2\sigma^{LD}}{R_{eq}} \tag{5-21}$$

Since equations (5-16) and (5-21) are combinations of equations (5-4), (5-6) and (5-3), (5-5) respectively, therefore we ultimately should solve two equilibrium equations, Equation (5-16)—the OFE for equilibrium of the curved solid precipitate phase, and Equation (5-21)—the Kelvin Equation for the equilibrium of the curved drop phase, simultaneously. Since there are four unknowns to be found: R_{eq}, R_{seq}, x_w^L, x_α^{limit} two more equations are needed to fully determine the unknowns. Mass conservation of the solute and water in the system yields:

$$N_\alpha^{init} = N_\alpha^S + N_\alpha^D \tag{5-22}$$

$$N_w^{init} = N_w^D + N_w^L \tag{5-23}$$

$$N_\alpha^D = N_w^D \frac{x_\alpha^{limit}}{(1-x_\alpha^{limit})} \tag{5-24}$$

$$N_\alpha^S = \frac{\rho^S V^S}{M_\alpha} = \frac{4\rho^S}{3M_\alpha} \pi R_s^{\,3} \tag{5-25}$$

$$N_w^L = N_o^{init} \frac{x_w^L}{(1-x_w^L)} \tag{5-26}$$

where N is the number of moles and the subscript o denotes the soybean oil component and the superscript *init* stands for the initial value. For simplicity we neglect any effects due to changes in the amount of any components adsorbed at interfaces, and so partition the moles of each component between the solid, drop and liquid phases only.

The initial numbers of moles of water, oil and solute are known and since the solid is within the drop, the following relation connects R_{eq} to R_{seq}:

$$V^D - V^S = \frac{4\pi}{3}\left(R_{eq}^3 - R_{seq}^3\right) = \frac{(N_w^D + N_\alpha^D)M^D}{\rho^D} \tag{5-27}$$

As it is clear, M^D and ρ^D which are molar mass and density of the drop, respectively, depend on x_α^{limit}:

$$M^D = M_w x_w^D + M_\alpha x_\alpha^{limit} \tag{5-28}$$

and in the case that the solute being considered is sodium chloride, the drop density is given by:[41]

$$\rho^D = \rho_{water} + 44.85c - 0.09634cT + 0.6136 \times 10^{-3}cT^2 - 2.712c^{1.5} + 1.009 \times 10^{-2}c^{1.5}T \tag{5-29}$$

where T is temperature in °C and c is molarity of NaCl which can be written in terms of sodium chloride mole fraction: $c = 10^{-3}\frac{\rho^D x_\alpha^{limit}}{M^D}$. Substituting equations (5-23) to (5-26) into equations (5-22) and (5-27) and making use of equations (5-28) and (5-29) and rearranging results in the following equations:

$$N_\alpha^{init} = \frac{4\rho^S}{3M_\alpha}\pi R_{seq}{}^3 + \left(N_w^{init} - N_o^{init}\frac{x_w^L}{(1-x_w^L)}\right)\frac{x_\alpha^{limit}}{(1-x_\alpha^{limit})} \tag{5-30}$$

$$\frac{4\pi}{3}\left(R_{eq}^3 - R_{seq}^3\right) = \frac{\left(N_w^{init} - N_o^{init}\frac{x_w^L}{(1-x_w^L)}\right)\left(1+\frac{x_\alpha^{limit}}{(1-x_\alpha^{limit})}\right)M^D}{\rho^D} \tag{5-31}$$

Now that we have four equations (5-16), (5-21), (5-30) and (5-31) in four unknowns: R_{eq}, R_{seq}, x_w^L, x_α^{limit} we can solve the equations simultaneously and find the equilibrium properties.

The procedure is to compare the calculated mole fraction of the solute within the drop phase using the before-precipitation equations $\left(x_\alpha^{D,bp}\right)$ with x_α^{limit}; so that if $x_\alpha^{D,bp}$ is bigger than x_α^{limit} then we set $x_\alpha^D = x_\alpha^{limit}$. However, since there is no explicit value for x_α^{limit} for the comparison at the beginning, we enter the after-precipitation calculation region by comparing $x_\alpha^{D,bp}$ with x_α^∞. So, if $x_\alpha^{D,bp} \geq x_\alpha^\infty$ we enter the precipitation region and can solve four equations (5-16), (5-21), (5-30) and (5-31) simultaneously to find four unknowns $R_{eq}, R_{seq}, x_w^L, x_\alpha^{limit}$. If this set of equations does not converge, then we have found that no precipitation occurred and we are still in the before-precipitation region. However, if at a specific amount of oil in the system this set of equations converges and we enter the precipitation region, any further divergence for this set of equations at a larger amount of oil in the system means that the system can no longer be at equilibrium with a drop present. Meanwhile, if the system of equations converges and we find the correct solubility limit we should check the validity of the calculation by comparing $x_\alpha^{D,bp}$ with x_α^{limit}. If $x_\alpha^{D,bp} \geq x_\alpha^{limit}$ then we can be assured that we are in the precipitation region and $x_\alpha^D = x_\alpha^{limit}$ and that the calculated R_{eq}, R_{seq}, and x_w^L are correct. But if we found that $x_\alpha^{D,bp} < x_\alpha^{limit}$ then we recognise that we have not entered the precipitation region and $x_\alpha^D = x_\alpha^{D,bp}$.

After doing the equilibrium calculation, we noticed that at certain conditions, more than one equilibrium answer is obtained. Therefore, by performing a free energy calculation we investigate the nature of each equilibrium answer and determine whether the equilibrium states are stable, metastable or unstable. The free energy calculation and stability analysis for the concentrating process of microdrops when the solute precipitates outside of the drop, and neglecting the role of solid precipitate–drop solution interfacial tension and the OFE, was

explained and completed in our previous paper.[6] Here, we summarize the main equations that are needed. Since the system is a closed volume system and consists of solid, drop, liquid, solid–drop and liquid–drop subsystems, its free energy is the summation of the Helmholtz free energies of its subsystems:

$$F = F^D + F^L + F^{LD} + F^S + F^{SL}$$

$$= -P^D V^D + \mu_{NaCl}^D N_{NaCl}^D + \mu_w^D N_w^D - P^L V^L + \mu_o^L N_o^L + \mu_w^L N_w^L + \sigma^{LD} A^{LD} + \mu_o^{LD} N_o^{LD} +$$

$$\mu_w^{LD} N_w^{LD} + \mu_{NaCl}^{LD} N_{NaCl}^{LD} - P^S V^S + \mu_{NaCl}^S N_{NaCl}^S + \sigma^{SL} A^{SL} + \mu_w^{SL} N_w^{SL} + \mu_{NaCl}^{SL} N_{NaCl}^{SL} \qquad (5\text{-}32)$$

By choosing one of the equilibrium points to be a reference state, and denoting properties of the reference state with the subscript 0, and applying constraints of constant system volume and constant numbers of moles for each component, the following equation is obtained for the free energy of the system with respect to the reference free energy:

$$F - F_0 = -\left(\frac{2\sigma^{LD}}{R_c}\right)\left(\frac{4}{3}\pi R^3\right) + \left(\frac{2\sigma^{LD}}{R_0}\right)\left(\frac{4}{3}\pi R_0^3\right) + \sigma^{LD}(4\pi R^2 - 4\pi R_0^2) + N_o^{init}\left(\mu_o^{eq} - \mu_{o,0}^{eq}\right) +$$

$$N_w^{init}\left(\mu_w^{eq} - \mu_{w,0}^{eq}\right) + N_{NaCl}^{init}\left(\mu_{NaCl}^{eq} - \mu_{NaCl,0}^{eq}\right) - \left(\frac{2\sigma^{SD}}{R_{sc}}\right)\left(\frac{4}{3}\pi Rs^3\right) + \left(\frac{2\sigma^{SD}}{R_{so}}\right)\left(\frac{4}{3}\pi R_{s0}^3\right) +$$

$$\sigma^{SD}\left(4\pi R_s^2 - 4\pi R_{s0}^2\right) \qquad (5\text{-}33)$$

In equation (5-33) R_c and R_{sc} are the Kelvin radius for the drop phase and the Ostwald–Freundlich radius for the solid phase, respectively. In addition, the differences between the chemical potentials of each component in the equilibrium states and the reference states are equal to:

$$\mu_w^{eq} - \mu_{w,0}^{eq} = \mu_w^L - \mu_{w,0}^L = R_u T ln\left(\frac{x_w^L}{x_{w,0}^L}\right) \qquad (5\text{-}34)$$

$$\mu_o^{eq} - \mu_{o,0}^{eq} = \mu_o^L - \mu_{o,0}^L = R_u T ln \left(\frac{x_o^L}{x_{0,0}^L} \right) \tag{5-35}$$

$$\mu_{NaCl}^{eq} - \mu_{NaCl,0}^{eq} = \mu_{NaCl}^D - \mu_{NaCl,0}^D = v_{NaCl} \left(\frac{2\sigma^{LD}}{R_c} - \frac{2\sigma^{LD}}{R_0} \right) + R_u T \left[k_{diss,NaCl}^* \left(ln \left(\frac{x_{NaCl}^D}{x_{NaCl,0}^D} \right) - \right. \right.$$
$$\left. \left. x_{NaCl}^D + x_{NaCl,0}^D \right) + 2B_{NaCl}^* k_{diss,NaCl}^{*2} \left(x_{NaCl}^D - x_{NaCl,0}^D - \frac{x_{NaCl}^{D^2}}{2} + \frac{x_{NaCl,0}^{D^2}}{2} \right) \right] \tag{5-36}$$

Since we are in the after-precipitation region and the solute mole fraction in the drop phase is constant and equal to the solubility limit, equation (5-36) will be simplified to:

$$\mu_{NaCl}^{eq} - \mu_{NaCl,0}^{eq} = \mu_{NaCl}^D - \mu_{NaCl,0}^D = v_{NaCl} \left(\frac{2\sigma^{LD}}{R_c} - \frac{2\sigma^{LD}}{R_0} \right) \tag{5-37}$$

It should also be mentioned that in the case of more than one equilibrium state, corresponding to each R_{eq} a separate x_α^{limit} will be obtained, so we have to separately draw the free energy diagram for each equilibrium x_α^{limit}. The procedure to find the nature of each equilibrium point is to first perform the equilibrium calculation as was explained above. Therefore, at each initial size and concentration of the solute, for each amount of oil in the system, the solubility limit, equilibrium drop size and solid size have been calculated. Then we choose one of the equilibrium solid sizes as R_{s0} and the corresponding equilibrium drop size and solubility limit as R_0 and $x_{\alpha,0}^{limit}$.

It should be noted that R and R_s are dependent, and this dependence can be found by fixing the solubility limit to $x_{limit,0}$ and making use of mass conservation equations. In order to use one mass conservation equation which relates R and R_s together, we rearrange equation (5-27) and make use of equations (5-22), (5-24) and (5-25) yielding:

$$\frac{4\pi}{3}\left(R^3 - R_s{}^3\right) = \frac{\left(\left(N_\alpha^{init} - \frac{4\rho^S}{3M_\alpha}\pi R_S{}^3\right)\left(1 + \frac{\left(1 - x_\alpha^{limit}\right)}{x_\alpha^{limit}}\right)\right)M^D}{\rho^D} \tag{5-38}$$

In order to draw the free energy we still need R_c and R_{sc}. The Kelvin radius, R_c, will be found by solving simultaneously the Laplace equation for the liquid–drop interface, equation (5-5), and the equality of chemical potentials of water in the drop phase and in the liquid phase, equation (5-3), which is equivalent to:[6]

$$R_c = \frac{2\sigma^{LD}v_w}{R_u T\left(k_{diss,\alpha}^* x_\alpha^{limit} + B_\alpha^*\left(k_{diss,\alpha}^* x_\alpha^{limit}\right)^2 + ln\left(\gamma_w^L x_w^L\right)\right)} \tag{5-39}$$

In the equations pertaining to free energy analysis such as equations (5-34), (5-35), (5-37) and (5-39) we allow x_w^L, x_o^L and R_c to vary with R and R_s so that we can do the stability analysis and draw free energy versus the size of the system. The dependence of x_w^L and x_o^L on R or R_s is found by using mass conservation equations (5-22) to (5-26):

$$x_w^L = \frac{N_w^{init} - \left(N_\alpha^{init} - \frac{4\rho^S}{3M_\alpha}\pi R_S{}^3\right)\frac{\left(1 - x_\alpha^{limit}\right)}{x_\alpha^{limit}}}{N_w^{init} - \left(N_\alpha^{init} - \frac{4\rho^S}{3M_\alpha}\pi R_S{}^3\right)\frac{\left(1 - x_\alpha^{limit}\right)}{x_\alpha^{limit}} + N_o^{init}} \tag{5-40}$$

$$x_o^L = 1 - x_w^L \tag{5-41}$$

Similarly to R_c, the Ostwald–Freundlich radius of the solid solute, R_{sc}, will be found by solving simultaneously the Laplace equation for the solid–drop interface, equation (5-6), and the equality of chemical potentials of solute in the drop phase and in the solid phase, equation (5-4), which is equivalent to the OF equation. Since we are in the after-precipitation region and the

solute mole fraction in the drop phase is constant and equal to the solubility limit, R_{sc} will be constant and equal to:

$$R_{seq} = \frac{2v_\alpha^S \sigma^{SD}}{R_u T \left(k_{diss,\alpha}^* \ln\left(\frac{x_\alpha^{limit}}{x_\alpha^\infty}\right) - k_{diss,\alpha}^*(x_\alpha^{limit} - x_\alpha^\infty) + 2B_\alpha^* k_{diss,\alpha}^{*2}\left[(x_\alpha^{limit} - x_\alpha^\infty) - \frac{1}{2}(x_\alpha^{limit^2} - x_\alpha^{\infty 2})\right] \right)} \quad (5\text{-}42)$$

Having all the parameters in the free energy equation (5-33), we can now perform the stability analysis.

5.3. Results and Discussion

The equilibrium calculations were performed for the concentrating of an aqueous drop which contains sodium chloride with initial concentration of two molar and three different initial diameters, a_{init}, of 18×10^{-6} m, 18×10^{-8} m and 18×10^{-9} m. Soybean oil was considered presaturated with water at 25 °C and then the system was heated to 35 °C. By increasing the amount of oil in the system, the equilibrium size and concentration of the solute are found for different amounts of available oil in the system. The main differences between this work and our previous paper[6] are that here we consider the solute to precipitate within the drop and also consider the effect of solid–drop interfacial tension on the equilibrium. Therefore, in this case, the solubility limit depends on both the solid size and the temperature.

Figure 5-2 shows the equilibrium volume of the drop per initial drop volume versus the oil volume per initial drop volume for three different initial drop sizes with and without the OFE role. It shows that for bigger initial sizes of the drop, the role of the OFE is insignificant, but upon decreasing the initial size, the OFE role becomes very important.

Figure 5-2 Equilibrium volume of the drop per initial drop volume versus the oil volume per initial drop volume for different initial drop diameters with and without the OFE role. The red oval regions are expanded in the insets.

Figure 5-3 shows the equilibrium mole fraction of the solute within the drop volume versus the oil volume per initial drop volume for three different initial drop sizes with and without the OFE role. It shows that when the OFE is not considered, the solubility limit would be constant, but in the case of application of the OFE, the solubility limit reaches its maximum amount at the onset of precipitation. By increasing the amount of oil in the system, more precipitation will occur and the size of solid precipitate will increase. Based on the OFE, solubility limit and solid size have an inverse relationship. Therefore, by increasing the amount of oil in the system, the solubility limit decreases more and more. As was mentioned previously, for smaller initial size of the drop

we noticed more than one equilibrium state. So we have done the free energy analysis to figure out which of the equilibrium states is more stable.

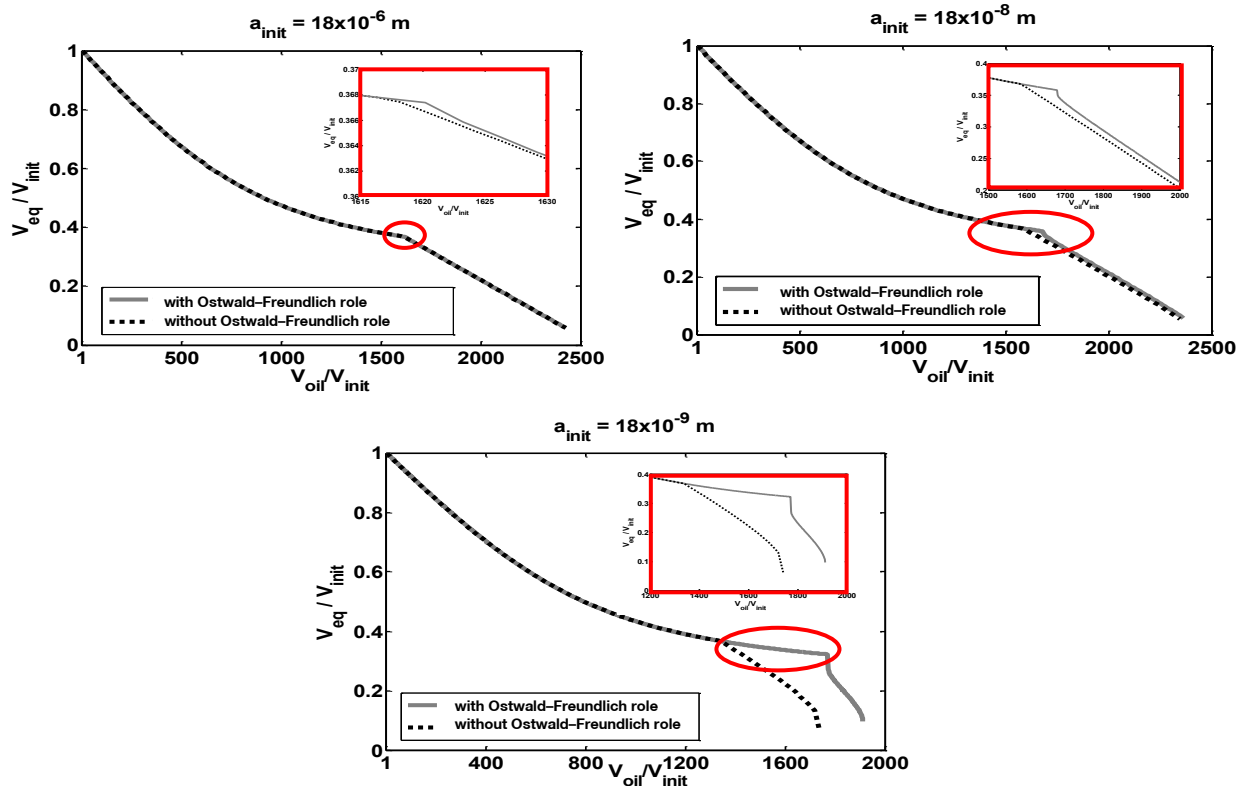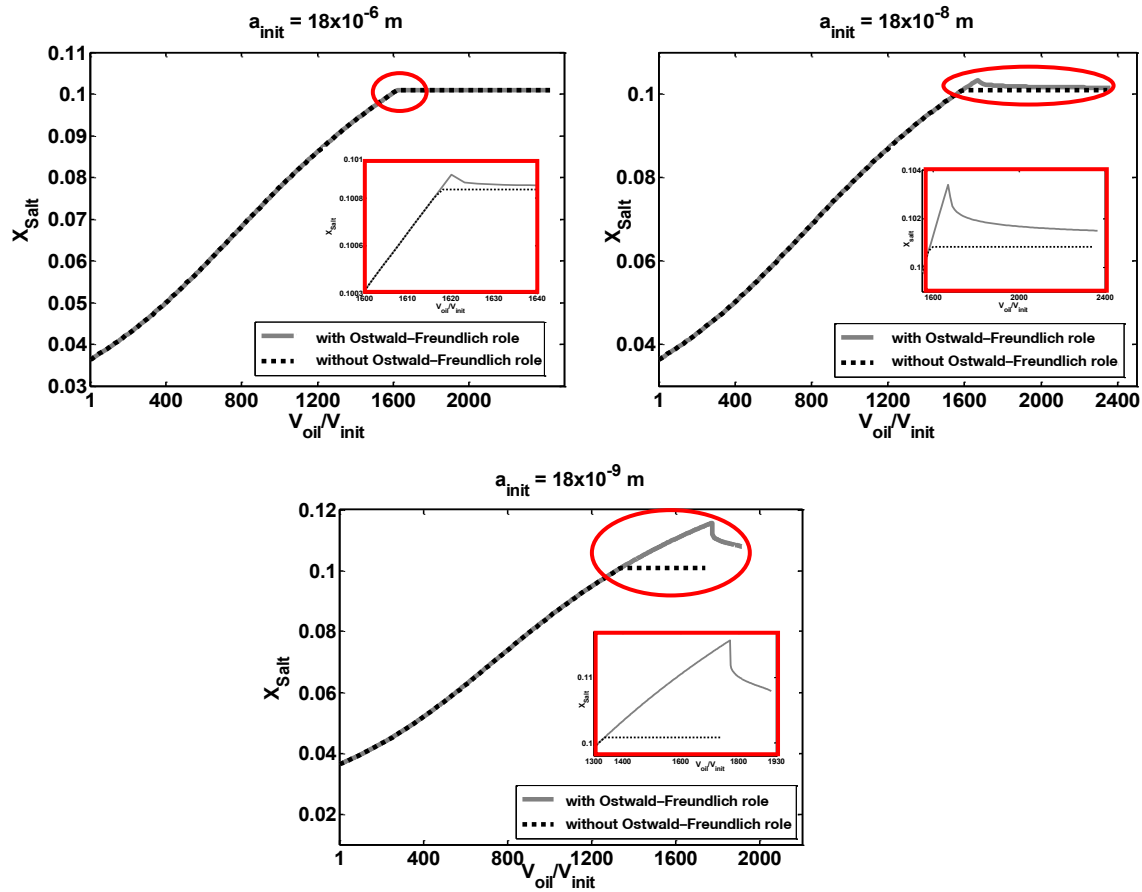Figure 5-3 Equilibrium mole fraction of the solute within the drop per initial drop volume versus the oil volume per initial drop volume for different initial drop diameters with and without the OFE role. The red oval regions are expanded in the insets.

Figure 5-4 a) Free energy versus the drop size and b) Free energy versus the solid size for three different amounts of oil in the system and an initial drop diameter of 18×10^{-6} m

Figure 5-4 shows the free energy versus the drop size and solid size for three different amounts of oil in the system at initial drop diameter of 18×10^{-6} m. Since the solid precipitates within the drop, the drops cannot shrink more than the maximum size of the solid which corresponds to the initial concentration of salt in the drop. As is illustrated in this figure, the systems have only one equilibrium state which corresponds to the minimum of the diagrams and confirms that they are stable equilibria. Figure 5-5 shows the Kelvin radius versus radius of the drop for a drop with initial drop size of 18×10^{-6} m for three different volumes of oil per initial volume of the drop. The intersections with the 45° line show the equilibrium sizes for each case which correspond very well with the minima in Figure 5-4 a.

Figure 5-5 Kelvin radius versus radius of the drop for a drop with initial drop size of 18×10^{-6} m for three different volumes of oil per initial volume of the drop. The intersections with the 45° line show the equilibrium sizes for each case.

Figure 5-6 shows the free energy versus the drop size and solid size for three different amounts of oil in the system and initial drop diameter of 18×10^{-8} m and Figure 5-7 shows the free energy versus the drop size and solid size for an oil volume of 1800 times the initial volume of the drop and initial drop diameter of 18×10^{-8} m. When the initial size of the drop is 18×10^{-8} m, we notice that for a lower amount of oil in the system, which means near the onset of precipitation, two acceptable equilibrium states exist (unacceptable equilibrium states pertain to the cases where the four equations (5-16), (5-21), (5-30) and (5-31) solve simultaneously but the resulting x_{NaCl}^{limit} is lower than $x_{\alpha}^{D,bp}$ which is not acceptable and indicates that the system is in the before-precipitation region) while for the higher amount of oil in the system, only one equilibrium state exists which corresponds to the stable equilibrium state.
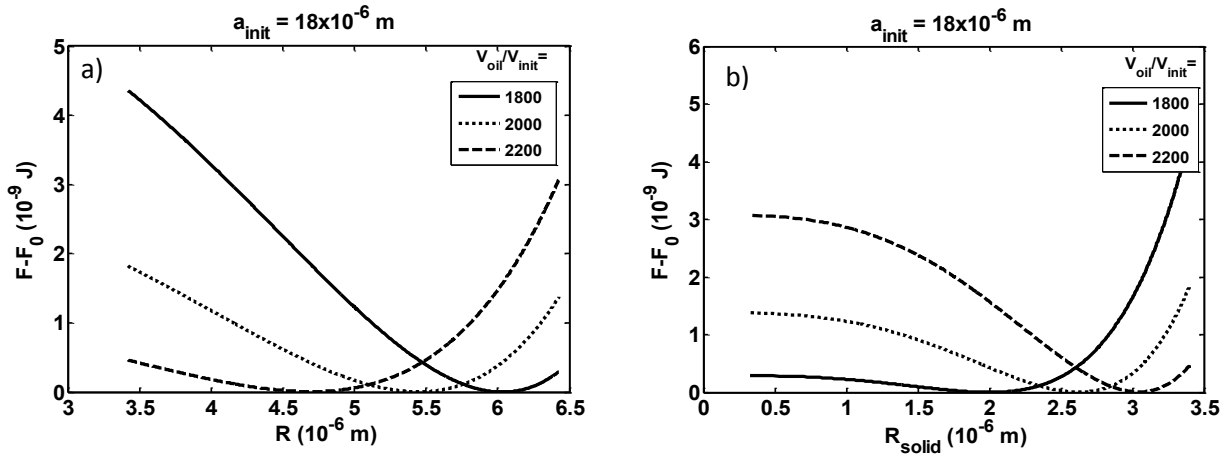
131
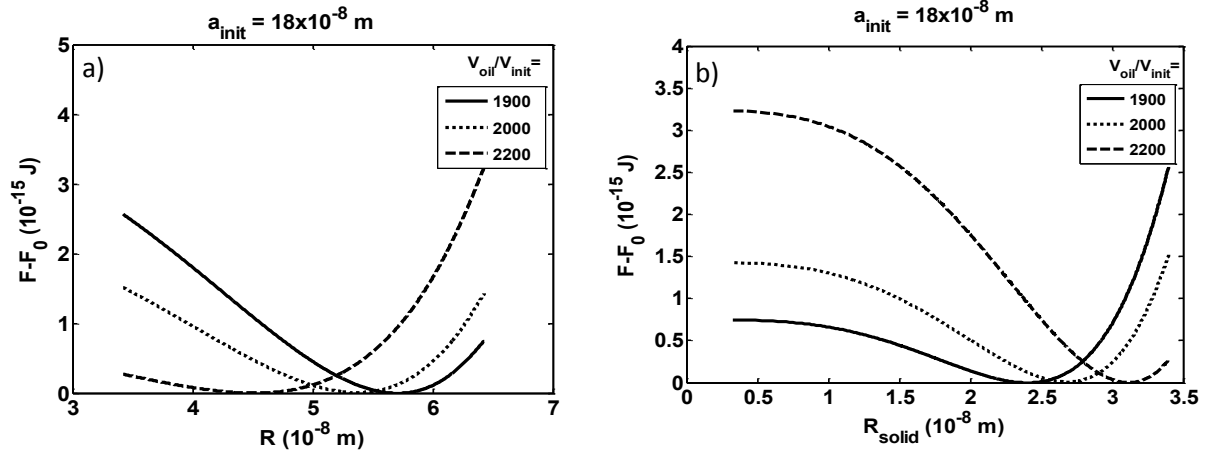
Figure 5-6 a) Free energy versus the drop size and b) Free energy versus the solid size for three different amounts of oil in the system and initial drop diameter of 18×10^{-8} m

As a result, in Figure 5-7 which is related to the lower amount of oil in the system near the onset of precipitation two equilibrium states exist, one minimum and one maximum. However, since each of the equilibrium sizes of the drop which corresponds to one equilibrium solid size matches only one x_{NaCl}^{limit}, we have to draw a free energy diagram for each x_{NaCl}^{limit} separately. Therefore, in Figure 5-7, parts a and c illustrate the minimum in free energy and therefore stable equilibrium state, for which $x_{NaCl}^{limit} = 0.1019$, while parts b and d pertain to the maximum in free energy and therefore unstable equilibrium state, for which $x_{NaCl}^{limit} = 0.1072$. In contrast, in Figure 5-6, for a higher amount of oil in the system only one equilibrium state exists which is the stable equilibrium. Figure 5-8 shows the Kelvin radius versus radius of the drop for a drop with initial drop size of 18×10^{-8} m for four different volumes of oil per initial volume of the drop. The intersection of the diagrams with the 45° line show the equilibrium sizes for each case which match very well with the extrema in Figures 5-6 and 5-7.

Figure 5-7 a) Free energy versus the drop size at $x_{Salt} = 0.1019$, b) Free energy versus the drop size at $x_{Salt} = 0.1072$, c) Free energy versus the solid size at $x_{Salt} = 0.1019$, d) Free energy versus the solid size at $x_{Salt} = 0.1072$, for oil volume per initial drop volume of 1800 and initial drop diameter of 18×10^{-8} m
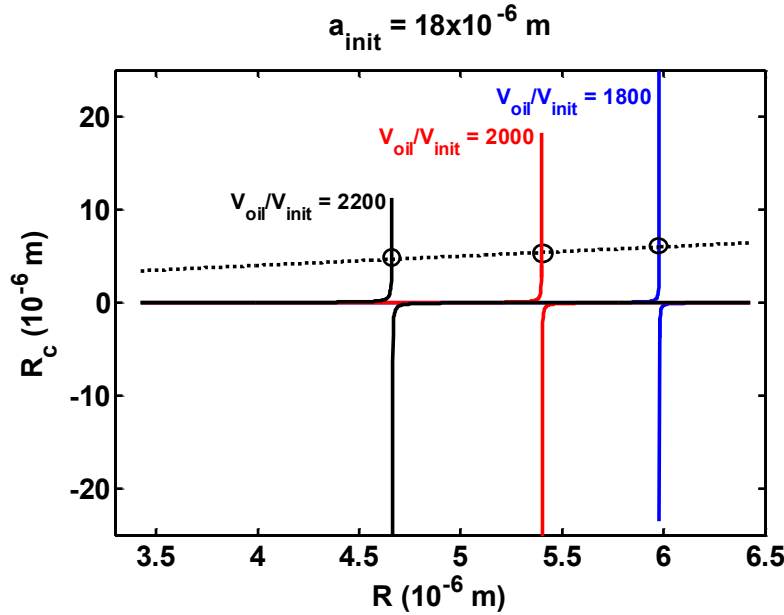
Figure 5-8 Kelvin radius versus radius of the drop for a drop with initial drop size of 18×10^{-8} m for four different volumes of oil per initial volume of the drop. The intersections with the 45° line show the equilibrium sizes for each case.

Figures 5-9 and 5-10 show the free energy diagrams for a drop with initial diameter of 18×10^{-9} m for two different amounts of oil in the system. When the initial size of the drop is 18×10^{-9} m, we found that for smaller amounts of oil in the system, near the onset of precipitation, two equilibrium states exist: one stable and one unstable equilibrium and that by increasing the amount of oil, the system encounters three equilibrium states: two unstable and one stable equilibrium state; the stable equilibrium is in between the two unstable states.

Figure 5-11 shows the Kelvin radius versus radius of the drop for a drop with initial drop size of 18×10^{-9} m for two different amounts of oil in the system. It can be seen that when dealing with this small size of a drop, the intersection of Kelvin radius curves with the 45° line which should correspond to the equilibrium states do not as accurately match the equilibrium sizes of the drop in the free energy diagrams, especially when the size of the drop goes below 5 nanometers (compare parts b and c in Figure 5-10 with part b in Figure 5-11).
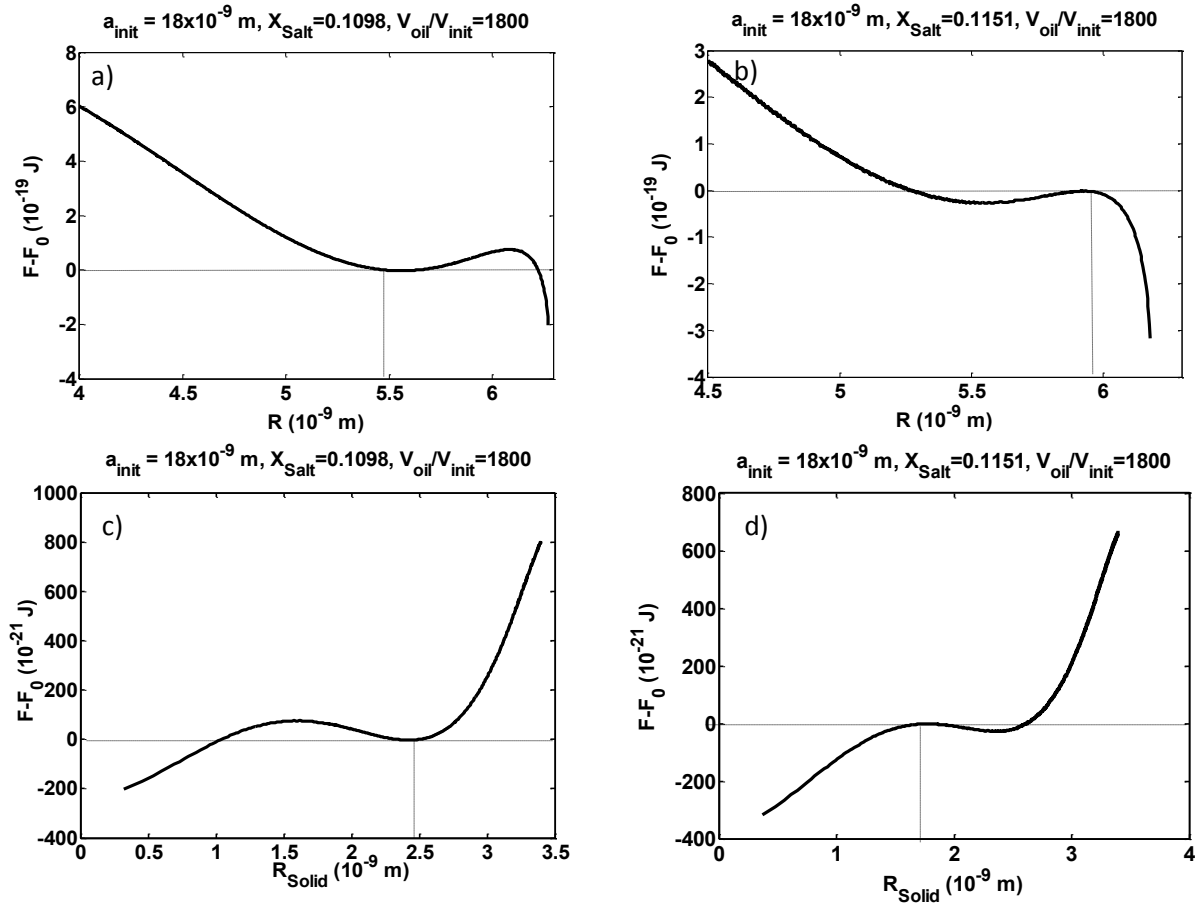
Figure 5-9 a) Free energy versus the drop size at $x_{Salt} = 0.1098$, b) Free energy versus the drop

size at $x_{Salt} = 0.1151$, c) Free energy versus the solid size at $x_{Salt} = 0.1098$, d) Free energy

versus the solid size at $x_{Salt} = 0.1151$, for oil volume per initial drop volume of 1800 at initial

drop diameter of 18×10^{-9} m
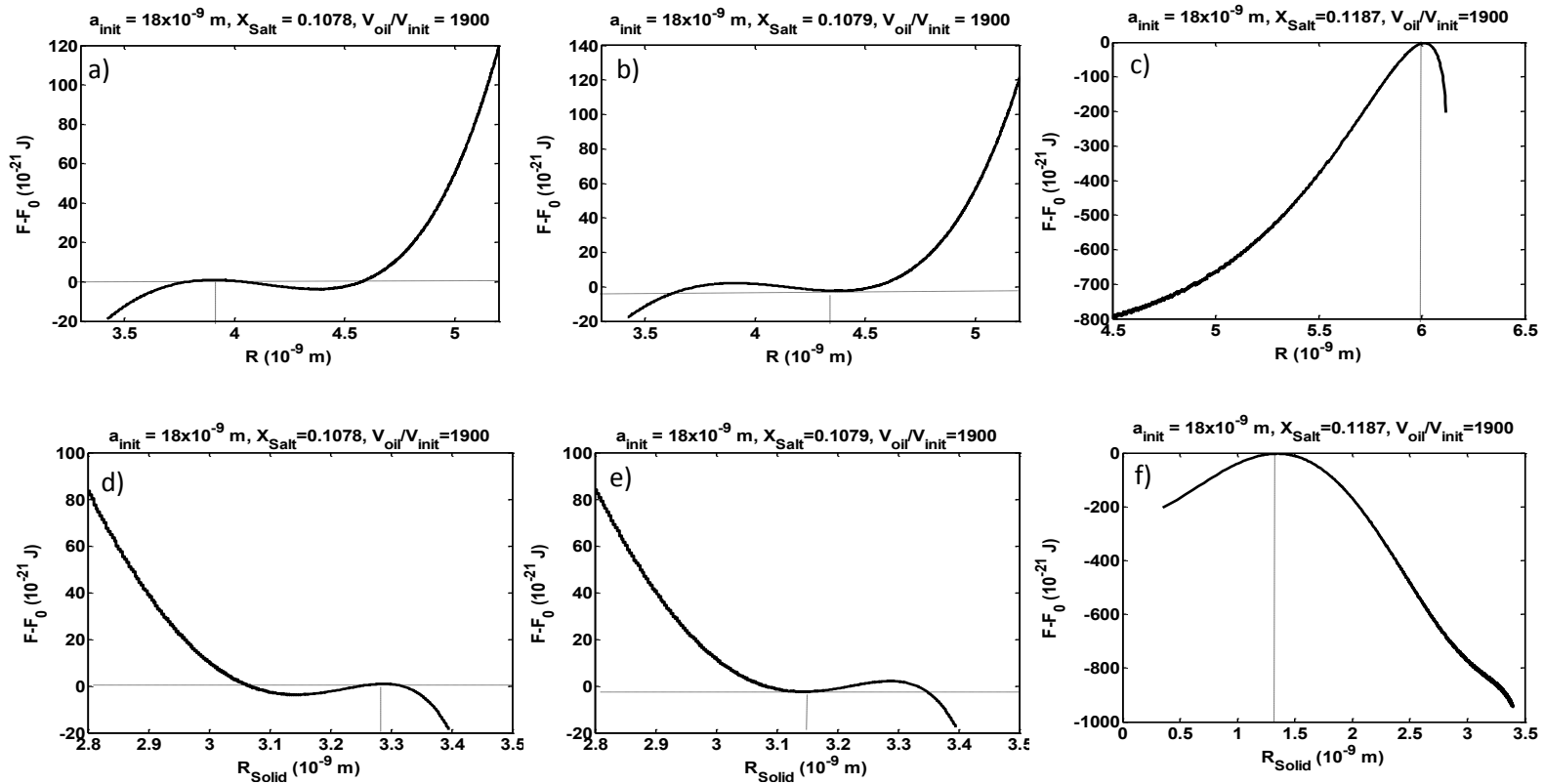
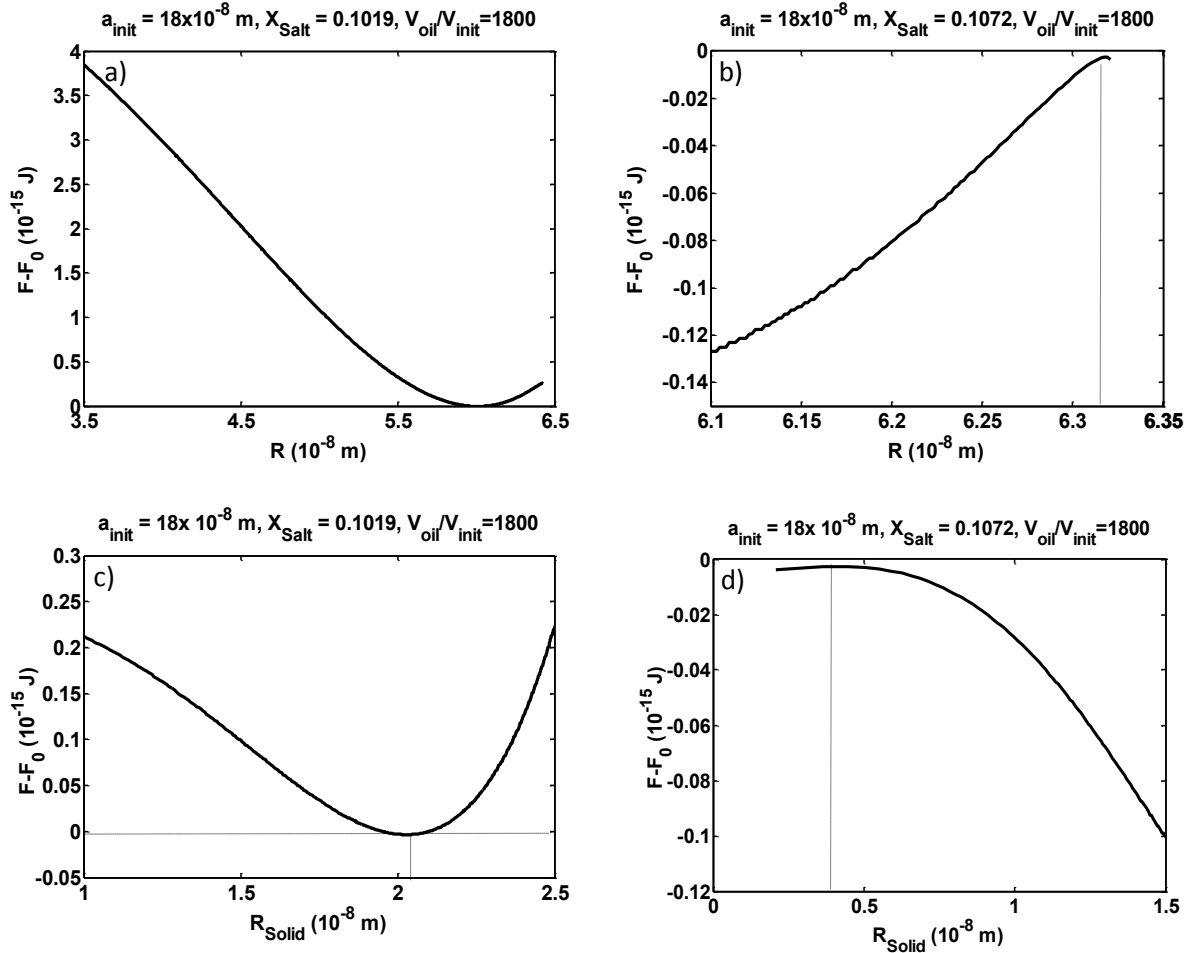Figure 5-10 a) Free energy versus the drop size at $x_{Salt} = 0.1078$, b) Free energy versus the drop size at $x_{Salt} = 0.1079$, c) Free energy versus the drop size at $x_{Salt} = 0.1187$, d) Free energy versus the solid size at $x_{Salt} = 0.1078$, e) Free energy versus the solid size at $x_{Salt} = 0.1079$, f) Free energy versus the solid size at $x_{Salt} = 0.1187$ for oil volume per initial drop volume of 1900 and initial drop diameter of 18×10^{-9} m
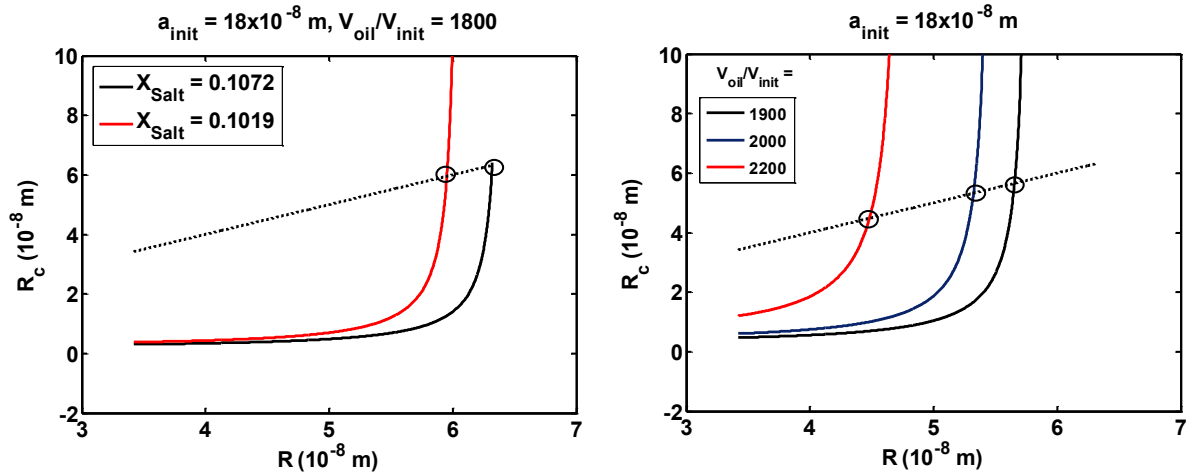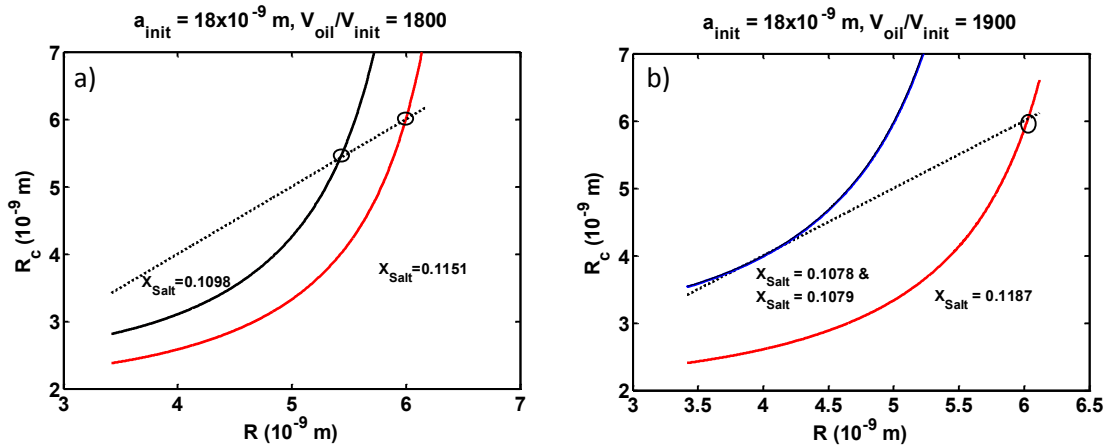
Figure 5-11 Kelvin radius versus radius of the drop for a drop with initial drop size of 18×10^{-9} m for two different volumes of oil per initial volume of the drop. The intersections with the 45° line show the equilibrium sizes for each case.

The Ostwald–Freundlich equation is an analog of the Kelvin equation relating the solubility limit to the solid size for the equilibrium of solid particles in their saturated solution. Here we investigate the role of this equation in microdrop concentrating processes including precipitations and, as expected, it was found that this role is more important for smaller initial sizes of the drop. In addition, it was found that by considering the role of the OFE, the onset of precipitation happens at a higher solubility limit and then by increasing the amount of oil in the system—which is accompanied by increasing the solute precipitation—the solubility limit decreases. The jump in solubility limit at the onset of precipitation which delays the precipitation with higher amounts of oil in the system is higher for a smaller initial size of the drop.

5.4. Conclusion

The non-ideal Ostwald–Freundlich equation is applied to the solute precipitates in microdrop concentrating process and the overall thermodynamic and stability analysis has been done. The final concentrations and sizes of the droplets are found for different initial sizes of the drop and

137

various oil volumes in the system. By considering the impact of the OFE the solubility limit is no longer constant and at the beginning of precipitation the solubility limit has its maximum value and then it will decrease upon further increasing the amount of oil.

The free energy analysis shows that for drops with initial diameters in the micrometer range there is only one stable equilibrium state and no unstable equilibrium, while by decreasing the initial size of the drop to 10^{-8} m we see two equilibrium states for an amount of oil which pertains to near the onset of precipitation and each of the states correspond to a different solubility limit. Stability analysis shows that the larger equilibrium size is unstable while the smaller one is stable. By increasing the amount of oil, the stable equilibrium size moves to the lower drop size and the unstable equilibrium size moves to the higher drop size. As was mentioned in our previous paper,[6] in this system, since a drop initially exists in the system and by increasing the concentration the drop shrinks, we move from right to left on the free energy diagram. When the initial size of the drop is about 10^{-8} m, the unstable equilibrium happens at almost the largest acceptable size of the drop (the largest acceptable size of the drop corresponds to the size at which precipitation initiates at each system) with a very small energy barrier (maximum in free energy) to be overcome. By increasing the amount of oil, since the unstable equilibrium moves further to the right of the diagram, we miss the unstable equilibrium.

When the initial drop diameter is about 10^{-9} m, we again see two equilibrium states for the amount of oil which pertains to near the onset of precipitation and each of the states corresponds to a different solubility limit. However, in this case, the unstable equilibrium happens farther from the utmost acceptable size of the drop and with a larger energy barrier. Therefore, by increasing the amount of oil, we will not miss this unstable equilibrium, even when the system meets another unstable equilibrium which is very close to the smallest acceptable size of the drop

(the smallest acceptable size of the drop corresponds to the size when almost all the water leaves the drop and all the solute precipitates). The stable equilibrium size of the drop lies between these two unstable equilibria. It seems that when the initial size of the drop is in the nanometer range, the system may not reach the stable equilibrium if it cannot overcome the energy barrier (height of the energy maximum corresponding to the largest acceptable size). In this situation, the solute may not precipitate at all unless the system is able to overcome the energy barrier. Generally speaking, in the case of a precipitated solute in water-in-oil emulsions different equilibrium states may occur depending on the system design parameters. Therefore, more care is required in designing such systems since an unexpected equilibrium may substantially affect the final results.

5.5. References

1. He, M.; Sun, C.; Chiu, D. T. Concentrating Solutes and Nanoparticles within Individual Aqueous Microdroplets. *Anal. Chem.* **2004***, 76*, 1222-1227.

2. Jeffries, G. D. M.; Kuo, J. S.; Chiu, D. T. Dynamic Modulation of Chemical Concentration in an Aqueous Droplet. *Angew. Chem. Int. Ed.* **2007***, 46*, 1326-1328.

3. Jeffries, G. D. M.; Kuo, J. S.; Chiu, D. T. Controlled Shrinkage and Re-Expansion of a Single Aqueous Droplet Inside an Optical Vortex Trap. *J. Phys. Chem. B.* **2007***, 111*, 2806-2812.

4. Bajpayee, A.; Edd, J. F.; Chang, A.; Toner, M. Concentration of Glycerol in Aqueous Microdroplets by Selective Removal of Water. *Anal. Chem.* **2010***, 82*, 1288-1291.

5. Eslami, F.; Elliott, J. A. W. Design of Microdrop Concentrating Processes. *J. Phys. Chem. B.* **2013***, 117*, 2205-2214.

6. Eslami, F.; Elliott, J. A. W. Stability Analysis of Microdrops during Concentrating Processes. *J. Phys. Chem. B.* **2014***, 118*, 3630-41.

7. Kojima, T.; Takayama, S. Microscale Determination of Aqueous Two Phase System Binodals by Droplet Dehydration in Oil. *Anal. Chem.* **2013***, 85*, 5213-5218.

8. Shim, J.; Cristobal, G.; Link, D. R.; Thorsen, T.; Jia, Y.; Piattelli, K.; Fraden, S. Control and Measurement of the Phase Behavior of Aqueous Solutions Using Microfluidics. *J. Am. Chem. Soc.* **2007***, 129*, 8825-8835.

9. Wang, B.; Shum, H. C.; Weitz, D. A. Fabrication of Monodisperse Toroidal Particles by Polymer Solidification in Microfluidics. *Chemphyschem* **2009**, *10*, 641-645.

10. Bajpayee, A.; Luo, T.; Muto, A.; Chen, G. Very Low Temperature Membrane-Free Desalination by Directional Solvent Extraction. *Energy Environ. Sci.* **2011**, *4*, 1672-1675.

11. Ward, C. A.; Levart, E. Conditions for Stability of Bubble Nuclei in Solid-Surfaces Contacting a Liquid-Gas Solution. *J. Appl. Phys.* **1984**, *56*, 491-500.

12. Ward, C. A.; Johnson, W. R.; Venter, R. D.; Ho, S.; Forest, T. W.; Fraser, W. D. Heterogeneous Bubble Nucleation and Conditions for Growth in a Liquid Gas System of Constant Mass and Volume. *J. Appl. Phys.* **1983**, *54*, 1833-1843.

13. Ward, C. A.; Tikuisis, P.; Venter, R. D. Stability of Bubbles in a Closed Volume of Liquid-Gas Solution. *J. Appl. Phys.* **1982**, *53*, 6076-6084.

14. Zargarzadeh, L.; Elliott, J. A. W. Comparative Surface Thermodynamic Analysis of New Fluid Phase Formation between a Sphere and a Flat Plate. *Langmuir* **2013**, *29*, 3610-3627.

15. Zargarzadeh, L.; Elliott, J. A. W. Surface Thermodynamic Analysis of Fluid Confined in a Cone and Comparison with the Sphere-Plate and Plate-Plate Geometries. *Langmuir* **2013**, *29*, 12950-12958.

16. Elliott, J. A. W.; Voitcu, O. On the Thermodynamic stability of Liquid Capillary Bridges. *Can. J. Chem. Eng.* **2007**, *85*, 692-700.

17. Eslami, F.; Elliott, J. A. W. Thermodynamic Investigation of the Barrier for Heterogeneous Nucleation on a Fluid Surface in Comparison with a Rigid Surface. *J. Phys. Chem. B.* **2011**, *115*, 10646-10653.

18. Mihranyan, A.; Stromme, M. Solubility of Fractal Nanoparticles. *Surf. Sci.* **2007**, *601*, 315-319.

19. Kaptay, G. On the Size and Shape Dependence of the Solubility of Nano-Particles in Solutions. *Int. J. Pharm.* **2012**, *430*, 253-257.

20. Defay, R.; Prigogine, I. *Surface Tension and Adsorption / R. Defay and I. Prigogine;* London, England : Longmans, 1966; English ed: 1966.

21. Ostwald, W. On the Assumed Isomerism of Red and Yellow Mercury Oxide and the Surface-Tension of Solid Bodies. *Zeitschrift Fur Physikalische Chemie--Stochiometrie Und Verwandtschaftslehre* **1900**, *34*, 495-503.

22. Freundlich, H. Kapillarchemie 1909. *Akademische Verlagsgessellschaft, Leipzig* .

23. Letellier, P.; Mayaffre, A.; Turmine, M. Solubility of Nanoparticles: Nonextensive Thermodynamics Approach. *J. Phys-Condens. Mat.* **2007**, *19*, 436229.

24. Johnson, K. C. Comparison of Methods for Predicting Dissolution and the Theoretical Implications of Particle-Size-Dependent Solubility. *J. Pharm. Sci.* **2012**, *101*, 681-689.

25. Shchekin, A. K.; Rusanov, A. I. Generalization of the Gibbs-Kelvin-Kohler and Ostwald–Freundlich equations for a liquid film on a soluble nanoparticle. *J. Chem. Phys.* **2008**, *129*, 154116.

26. Shchekin, A. K.; Shabaev, I. V.; Rusanov, A. I. Thermodynamics of Droplet Formation Around a Soluble Condensation Nucleus in the Atmosphere of a Solvent Vapor. *J. Chem. Phys.* **2008**, *129*, 214111.

27. Van Eerdenbrugh, B.; Vermant, J.; Martens, J. A.; Froyen, L.; Van Humbeeck, J.; Van den Monter, G.; Augustijns, P. Solubility Increases Associated with Crystalline Drug Nanoparticles: Methodologies and Significance. *Mol. Pharm.* **2010**, *7*, 1858-1870.

28. Nielsen, A.; Sohnel, O. Interfacial Tensions Electrolyte Crystal-Aqueous Solution, from Nucleation Data. *J. Cryst. Growth* **1971**, *11*, 233-&.

29. Sohnel, O. Electrolyte Crystal Aqueous-Solution Interfacial-Tensions from Crystallization Data. *J. Cryst. Growth* **1982**, *57*, 101-108.

30. Bennema, P.; Sohnel, O. Interfacial Surface-Tension for Crystallization and Precipitation from Aqueous-Solutions. *J. Cryst. Growth* **1990**, *102*, 547-556.

31. Christoffersen, J.; Rostrup, E.; Christoffersen, M. R. Relation between Interfacial Surface-Tension of Electrolyte Crystals in Aqueous Suspension and their Solubility - a Simple Derivation Based on Surface Nucleation. *J. Cryst. Growth* **1991**, *113*, 599-605.

32. Mersmann, A. Calculation of Interfacial-Tensions. *J. Cryst. Growth* **1990**, *102*, 841-847.

33. Sangwal, K. On the Estimation of Surface Entropy Factor, Interfacial-Tension, Dissolution Enthalpy and Metastable Zone-Width for Substances Crystallizing from Solution. *J. Cryst. Growth* **1989**, *97*, 393-405.

34. Yan, Z. L.; Elliott, J. A. W.; Masliyah, J. H. Roles of Various Bitumen Components in the Stability of Water-In-Diluted-Bitumen Emulsions. *J. Colloid. Interface Sci.* **1999**;220(2):329-337.

35. Vazquez, D.; Mansoori, G. A. Identification and Measurement of Petroleum Precipitates. *J. Petrol. Sci. Eng.* **2000**, *26*, 49-55.

36. Prickett, R. C.; Elliott, J. A. W.; McGann, L. E. Application of the Multisolute Osmotic Virial Equation to Solutions Containing Electrolytes. *J. Phys. Chem. B.* **2011**, *115*, 14531-14543.

37. Zielinski, M. W.; McGann, L. E.; Nychka, J. A.; Elliott, J. A. W. Comparison of Non-Ideal Solution Theories for Multi-Solute Solutions in Cryobiology and Tabulation of Required Coefficients. In Press *Cryobiology*, Accepted August 13, **2014**.

38. Design Institute for Physical Properties, Sponsored,by AIChE DIPPR Project 801 - Full Version.

39. Pinho, S. P.; Macedo, E. A. Solubility of NaCl, NaBr, and KCl in Water, Methanol, Ethanol, and their Mixed Solvents. *J. Chem. Eng. Data* **2005***, 50*, 29-32.

40. Hilder, M. H. The Solubility of Water in Edible Oils and Fats. *J. Am. Oil Chem. Soc.* **1968***, 45*, 703-707.

41. Novotny, P.; Sohnel, O. Densities of Binary Aqueous Solutions of 306 Inorganic Substances. *J. Chem. Eng. Data* **1988***, 33*, 49-55.

Chapter 6: Conclusion

Theoretical descriptions of droplets in two systems of recent interest have been developed by means of Gibbsian composite-system surface thermodynamics. One of the systems pertains to nucleation on soft surfaces which has many applications and the next system is relevant to microdrop concentrating processes that are mainly applicable in microfluidic technologies.

By considering a fluid surface as an extremely soft material, we compared the energy barrier for nucleation on a fluid surface with that for nucleation on a rigid surface with the same interfacial tensions as in the fluid case and found a smaller energy barrier for the fluid substrate which implies easier nucleation. This work is the first to provide a mathematical justification for the observed easier nucleation on soft surfaces. Furthermore, by exploring the role of each term in the free energy of the system it was found that although deformation of the substrate in the case of nucleation on a fluid surface increases the substrate–drop surface area, the liquid–vapor surface area decreases to such an extent that the ultimate energy barrier for the system is lowered to below that for the rigid substrate.

The microdrop concentrating process was the next focus of this thesis which has many applications especially in biotechnology. The system consists of water-in-oil emulsions where the water droplets contain the solute of interest that is going to be concentrated by dissolution of water into the oil phase. Two types of solute—with and without a solubility limit—have been investigated. In the case of a solute with a solubility limit, since the solute precipitates in solid form after the solution reaches its saturation concentration, two scenarios are possible: either the solid leaves the droplet or the solid remains within the droplet. We first provide an equilibrium

thermodynamic description of the process for the first scenario, ignoring any role of precipitate curvature, and explore the role in the process of design parameters such as temperature, oil volume and the initial concentration of the solute. It was found that the equilibrium drop concentration and the equilibrium drop size of both types of solutes will increase and decrease respectively by increasing the temperature or increasing the oil volume of the system. However, in the case of limited solubility solutes, after reaching the saturation concentration the equilibrium concentration will remain constant and the decreasing trend for equilibrium drop size will change entirely so that the drop can shrink completely (all water dissolving into the oil) while this is not possible for unlimited solubility solutes.

Furthermore, exploring the role of the initial drop size we found that there may be more than one equilibrium state for some cases. This led us to analyze the system from the stability point of view. Stability analysis showed that in the case of complete dissolution of the solute in water— either in the case of an unlimited solubility solute or a limited solubility solute before its saturation limit is reached and the solid precipitates—the system has only one stable equilibrium state. However, precipitation of the solid in the system may result in one, two or three equilibrium states depending on the amount of oil and initial drop size. Complete disappearance of the drop, *i.e.*, the drop radius is R_{eq0}, is always one of the equilibrium states which corresponds to a minimum in the free energy diagram. Two other equilibrium states may occur in the system; the smaller size, R_{eq1}, corresponds to the unstable equilibrium and the larger one, R_{eq2}, matches to the other minimum in the free energy diagram. The competition between the free energy of R_{eq0} and that of R_{eq2} determines which of them is the stable equilibrium in a given circumstance: the global minimum would be the stable equilibrium and the local minimum would be the metastable

one. Based on this stability analysis, we also predict a hysteresis path for droplet shrinkage through decreasing the oil volume.

Afterward, we focus on the second scenario where the solid precipitate remains within the droplet. In addition, since we had neglected the role of solid–drop interfacial tension in the first scenario we added this complexity to this second analysis and explored the role of a non-ideal Ostwald–Freundlich equation (OFE)—which describes the effect of solid curvature on solubility—on microdrop concentrating processes. Without considering the role of solid–drop interfacial tension the solubility limit depends only on temperature while by applying the OFE the solubility limit depends on solid size, temperature and solid–drop interfacial tension and at the beginning of precipitation the solubility limit has its maximum amount and then it will decrease upon increasing the amount of oil. In this case, since the solid remains within the droplet complete disappearance of the drop will not occur. Depending on the initial drop size and oil volume in the system different equilibrium states occur. However, regardless of these dependencies one stable equilibrium state exists in all cases. For micrometer initial drop sizes, this stable equilibrium is the only equilibrium state of the system but by decreasing the initial droplet size two other equilibrium states, both of which are unstable equilibrium states—one smaller and one larger than the stable one—may occur in the system. In microdrop concentrating processes, since a drop initially exists in the system and by increasing the concentration the drop shrinks, we move from right to left on the free energy diagram. As a result the presence of an unstable equilibrium at a larger drop size may not allow to precipitation of the solute at all unless the system is able to overcome the energy barrier.

Generally speaking, although continuous drop size change by changing the amount of oil in these systems is expected, an abrupt change may happen in microdrop size due to the change in

thermodynamic stability of different equilibrium states. Acquisition of this knowledge will enable the accurate design of microdrop concentrating processes. This knowledge is not only applicable in the microfluidics and biotechnology systems that motivated this work but also may be useful in other industries including water-in-oil emulsions in the oil industry in which salts are present in aqueous droplets or other emulsion scenarios in which a droplet surrounded by a fluid phase which controls the droplet size by dissolution contains a solute that may or may not precipitate.

6.1. Limitations and Future works

Throughout this thesis the role of gravity has been ignored. The accuracy of this assumption can be examined by means of the Bond number which is a dimensionless number equal to the ratio of gravitational to surface tension forces:

$$Bo = \frac{\Delta \rho g R^2}{\gamma} \tag{6-1}$$

In Chapter 2 where we considered nucleation of water on dodecane at 22 °C the density of dodecane is 748.4 kg/m^3 and the density of water is 997.7686 kg/m^3. As a result the Bond number at the Kelvin radius is:

$$Bo = \frac{\Delta \rho g R^2}{\gamma} = \frac{249.3686 \frac{kg}{m^3} \times 9.81 \frac{m}{s^2} \times \left(4.9072 \times 10^{-8} m\right)^2}{53.7 \times 10^{-3} \frac{N}{m}} = 1.097 \times 10^{-10} \tag{6-2}$$

In Chapters 3, 4 and 5 we considered an aqueous drop of glycerol or sodium chloride in soybean oil between 25-35 °C. As an illustration, at 30 °C with the molarity of the solute being set at 3 molar, the density of the sodium chloride solution is 1112.7 kg/m^3, the density of the glycerol solution is 1054.4 kg/m^3, and the density of soybean oil is 917.4775 kg/m^3. For drop radius between $9 \times 10^{-6} m$ and $9 \times 10^{-9} m$ and the drop–oil surface tension of 22.8 mN/m, the Bond numbers for the glycerol solution and sodium chloride solution are respectively:

$$6.456 \times 10^{-12} \leq Bo \leq 6.456 \times 10^{-6} \tag{6-3}$$

$$4.424 \times 10^{-12} \leq Bo \leq 4.424 \times 10^{-6} \tag{6-4}$$

These small Bond numbers verify that gravitational effects can be ignored in comparison with the surface effects.

Another limitation of our work is our setting of the for drop–oil surface tension to be equal to the pure water–soybean oil surface tension while in reality the drop phase become highly concentrated and its surface tension would depend on the mole fraction of the drop constituents.

We have also ignored the role of adsorption in this work—since we have enough complexity in our system—which could be improved upon in future by making use of the Gibbs adsorption equation and using an appropriate adsorption isotherm.

Throughout this thesis we have investigated the systems at equilibrium and where the intensive properties of the systems reach their final value without any macroscopic change. While prior to reaching the equilibrium, the kinetics of the system determine when and how it will reach the equilibrium, note that the equilibrium state determines the driving force towards equilibrium for the systems. In addition, in cases for which the kinetics are very rapid and the equilibrium time scale is on the order of minutes—such as for the microfluidic system—thermodynamics and the equilibrium information of the systems provide a good perspective for the qualitative behaviour of the system.

Appendix: Numerical Methods and Flowcharts:

The calculation procedures in Chapters 3, 4 and 5 are numerical and are done using the Matlab software. However, due to the high sensitivity of equations to the first guess and the probability of multiple answers for the set of equations, we did not use the current software functions such as fsolve. Instead, we first choose a dimensionless variable that has a confined range such as $\frac{R}{a_{init}}$ that is between 0 and 1. Then by using a very small step such as $a_{init} \times 10^{-4}$ we find the amount of the objective function. Since the roots of the function would be found when f(variables)=0, wherever the function value goes from positive to negative or vice versa we obtain the roots. This method is primitive but for our case of dealing with very small magnitudes and the potential of several roots, it is a trusted method.

Solution Flowchart for Chapter 3:

Before precipitation region:

Simultaneously solving

(3-15), (3-16),

(3-17), (3-19)

and (3-26)

R_{eq} ☑
x_w^D ☑
x_w^L ☑
$x_\alpha^{D,bp}$ ☑
x_o^L ☑

If $x_\alpha^{D,bp} > x_\alpha^\infty$?

Yes

No

Still in before precipitation region

In precipitation region: $x_\alpha^D = x_\alpha^\infty$

If solving the set of equations ((3-17), (3-19), (3-26), (3-29)) converges?

No

No equilibrium with drop present

Yes

R_{eq} ☑
N_α^S ☑
x_w^L ☑
x_o^L ☑

Solution Flowchart for Chapter 5:

Certainly in precipitation region
R_{eq} ☑
R_{seq} ☑
x_w^L ☑
x_α^{limit} ☑

If $x_\alpha^{D,bp} > x_\alpha^\infty$?

Yes

If solving the set of equations ((5-16), (5-21), (5-30), (5-31)) converges?

Yes

No

No

Still in before precipitation region

No

Has the system previously entered precipitation region?

Yes

No equilibrium with drop present

No

Yes

If $x_\alpha^{D,bp} > x_\alpha^{limit}$?

Regression Statistics for Figure 3-3

This table is produced by Excel.

Regression Statistics	
Multiple R	0.995883071
R Square	0.991783092
Adjusted R Square	0.99013971
Standard Error	0.001609122
Observations	7

ANOVA

	df	SS	MS	F	Significance F
Regression	1	0.001562631	0.001562631	603.5013799	2.08415E-06
Residual	5	1.29464E-05	2.58927E-06		
Total	6	0.001575577			

	Coefficients	Standard Error	t Stat	P-value	Lower 95%	Upper 95%
Intercept	0.034642249	0.001003239	34.53041661	3.83178E-07	0.032063342	0.037221156
X Variable 1	0.000842778	3.43063E-05	24.56626508	2.08415E-06	0.000754591	0.000930965

The 95% confidence values for the linear coefficient and intercepts of equation 3-30 are given in the bottom right entries of this table.

Bibliography

1. Marmur, A. Wetting on Hydrophobic Rough Surfaces: To Be Heterogeneous or Not to Be? *Langmuir* **2003***, 19*, 8343-8348.

2. Milne, A. J. B.; Elliott, J. A. W.; Zabeti, P.; Zhou, J.; Amirfazli, A. Model and Experimental Studies for Contact Angles of Surfactant Solutions on Rough and Smooth Hydrophobic Surfaces. *Phys. Chem. Chem. Phys.* **2011***, 13*, 16208-16219.

3. Sheng, Y.; Jiang, S.; Tsao, H. Effects of Geometrical Characteristics of Surface Roughness on Droplet Wetting. *J. Chem. Phys.* **2007***, 127*, 234704.

4. Bittoun, E.; Marmur, A. The Role of Multiscale Roughness in the Lotus Effect: Is It Essential for Super-Hydrophobicity? *Langmuir* **2012***, 28*, 13933-13942.

5. Marmur, A. Underwater Superhydrophobicity: Theoretical Feasibility. *Langmuir* **2006***, 22*, 1400-1402.

6. Marmur, A. The Lotus Effect: Superhydrophobicity and Metastability. *Langmuir* **2004***, 20*, 3517-3519.

7. Li, W.; Amirfazli, A. Microtextured Superhydrophobic Surfaces: A Thermodynamic Analysis. *Adv. Colloid Interface Sci.* **2007***, 132*, 51-68.

8. Kwon, Y.; Patankar, N.; Choi, J.; Lee, J. Design of Surface Hierarchy for Extreme Hydrophobicity. *Langmuir* **2009***, 25*, 6129-6136.

9. Gibbs, J. W. On the Equilibrium of Heterogeneous Substances. *Trans. Conn. Acad. Arts Sci.3* **1876**, 108–248; **1878**, 343–524, in "The Scientific Papers of J. Willard Gibbs," Ox Bow, Woodridge, CT (1993), Vol. I, pp. 55–353.

10. Callen, H. B. *Thermodynamics and an Introduction to Thermostatistics;* Wiley: New York, 1985; pp 36.

11. Hunter, R. J. *Introduction to Modern Colloid Science;* Oxford University Press Inc.: New York, 1993; Vol. 1, pp 344.

12. Ward, C. A.; Johnson, W. R.; Venter, R. D.; Ho, S.; Forest, T. W.; Fraser, W. D. Heterogeneous Bubble Nucleation and Conditions for Growth in a Liquid Gas System of Constant Mass and Volume. *J. Appl. Phys.* **1983***, 54*, 1833-1843.

13. Elliott, J. A. W. On the Complete Kelvin Equation. *Chem. Eng. Educ.* **2001***, 35*, 274-278.

14. McGaughey, A. J. H.; Ward, C. A. Droplet Stability in a Finite System: Consideration of the Solid-Vapor Interface. *J. Appl. Phys.* **2003**, *93*, 3619-3626.

15. Ghasemi, H.; Ward, C. A. Surface Tension of Solids in the Absence of Adsorption. *J. Phys. Chem. B.* **2009**, *113*, 12632-12634.

16. Ward, C. A.; Wu, J. Effect of Adsorption on the Surface Tensions of Solid-Fluid Interfaces. *J. Phys. Chem. B.* **2007**, *111*, 3685-3694.

17. Ghasemi, H.; Ward, C. A. Sessile-Water-Droplet Contact Angle Dependence on Adsorption at the Solid-Liquid Interface. *J. Phys. Chem. C* **2010**, *114*, 5088-5100.

18. Wu, J.; Farouk, T.; Ward, C. A. Pressure Dependence of the Contact Angle. *J. Phys. Chem. B.* **2007**, *111*, 6189-6197.

19. Forest, T. W.; Ward, C. A. Homogeneous Nucleation of Bubbles in Solutions at Pressures Above Vapor-Pressure of Pure Liquid. *J. Chem. Phys.* **1978**, *69*, 2221-2230.

20. Ward, C. A.; Levart, E. Conditions for Stability of Bubble Nuclei in Solid-Surfaces Contacting a Liquid-Gas Solution. *J. Appl. Phys.* **1984**, *56*, 491-500.

21. Ward, C. A.; Tikuisis, P.; Venter, R. D. Stability of Bubbles in a Closed Volume of Liquid-Gas Solution. *J. Appl. Phys.* **1982**, *53*, 6076-6084.

22. Attard, P. Thermodynamic Analysis of Bridging Bubbles and a Quantitative Comparison with the Measured Hydrophobic Attraction. *Langmuir* **2000**, *16*, 4455-4466.

23. Elliott, J. A. W.; Voitcu, O. On the Thermodynamic Stability of Liquid Capillary Bridges. *Can. J. Chem. Eng.* **2007**, *85*, 692-700.

24. Zargarzadeh, L.; Elliott, J. A. W. Comparative Surface Thermodynamic Analysis of New Fluid Phase Formation between a Sphere and a Flat Plate. *Langmuir* **2013**, *29*, 3610-3627.

25. Zargarzadeh, L.; Elliott, J. A. W. Surface Thermodynamic Analysis of Fluid Confined in a Cone and Comparison with the Sphere-Plate and Plate-Plate Geometries. *Langmuir* **2013**, *29*, 12950-12958.

26. Reiss, H.; Koper, G. The Kelvin Relation - Stability, Fluctuation, and Factors Involved in Measurement. *J. Phys. Chem.* **1995**, *99*, 7837-7844.

27. Fisher, L. R.; Israelachvili, J. N. Experimental Studies on the Applicability of the Kelvin Equation to Highly Curved Concave Menisci. *J. Colloid Interface Sci.* **1981**, *80*, 528-541.

28. Sajadinia, S. H.; Sharif, F. Thermodynamic Analysis of the Wetting Behavior of Dual Scale Patterned Hydrophobic Surfaces. *J. Colloid Interface Sci.* **2010**, *344*, 575-583.

29. Li, W.; Amirfazli, A. A Thermodynamic Approach for Determining the Contact Angle Hysteresis for Superhydrophobic Surfaces. *J. Colloid Interface Sci.* **2005**, *292*, 195-201.

30. Zhang, H.; Li, W.; Cui, D.; Hu, Z.; Xu, L. Design of Lotus-Simulating Surfaces: Thermodynamic Analysis Based on a New Methodology. *Colloid Surface A.* **2012***, 413*, 314-327.

31. Long, J.; Hyder, M. N.; Huang, R. Y. M.; Chen, P. Thermodynamic Modeling of Contact Angles on Rough, Heterogeneous Surfaces. *Adv. Colloid Interface Sci.* **2005***, 118*, 173-190.

32. Wenzel, R. Resistance of Solid Surfaces to Wetting by Water. *Ind. Eng. Chem.* **1936***, 28*, 988-994.

33. Cassie, A.; Baxter, S. Wettability of Porous Surfaces. *T. Faraday Soc.* **1944***, 40*, 0546-0550.

34. Extrand, C. W.; Kumagai, Y. Contact Angles and Hysteresis on Soft Surfaces. *J. Colloid Interface Sci.* **1996***, 184*, 191-200.

35. Pericet-Camara, R.; Auernhammer, G. K.; Koynov, K.; Lorenzoni, S.; Raiteri, R.; Bonaccurso, E. Solid-Supported Thin Elastomer Films Deformed by Microdrops. *Soft Matter* **2009***, 5*, 3611-3617.

36. Pericet-Camara, R.; Best, A.; Butt, H.; Bonaccurso, E. Effect of Capillary Pressure and Surface Tension on the Deformation of Elastic Surfaces by Sessile Liquid Microdrops: An Experimental Investigation. *Langmuir* **2008***, 24*, 10565-10568.

37. Carre, A.; Gastel, J. C.; Shanahan, M. E. R. Viscoelastic Effects in The Spreading of Liquids. *Nature* **1996***, 379*, 432-434.

38. Jerison, E. R.; Xu, Y.; Wilen, L. A.; Dufresne, E. R. Deformation of an Elastic Substrate by a Three-Phase Contact Line. *Phys. Rev. Lett.* **2011***, 106*, 186103.

39. Lester, G. R. Contact Angles of Liquids at Deformable Solid Surfaces. *J. Colloid Sci.* **1961***, 16*, 315-&.

40. Rusanov, A. I. Theory of Wetting of Elastically Deformed Bodies .1. Deformation with a Finite Contact-Angle. *Colloid J. Ussr+* **1975***, 37*, 614-622.

41. Shanahan, M. E. R.; de Genns, P. G. In *Adhesion 11;* Allen, K. W., Ed.; Elsevier Applied Science Publ: London, 1987; Vol. 11, pp 71-81.

42. Shanahan, M. E. R. The Spreading Dynamics of a Liquid-Drop on a Viscoelastic Solid. *J. Phys. D. Appl. Phys.* **1988***, 21*, 981-985.

43. Shanahan, M. E. R.; Carre, A. Spreading and Dynamics of Liquid Drops Involving Nanometric Deformations on Soft Substrates. *Colloid Surf. A.* **2002***, 206*, 115-123.

44. White, L. R. The Contact Angle on an Elastic Substrate. 1. The Role of Disjoining Pressure in the Surface Mechanics. *J. Colloid Interface Sci.* **2003***, 258*, 82-96.

45. Yu, Y.; Zhao, Y. Elastic Deformation of Soft Membrane with Finite Thickness Induced by a Sessile Liquid Droplet. *J. Colloid Interface Sci.* **2009**, *339*, 489-494.

46. Kern, R.; Muller, P. Deformation of an Elastic Thin Solid Induced by a Liquid Droplet. *Surf Sci.* **1992**, *264*, 467-494.

47. Yu, Y.; Yang, Z.; Zhao, Y. Role of Vertical Component of Surface Tension of the Droplet on the Elastic Deformation of PDMS Membrane. *J. Adhes. Sci. Technol.* **2008**, *22*, 687-698.

48. Style, R. W.; Dufresne, E. R. Static Wetting on Deformable Substrates, from Liquids to Soft Solids. *Soft Matter* **2012**, *8*, 7177-7184.

49. Shanahan, M. E. R. The Influence of Solid Micro-Deformation on Contact-Angle Equilibrium. *J. Phys. D. Appl. Phys.* **1987**, *20*, 945-950.

50. Olives, J. Surface Thermodynamics, Surface Stress, Equations at Surfaces and Triple Lines for Deformable Bodies. *J. Phys. Condens. Mat.* **2010**, *22*, 085005.

51. Olives, J. Green's Formula and Singularity at a Triple Contact Line. Example of Finite-Displacement Solution. *Int. J. Solids Struc.* **2014**, *51*, 314-324.

52. Style, R. W.; Boltyanskiy, R.; Che, Y.; Wettlaufer, J. S.; Wilen, L. A.; Dufresne, E. R. Universal Deformation of Soft Substrates Near a Contact Line and the Direct Measurement of Solid Surface Stresses. *Phys. Rev. Lett.* **2013**, *110*, 066103.

53. Squires, T. M. Drops on Soft Surfaces Learn the Hard Way. *P. Natl. Acad. Sci. USA.* **2013**, *110*, 12505-12506.

54. Style, R. W.; Che, Y.; Park, S. J.; Weon, B. M.; Je, J. H.; Hyland, C.; German, G. K.; Power, M. P.; Wilen, L. A.; Wettlaufer, J. S.; Dufresne, E. R. Patterning Droplets with Durotaxis. *P. Natl. Acad. Sci. USA.* **2013**, *110*, 12541-12544.

55. Sokuler, M.; Auernhammer, G. K.; Roth, M.; Liu, C.; Bonaccurso, E.; Butt, H. The Softer the Better: Fast Condensation on Soft Surfaces. *Langmuir* **2010**, *26*, 1544-1547.

56. Bremond, N.; Bibette, J. Exploring Emulsion Science with Microfluidics. *Soft Matter* **2012**, *8*, 10549-10559.

57. Chiu, D. T.; Lorenz, R. M.; Jeffries, G. D. M. Droplets for Ultrasmall-Volume Analysis. *Anal. Chem.* **2009**, *81*, 5111-5118.

58. Huebner, A.; Sharma, S.; Srisa-Art, M.; Hollfelder, F.; Edel, J. B.; deMello, A. J. Microdroplets: A Sea of Applications? *Lab Chip* **2008**, *8*, 1244-1254.

59. Kuo, J. S.; Chiu, D. T. Controlling mass Transport in Microfluidic Devices. *Annu. Rev. Anal. Chem.* **2011**, *4*, 275-296.

60. He, M.; Sun, C.; Chiu, D. T. Concentrating Solutes and Nanoparticles within Individual Aqueous Microdroplets. *Anal. Chem.* **2004**, *76*, 1222-1227.

61. Shim, J.; Cristobal, G.; Link, D. R.; Thorsen, T.; Jia, Y.; Piattelli, K.; Fraden, S. Control and Measurement of the Phase Behavior of Aqueous Solutions using Microfluidics. *J. Am. Chem. Soc.* **2007**, *129*, 8825-8835.

62. Ji, J.; Nie, L.; Li, Y.; Yang, P.; Liu, B. Simultaneous Online Enrichment and Identification of Trace Species Based on Microfluidic Droplets. *Anal. Chem.* **2013**, *85*, 9617-9622.

63. Bajpayee, A.; Edd, J. F.; Chang, A.; Toner, M. Concentration of Glycerol in Aqueous Microdroplets by Selective Removal of Water. *Anal. Chem.* **2010**, *82*, 1288-1291.

64. Kojima, T.; Takayama, S. Microscale Determination of Aqueous Two Phase System Binodals by Droplet Dehydration in Oil. *Anal. Chem.* **2013**, *85*, 5213-5218.

65. Wang, B.; Shum, H. C.; Weitz, D. A. Fabrication of Monodisperse Toroidal Particles by Polymer Solidification in Microfluidics. *Chemphyschem* **2009**, *10*, 641-645.

66. Wu, T.; Hirata, K.; Suzuki, H.; Xiang, R.; Tang, Z.; Yomo, T. Shrunk to Femtolitre: Tuning High-Throughput Monodisperse Water-In-Oil Droplet Arrays for Ultra-Small Micro-Reactors. *Appl. Phys. Lett.* **2012**, *101*, 074108.

67. Bajpayee, A.; Luo, T.; Muto, A.; Chen, G. Very Low Temperature Membrane-Free Desalination by Directional Solvent Extraction. *Energy Environ. Sci.* **2011**, *4*, 1672-1675.

68. Jeffries, G. D. M.; Kuo, J. S.; Chiu, D. T. Dynamic Modulation of Chemical Concentration in an Aqueous Droplet. *Angew. Chem. Int. Ed.* **2007**, *46*, 1326-1328.

69. Jeffries, G. D. M.; Kuo, J. S.; Chiu, D. T. Controlled Shrinkage and Re-Expansion of a Single Aqueous Droplet inside an Optical Vortex Trap. *J. Phys. Chem. B*. **2007**, *111*, 2806-2812.

70. Shen, A. Q.; Wang, D.; Spicer, P. T. Kinetics of Colloidal Templating Using Emulsion Drop Consolidation. *Langmuir* **2007**, *23*, 12821-12826.

71. Debenedetti, Thermodynamics: When a Phase is Born. P. G. *Nature* **2006**, *441*, 168-169.

72. Leach, R. N.; Stevens, F.; Langford, S. C.; Dickinson, J. T. Dropwise Condensation: Experiments and Simulations of Nucleation and Growth of Water Drops in a Cooling System. *Langmuir* **2006**, *22*, 8864-8872.

73. Family, F.; Meakin, P. Scaling of the Droplet-Size Distribution in Vapor-Deposited Thin-Films. *Phys. Rev. Lett.* **1988**, *61*, 428-431.

74. Shanahan, M. E. R. Contact-Angle Equilibrium on Thin Elastic Solids. *J. Adhesion* **1985**, *18*, 247-267.

75. Shanahan, M. E. R. Equilibrium of Liquid-Drops on Thin Plates - Plate Rigidity and Stability Considerations. *J. Adhesion* **1987***, 20*, 261-274.

76. Nepomnyashchy, A. A.; Golovin, A. A.; Tikhomirova, A. E.; Volpert, V. A. Nucleation and Growth of Droplets at a Liquid-Gas Interface. *Phys. Rev. E.* **2006***, 74*, 021605.

77. Jarvis, T. J.; Donohue, M. D.; Katz, J. L. Bubble Nucleation Mechanisms of Liquid Droplets Superheated in Other Liquids. *J. Colloid Interface Sci.* **1975***, 50*, 359-368.

78. Toshev, B. V.; Avramov, M. Z. On the Thermodynamic Stability of Small Droplets at Positive Line Tension*. Colloid Surface A.* **1993***, 75*, 33-37.

79. Toshev, B. V. Equilibrium and Stability of Spherical Cap-Shaped Liquid Drops*. Colloid surface A.* **1996***, 108*, 133-135.

80. Ward, C. A.; Sasges, M. R. Effect of Gravity on Contact Angle: A Theoretical Investigation*. J. Chem. Phys.* **1998***, 109*, 3651-3660.

81. Goebel, A.; Lunkenheimer, K. Interfacial Tension of the Water/N-alkane Interface. *Langmuir* **1997***, 13*, 369-372.

82. Chiu, D. T. Micro- and Nano-Scale Chemical Analysis of Individual Sub-Cellular Compartments. *TrAC - Trend Anal. Chem.* **2003***, 22*, 528-536.

83. Sgro, A. E.; Allen, P. B.; Chiu, D. T. Thermoelectric Manipulation of Aqueous Droplets in Microfluidic Devices. *Anal. Chem.* **2007***, 79*, 4845-4851.

84. He, M.; Edgar, J. S.; Jeffries, G. D. M.; Lorenz, R. M.; Shelby, J. P.; Chiu, D. T. Selective Encapsulation of Single Cells and Subcellular Organelles into Picoliter- and Femtoliter-Volume Droplets. *Anal. Chem.* **2005***, 77*, 1539-1544.

85. Gadd, J. C.; Kuyper, C. L.; Fujimoto, B. S.; Allen, R. W.; Chiu, D. T. Sizing Subcellular Organelles and Nanoparticles Confined within Aqueous Droplets. *Anal. Chem.* **2008***, 80*, 3450-3457.

86. Hilder, M. H. The Solubility of Water in Edible Oils and Fats. *J. Am. Oil Chem. Soc.* **1968***, 45*, 703-707.

87. Prickett, R. C.; Elliott, J. A. W.; McGann, L. E. Application of the Osmotic Virial Equation in Cryobiology. *Cryobiology* **2010***, 60*, 30-42.

88. Elliott, J. A. W.; Prickett, R. C.; Elmoazzen, H. Y.; Porter, K. R.; McGann, L. E. A Multisolute Osmotic Virial Equation for Solutions of Interest in Biology. *J. Phys. Chem. B.* **2007***, 111*, 1775-1785.

89. Pinho, S. P.; Macedo, E. A. Solubility of NaCl, NaBr, and KCl in Water, Methanol, Ethanol, and their Mixed Solvents. *J. Chem. Eng. Data* **2005***, 50*, 29-32.

90. Prickett, R. C.; Elliott, J. A. W.; McGann, L. E. Application of the Multisolute Osmotic Virial Equation to Solutions Containing Electrolytes. *J. Phys. Chem. B.* **2011***, 115*, 14531-14543.

91. Perkins, E. G. In *Physical Properties of Soybeans;* Erickson, D. R., Ed.; Practical Handbook of Soybean Processing and Utilization; AOCS Press: Champaign,IL, 1995; pp 29-38.

92. Wang, T. In *Soybean Oil;* Gunstone, F. D., Ed.; Vegetable Oils in Food Technology : Composition, Properties, and Uses; Blackwell ; CRC Press: Osney Mead, Oxford; Boca Raton, 2002; pp 90-103.

93. Hammond, E. G.; Johnson, L. A.; White, P. J.; Wang, T.; Su, C. In *Soybean Oil;* Shahidi, F., Ed.; Bailey's Industrial oil and fat products; Wiley: New York, 1979; pp 577-653.

94. Novotny, P.; Sohnel, O. Densities of Binary Aqueous Solutions of 306 Inorganic Substances. *J. Chem. Eng. Data* **1988***, 33*, 49-55.

95. Design Institute for Physical Properties, Sponsored,by AIChE DIPPR Project 801 - Full Version.

96. Theberge, A. B.; Courtois, F.; Schaerli, Y.; Fischlechner, M.; Abell, C.; Hollfelder, F.; Huck, W. T. S. Microdroplets in Microfluidics: An Evolving Platform for Discoveries in Chemistry and Biology. *Angew. Chem. int. Edit.* **2010***, 49*, 5846-5868.

97. Joensson, H. N.; Svahn, H. A. Droplet Microfluidics-A Tool for Single-Cell Analysis. *Angew. Chem. int. Edit.* **2012***, 51*, 12176-12192.

98. Lagus, T. P.; Edd, J. F. A eview of the Theory, Methods and Recent Applications of High-Throughput Single-Cell Droplet Microfluidics. *J. Phys. D. Appl. Phys.* **2013***, 46*, 114005.

99. Eslami, F.; Elliott, J. A. W. Design of Microdrop Concentrating Processes. *J. Phys. Chem. B.* **2013***, 117*, 2205-2214.

100. Wang, B.; Shum, H. C.; Weitz, D. A. Fabrication of Monodisperse Toroidal Particles by Polymer Solidification in Microfluidics. *Chemphyschem* **2009***, 10*, 641-645.

101. Vogelsberger, W. Use of Chemical-Potentials in the Condensation of a Pure Vapor. *Chem. Phy. Lett.* **1979***, 64*, 601-604.

102. Eslami, F.; Elliott, J. A. W. Thermodynamic Investigation of the Barrier for Heterogeneous Nucleation on a Fluid Surface in Comparison with a Rigid Surface. *J Phys Chem B* **2011***, 115*, 10646-10653.

103. Zielinski, M. W.; McGann, L. E.; Nychka, J. A.; Elliott, J. A. W. Comparison of Non-Ideal Solution Theories for Multi-Solute Solutions in Cryobiology and Tabulation of Required Coefficients. In Press *Cryobiology*, Accepted August 13, **2014**.

104. Eslami, F.; Elliott, J. A. W. Stability Analysis of Microdrops during Concentrating Processes. *J. Phys. Chemi. B.* **2014**, *118*, 3630-41.

105. Mihranyan, A.; Stromme, M. Solubility of Fractal Nanoparticles. *Surf. Sci.* **2007**, *601*, 315-319.

106. Kaptay, G. On the Size and Shape Dependence of the Solubility of Nano-Particles in Solutions. *Int. J. Pharm.* **2012**, *430*, 253-257.

107. Ostwald, W. On the Assumed Isomerism of Red and Yellow Mercury Oxide and the Surface-Tension of Solid Bodies. *Zeitschrift Fur Physikalische Chemie--Stochiometrie Und Verwandtschaftslehre* **1900**, *34*, 495-503.

108. Freundlich, H. Kapillarchemie 1909. *Akademische Verlagsgessellschaft, Leipzig* .

109. Defay, R.; Prigogine, I. *Surface Tension and Adsorption / R. Defay and I. Prigogine;* London, England : Longmans, 1966; English ed: 1966; .

110. Letellier, P.; Mayaffre, A.; Turmine, M. Solubility of Nanoparticles: Nonextensive Thermodynamics Approach. *J. Phys-Condens. Mat.* **2007**, *19*, 436229.

111. Johnson, K. C. Comparison of Methods for Predicting Dissolution and the Theoretical Implications of Particle-Size-Dependent Solubility. *J. Pharm. Sci.* **2012**, *101*, 681-689.

112. Shchekin, A. K.; Rusanov, A. I. Generalization of the Gibbs-Kelvin-Kohler and Ostwald–Freundlich equations for a liquid film on a soluble nanoparticle. *J. Chem. Phys.* **2008**, *129*, 154116.

113. Shchekin, A. K.; Shabaev, I. V.; Rusanov, A. I. Thermodynamics of Droplet Formation Around a Soluble Condensation Nucleus in the Atmosphere of a Solvent Vapor. *J. Chem. Phys.* **2008**, *129*, 214111.

114. Van Eerdenbrugh, B.; Vermant, J.; Martens, J. A.; Froyen, L.; Van Humbeeck, J.; Van den Monter, G.; Augustijns, P. Solubility Increases Associated with Crystalline Drug Nanoparticles: Methodologies and Significance. *Mol. Pharm.* **2010**, *7*, 1858-1870.

115. Nielsen, A.; Sohnel, O. Interfacial Tensions Electrolyte Crystal-Aqueous Solution, from Nucleation Data. *J. Cryst. Growth* **1971**, *11*, 233-&.

116. Sohnel, O. Electrolyte Crystal Aqueous-Solution Interfacial-Tensions from Crystallization Data. *J. Cryst. Growth* **1982**, *57*, 101-108.

117. Bennema, P.; Sohnel, O. Interfacial Surface-Tension for Crystallization and Precipitation from Aqueous-Solutions. *J. Cryst. Growth* **1990**, *102*, 547-556.

118. Christoffersen, J.; Rostrup, E.; Christoffersen, M. R. Relation between Interfacial Surface-Tension of Electrolyte Crystals in Aqueous Suspension and their Solubility - a Simple Derivation Based on Surface Nucleation. *J. Cryst. Growth* **1991**, *113*, 599-605.

119. Mersmann, A. Calculation of Interfacial-Tensions. *J. Cryst. Growth* **1990***, 102*, 841-847.

120. Sangwal, K. On the Estimation of Surface Entropy Factor, Interfacial-Tension, Dissolution Enthalpy and Metastable Zone-Width for Substances Crystallizing from Solution. *J. Cryst. Growth* **1989***, 97*, 393-405.

121. Yan, Z. L.; Elliott, J. A. W.; Masliyah, J. H. Roles of Various Bitumen Components in the Stability of Water-In-Diluted-Bitumen Emulsions. *J. Colloid. Interface Sci*. **1999**;220(2):329-337.

122. Vazquez, D.; Mansoori, G. A. Identification and Measurement of Petroleum Precipitates. *J. Petrol. Sci. Eng.* **2000***, 26*, 49-55.